statistical analysis of triggered landslides: implication for earthquake and weather controls

Lucile Tatard

▶ **To cite this version:**

Lucile Tatard. statistical analysis of triggered landslides: implication for earthquake and weather controls. Geophysics [physics.geo-ph]. Université Joseph-Fourier - Grenoble I, 2010. English. NNT : . tel-00498011

HAL Id: tel-00498011
https://theses.hal.science/tel-00498011

Submitted on 6 Jul 2010

HAL is a multi-disciplinary open access archive for the deposit and dissemination of scientific research documents, whether they are published or not. The documents may come from teaching and research institutions in France or abroad, or from public or private research centers.

L'archive ouverte pluridisciplinaire **HAL**, est destinée au dépôt et à la diffusion de documents scientifiques de niveau recherche, publiés ou non, émanant des établissements d'enseignement et de recherche français ou étrangers, des laboratoires publics ou privés.

Thesis submitted for the Degree of
Doctor of Philosophy in Geology (University of Canterbury) and
Docteur en Géophysique (Université de Grenoble, ED TUE)

Statistical analysis of triggered landslides : implications for earthquake and weather controls

Lucile Tatard

Thesis prepared under a cotutelle arrangement between Laboratoire de Géophysique Interne et Tectonophysique (Grenoble, France) and Department of Geological Sciences (Christchurch, New Zealand)
Thesis defended on the 9th of February 2010

PhD Committee:

Fausto Guzzetti	IRPI CNR - Perugia	(Examiner)
David Petley	IHRR - Durham	(Examiner)
David Amitrano	LGIT - Grenoble	(Oral Examiner)
Fabrice Cotton	LGIT - Grenoble	(Oral Examiner)
Jean-Philippe Malet	EOST - Strasbourg	(Oral Examiner)
Tim Davies	DGS - Christchurch	(Supervisor)
Stéphane Garambois	LGIT - Grenoble	(Supervisor)
Jean-Robert Grasso	LGIT - Grenoble	(Supervisor)

Contents

Abstract

We first review, in five sections, the external perturbations and their associated processes which can lead to landslide failure: i) increase of slope angle, ii) increase of load applied to the slope, iii) rise of groundwater level and pore pressure, iv) frost weathering processes and v) earthquake loading.

Second, we analyse the New Zealand landslide catalogue, including all landslides recorded in New Zealand between 1996 and 2004, in time and rate and find a strong correlation in landslide occurrences. The time correlation between landslide occurrences for events occurring more than 10 days apart is not driven by earthquake-landslide nor landslide-landslide interactions. We suggest the climate-landslide interactions drive most of New Zealand landslide dynamics, non-linearly and beyond the empirically reported daily correlation.

Third, we compare the occurrence of landslides in time, space and rate of New Zealand, Yosemite cliffs (California, USA), Grenoble cliffs (Isère, French Alps), Val d'Arly cliffs (Haute-Savoie, French Alps), Australia and Wollongong (New South Wales, Australia) as indicated by the corresponding catalogues. Landslides are found to be correlated to each other in time for all catalogues. The New Zealand, Yosemite, Australia and Wollongong landslide daily rates between 1 and 1000 events per day are well fitted by a power law, suggesting that the same mechanism(s) are driving both the large landslide daily crises and the single events. The joint analysis of the six catalogues reveals parameters that allow sorting of the relative landslide occurrences in each of the six areas. From the most re-active landslide area (New Zealand) to the least re-active area (Grenoble), the global trends of the different parameters are: i) decreasing departure from randomness; ii) decreasing

maximum daily rates and area over which the trigger operates; iii) decreasing landslide triggering for landslides occurring one day apart; and iv) decreasing global interaction among earthquake, rainfall and temperature.

Fourth, we compare earthquake aftershock spatial distributions with the spatial distributions of landslides triggered by the Chi-Chi M_W7.6 earthquake (Taiwan), by the M_W7.6 Kashmir earthquake (Pakistan), by the M_W7.2 Fiordland earthquake (New Zealand), by the M_W6.6 Northridge earthquake (California) and by the M_W5.6 Rotoehu earthquake (New Zealand). We show the seismic aftershock and landslide normalised number of events to display roughly similar patterns with distances for given seismic events. When comparing the five landslide - aftershock distribution pairs for a given mainshock, however, we do not find a clear common pattern. Then we compare landslide and aftershock distance distributions with ground motion observations (Peak Ground Acceleration, Peak Ground Velocity and Peak Ground Displacement) and we find no linear scaling of the number of landslides or aftershocks with any of the ground motion variables. We suggest that landslides and aftershocks are driven by the same mechanisms and shed light on the Peak Ground Displacement and static stress changes on landslide triggering. Last, we show that there may be an influence of the local conditions (antecedent soil water status) and of the earthquake mechanism (surface rupturing earthquake versus buried earthquake) on the spatial distribution of the earthquake-triggered landslides.

Résumé

Dans un premier temps, nous nous intéressons aux perturbations extérieures pouvant déclencher des glissements de terrain: i) augmentation de l'angle de la pente, ii) augmentation de la charge appliquée sur la pente, iii) augmentation du niveau de la nappe phréatique et de la pression de pore associée, iv) processus de gel et dégel et v) chargement sismique de la pente.

Dans un deuxième temps, nous analysons les séries temporelles des glissements de terrain de Nouvelle-Zélande en temps et en taux et mettons en évidence une corrélation dans les occurrences de glissements. Cette corrélation entre les occurrences de glissement de terrain, pour des glissements de terrain ayant lieu à plus de dix jours d'écart n'est pas due aux interactions glissement-séisme ou aux interactions glissement-glissement mais aux interactions glissement-climat. Nous suggérons que les interactions glissement-climat contrôlent la plupart de l'activité glissement de terrain en Nouvelle-Z'élande. Ces interactions sont non linéaires et jouent à des échelles de temps supérieures à la journée.

Dans un troisième temps, nous comparons les occurrences des glissements de terrain en temps, espace et taux pour la Nouvelle-Zélande, le Yosemite (Californie, Etats-Unis d'Amérique), Grenoble (Isère, France), Val d'Arly (Haute-Savoie, France), l'Australie et le Wollongong (New South Wales, Australie). Les glissements présentent une corrélation en temps pour tous les catalogues. Les taux journaliers de glissements de la Nouvelle-Zélande, du Yosemite, de l'Australie et du Wollongong acceptent une loi puissance pour

des taux variant de 1 à 1000 glissements/jour. Cela suggère que les mêmes méchanismes sont à l'oeuvre pour le déclenchement de plusieurs centaines de glissements comme pour le déclenchement d'un seul glissement. L'analyse jointe de ces 6 catalogues nous a permis de dériver des paramètres permettant de classer la dynamique de chaque endroit en terme de glissements. Si l'on classe les six zones géographiques de la plus re-active (Nouvelle-Zélande) à la moins re-active (Grenoble), les tendances générales des paramètres sont les suivantes: i) les occurrences de glissement de terrain en temps sont plus proche d'une distribution aléatoire, ii) baisse du taux maximum de glissements de terrain à la journée et de la taille de la zone sur laquelle le déclencheur opère, iii) baisse du nombre de glissements déclenchés à un jour d'écart et iv) baisse de l'interaction globale des glissements de terrain avec la sismicité, la pluie et la température.

Dans un quatrième temps, nous comparons les distributions en espace des répliques sismiques et des glissements de terrain déclenchés par les séismes de Chi-Chi (Mw7.6 - Taiwan), du Kashmir (Mw7.6 - Pakistan), de Fiordland (Mw7.2 - NZ), de Northridge (Mw6.6 - Californie) et de Rotoehu (MW5.6 - NZ). Le nombre de répliques sismiques et de glissements présentent des distributions spatiales (distance à lépicentre, l'hypocentre, la faille en profondeur, la faille en surface...) similaires, pour un événement sismique donné. Cependant, les distributions spatiales des répliques et des glissements de terrain pour les les cinq événements sismiques, ne sont pas similaires. Nous ne trouvons pas de réponse linéaire entre les glissements et/ou les répliques et les observations de mouvements du sol (accélération maximale du sol, vitesse maximale du sol et déplacmenent maximal du sol). Nous suggérons que les glissements et les répliques sismiques sont contrôlés par les mêmes méchanismes et donc qu'il existe un rôle de la contrainte statique sur le déclenchement des glissements de terrain. Enfin, nous montrons une possible dépendance des distributions spatiales des glissements de terrain au type de séisme (séisme rupturant la surface contre séisme enfoui) et aux conditions locales (état hydrique du sol).

Aknowledgement - Remerciements

Des remerciements! c'est cool les remerciements! certes, c'est un peu long..... certes des double-remerciements, liés à une thèse en cotutelle, c'est encore plus long... mais sans vous tous, qui serais-je? où serais-je?

BREF! :-)

Mes premiers remerciements s'adressent tout naturellement à mes directeurs de thèse: merci Jean-Robert pour toutes tes idées, ton enthousiasme et cette approche particulière de la science qui, visiblement, porte ces fruits! Merci Stéphane pour m'avoir aidée à garder le cap, pour les conseils, les corrections et toutes ces petites choses indispensables qui m'ont clairement aidée à venir à bout de cette thèse. Thank you, Tim, for introducing me to a physical approach of landsliding. Thanks also for the diverse opportunities you gave me and which highly improved my understanding of NZ landsliding notably. Dans la catégorie pas directeur de thèse mais pas loin, merci Agnès, pour toute ton aide mathématique/statistique/matlabistique qui a beaucoup apporté à cette thèse.

Dans la catégorie rapporteurs, thank you very much David Petley and Fausto Guzzetti for reporting my thesis and for the very interesting discussions you raised. I do hope I'll have the chance to work with you in the near future. Dans la catégorie membres du jury, je remercie vivement David Amitrano, Fabrice Cotton et Jean-Philippe Malet d'avoir accepté d'être membre du jury et de s'être intéressés de prêt à cette thèse!

Dans la catégorie "Merci pour le coup de main, vous êtes nombreux et je vous en

suis ô combien reconnaissante!", merci Brice Randrianasolo, Philippe Guéguen et Erwan Pathier pour l'aide sur les différents logiciels de SIG, merci Guillaume Daniel pour le petit programme matlab qui calcule des magnitudes de complétude à merveille!, merci Pierre Gouedard pour ton aide matlabienne et linuxiote, merci Elisabeth pour l'aide LaTeX + le reste!, merci merci merci! Paola pour la multi aide sur à peu prêt tous les domaines possibles! Et non, je ne t'oublierai pas, merci Jacques pour toute l'aide que tu m'as apportée pendant la première année! (et une spéciale dédicace aux deux sports que nous avons inventés!). Thanks also to Aaron Clauset for letting available his matlab codes on power laws: finding his article and associated codes was such a turning point during my thesis!! Also thanks a lot Mauri McSaveney for the fieldwork and interesting discussions... Pour les discussions intéressantes, je repasse au français avec des mercis Romain et Pierre ainsi qu'un special round of thanks pour Anne-Marie, Pascal, Florence, Shaz, Agnès pour les corrections pre-soutenance!

Dans la catégorie "bases de données", oh yeah I did use quite some landslide and earthquake databases.... thanks a lot to Grant Dellow for all the help on the NZ landslide catalogue! but also thanks a lot to, by country: Gerald Wieczoreck, Randall Jibson, David Keefer, John Michael for the USA related databases, to Didier Hantz, François Thouvenot, Céline Beauval for the France related databases, to Monica Osuchowski, Phil Flentje and Mark Leonard for the Australia related databases, to Kuo-Fong Ma for the Taiwan related databases and to Hiroshi Sato for the Pakistan related database.

Dans la catégorie "terrain", Yes! there was some fieldwork performed for this thesis and well no, it did not worked out exactly how we would have liked it to (and this might be the reason why you'll read nothing about it in this thesis!) but I'm pretty sure I should thank a lot Brendan Duffy, Michael Finnemore, Sam Hampton, Tom Wilson and David Nobes for helping me out on the field. Neither GPR, electrics or seismics were easy on this really, really! steep landslide slope! (how precious was this expression on your faces when you first saw it, ahah!)

Catégorie administratif: Je voudrai remercier les équipes administratives françaises et

néo-zélandaises pour leur aide et leur bonne humeur sans faille: merci Zoubida, France, Jacques, Karine, Jean-Marc et toutes les autres, merci Sylvianne et Christine, thank you very much Pat and Janet for helping me out in NZ! that was quite nice to have people to rely on, especially when coming somewhere like the other end of the world :-) Thanks a lot to Sonia Marshall as well for helping me out with the last minute paperworks!

Merci beaucoup Rodolphe, Patrick, Ghislain et Hafid pour la catégorie informatique. Thank you so much, John, for all the help you provided me!

Et fi des catégories, me voilà enchaînant sur la bonne humeur du LGIT et de ses thésards et autres postdoc et stagiaires! merci à eux tous! dois-je vraiment les citer? sûrement, mais c'est rude, forcément je vais en oublier! (heya Pierre, Lolo, Yvi, Guillaume, Jacques, Antho, Soline, Alexis, Fabien, Ben, Thom, Paola, Eli, Louis, Seb, Aloé, Mat(t)hieux, Agathe, Soumaya, Oliviers, Gwen, Tahir, Florence, Clara, Mathildes, Bérénice, Steph, Romain, Manu, Dimitri, Elodie, Marie, Bastien, Cahtee, Célines et tous les autres!) et le LGCA? puis-je l'oublier le LGCA? bé non, finalement c'est un peu mon labo aussi, et ce, avant toute fusion consommée (houyou Shaz, Benoît, Vince, Thom, Marions, Jérémie, Seb, Romain, Fabinou, Pierre, Chichi, Jérôme, Antoine, Charlotte, Marc, Marie, TSL, Thibault, Christoph and so on)! et les poteaux de 3SR? heya Ha, Bastien, Christophe, Rachel! et aussi heya là bas, en histoire, Nadège! Et les vieux compagnons de promo: magis02 j'ai nommé! une pensée à eux tous et en particulier Delphine, Olivier, Johan, Julien, Sam, Sylvain, Shaz, Corentin, Nadaya et les friends related Marie, Antwan, Benj, Elo, Mathilde, Pierrick, Jérémie... J'espère qu'on se referra une épopée à l'islandaise one of these days!

Down there, who would I like to say howdie & thanks for everything? people like Anja, Elke, Ali, Rose, Sam, Tom, Kate, Olivia, Guillaume, Jesse, Natalya, Scott, Chad and also the Iranian dream team: Sohrab, Bita, Masoud, Mostafa, Amin, Ali G., Zohreh, Nicola (yes you are Iranian to me!) and Ehsan (what a trip we had!). Diane and Danny: thank you for your hospitality and the great farm tour! And, let me not forget the Tika Palacers, who highly contributed to make this experience in NZ something quite incredible

and unforgettable... thank you so much SuperJames! Andymoioui! Tania-Laura P.! Julie-Bonbon-Olive-Emeu-Crêpe (je sais plus l'ordre!!)! and Basile le crocodile! To all of you my NZ friends, I really hope to see you soon, either in France or in NZ (or anywhere actually!)!

J'en profite pour remercier solennellement et éternellement une armée, celle qui m'aida, sans faillir, à la préparation du pôt de thèse. D'un côté, le bataillon quiche (merci Fabien, Mathieu, Soumaya, Mathildes, Aurore, Gwen!), de l'autre côté, le bataillon tarte (merci Elodie, Manu, Florence, Agathe, Romain, Dimitri, Tahir!), sans oublier l'inénarable agent double: merci Shasa!, et les renforts de Paris qui m'ont permis de venir à bout de cette bataille (merci la familia!). Miam miam les papilles! MERCI à eux tous, donc!

Dans la catégorie plus vraiment la thèse mais source de motivation et de remotivation, je voudrai dire un grand merci aux rainbow swingers - aussi connu sous le nom bien moins funky de Ensemble Vocal Universitaire de Grenoble (répète ses merveilleux chants du monde tous les mercredis soirs à l'ARSH soit dit en passant!) et à Boréale, pour, au-delà de ses performances musicales, m'avoir fait découvrir le folk et ouvert les portes de la DANSE! In New Zealand, I am very grateful to the Farandol Folkdancers and their weekly jig and so very very grateful to The Muse Community Music Trust (I so damn wish there would be one association like yours in every cities of every countries!).

Et je ne peux point laisser aller ces remerciements sans inclure les old friends, les déjantés, les Bouboulonnais! heya Nath, Maïs, Alion sauvage, Yas le putois, Aurel, Loulou1664 sans oublier ma petite Félina, qui s'est mariée!, et mes poteaux géologues des débuts, j'ai nommé Jorge et Steph! Enfin, merci la familia Grenobloise des Labanieh pour votre présence, votre bonne humeur et votre leçon de vie quotidienne... Et MERCI la real familia, pour votre soutien sans faille pendant toutes ces looooooooooongues années d'études! :-)

As a conclusion to this acknowledgement section, a special thank to Anja for introduc-

ing me to Vipassanna and E. Tolle's books (ok, this is not directly PhD related but it does include it though! and transcend it as well!). Thank you for showing me the door... giving me some keys... I know the rest is just on me! ;-)

Now, it looks to me that it would be a good idea to finish with three quotes from E. Tolle, so let's do that!

"Your mind is an instrument, a tool. It is there to be used for a specific task, and when the task is completed, you lay it down. As it is, I would say about 80 to 90 percent of most people's thinking is not only repetitive and useless, but because of its dysfunctional and often negative nature, much of it is also harmful. Observe your mind and you will find this to be true. It causes a serious leakage of vital energy."

"The present moment has always been available to spiritual seekers, but as long as you are seeking you are not available to the present moment. Seeking implies that you are looking to the future for some answer, or for some achievement, spiritual or otherwise. Everybody is in the seeking mode, seeking to add something to who they are, whether it be money, relationships, possessions, knowledge, status... or spiritual attainment."

"Those who have not found their true wealth, which is the radiant joy of Being and the deep, unshakable peace that comes with it, are beggars, even if they have great material wealth. They are looking outside for scraps of pleasure or fulfillment, for validation, security, or love, while they have a treasure within that not only includes all those things but is infinitely greater than anything the world can offer."

bah voilà, c'est fait!

May you all be happy! - Soyez heureux!
⌊ et puis bonne lecture de cette thèse, surtout! ⌋

General introduction

Landslides and rockfalls, as well as earthquakes, volcanic eruptions and other natural hazards, are not fully understood and it is not yet possible to forecast with confidence their occurrences or their characteristics. In general, triggering of instabilities in geosystems is a complex problem encompassing different scales and mechanisms, from the micro scale where defects of the crystalline network such as dislocations and microcracks govern deformation properties, to the macro scale where defects of the geomaterial such as fractures and faults influence the geosystem global behaviour. Causes of failure in geosystems can be classified into two categories: i) exogenous causes such as precipitation events and associated pore pressure changes, and seismic waves and their associated stress changes and ii) endogenous causes such as geochemical deterioration, creep deformation, microcracking and microplasticity (Alava et al., 2008).

As it is difficult to deal with the general problem of natural hazard occurrences as a whole, one approach is to restrict the analysis to how and when instabilities are triggered and the role of potential external disturbances. These different questions have been addressed in various ways, depending on the geological hazard involved, *e.g.* earthquakes, volcanoes or landslides, and we review them shortly below.

There have been many studies on seismicity triggering patterns since the 1970s, based on the expansion of local seismicity networks, generating good quality earthquake databases. While earthquake triggering is still poorly understood, some models which reproduce earth-

quake patterns (e.g. ETAS model, Ogata, 1988; rate-and-state model, Dieterich, 1994) and the role of external disturbances on earthquake triggering have been investigated. Triggering of an earthquake by another earthquake is the process which has been most studied. Helmstetter (2003) showed that any magnitude of earthquake could be triggered by an earthquake, of any magnitude. Other statistical studies showed that earthquakes could also be induced by other external perturbations such as "slow" earthquakes (e.g. Segall et al., 2006), rainfall (e.g. Muço, 1999; Ogasawara et al., 2002; Hainzl et al., 2006), volcanic activity (e.g. Dieterich et al., 2000; Špičák and Horálek, 2001), deep crust degassing (e.g. Chiodini et al., 2004; Miller et al., 2004) and human activities (see McGarr et al., 2002 for a review).

The processes driving triggering of volcanism are also poorly understood. Analysis of instrumental volcanic eruption databases demonstrates the influence of earthquakes on volcanic eruption triggering (e.g. Linde and Sacks, 1998; Manga and Brodsky, 2006; Lemarchand and Grasso, 2007), but the processes of eruption triggering by earthquakes are still unknown, and research is ongoing.

Returning to landslide triggering, past and present landslide studies are usually deterministic in nature, dealing with engineering and mitigation aspects of landslides, as well as process-based studies or case investigations. Process-based studies analyse the triggering mechanisms and properties of external perturbations such as large ($M > 4$) nearby earthquakes (for a review see Keefer, 2002) and heavy rain (see De Vita et al., 1998 for a list of references). There are few available continuous landslide databases extending over time periods longer than one year, and their no systematic analysis in time, space and rate, along with the assessment of possible earthquake-landslide, weather-landslide and landslide-landslide interactions, has yet been carried out.

This thesis firstly aims to achieve such a systematic analysis of six landslide databases, irrespective of the landslide type or the local conditions (geology, geomorphological history of the slope, etc...). Note that the term landslide is used in this study as a generic term for mass movement processes, and more precisely for any episode of movement provided

there is a period without movement ("waiting time") between successive movement events. It encompasses all falls, topples, slides, spreads and flows involving either rocks, debris or earth materials.

The outline of this thesis is as follows:

In the first chapter, we review the external perturbations which can lead to landslide failure and associated processes in five sections: i) increase of slope angle, ii) increase of load applied to the slope, iii) rise of groundwater level and pore pressure, iv) frost weathering processes and v) earthquake loading.

In chapter 2, we apply statistical tools used for the analysis of other geosystems, such as earthquakes and volcanic eruptions, to the analysis of the 1996-2004 New Zealand landslide database. We study the New Zealand landslide series in time and rate and investigate the landslide-landslide, landslide-climate and landslide-earthquake interactions.

In chapter 3, we extend our analysis to five other landslide databases, with the objective of assessing and comparing landslide dynamics. We compare the landslide dynamics in time, space and rate of New Zealand, Yosemite cliffs (California, USA), Grenoble cliffs (Isère, French Alps), Val d'Arly cliffs (Haute-Savoie, French Alps), Australia and Wollongong (New South Wales, Australia). The joint analysis of the six catalogues allows us to derive parameters that represent the relative landslide dynamics in each of the six areas. Landslide dynamics include here both the slope susceptibilities and the applied forcings for a given area. The parameters used for the comparison are i) deviation from randomness of the landslide occurrence time distributions, ii) exponent of daily rate power-law and maximum area impacted during a daily landslide crisis, iii) triggering of landslides for events occurring one day apart and iv) intensity of correlation to seismicity, rainfall and temperature.

In chapter 4, we compare earthquake aftershock spatial distributions with landslide spatial distributions triggered by the Chi-Chi M_W7.6 earthquake (Taiwan), by the M_W7.6 Kashmir earthquake (Pakistan), by the M_W7.2 Fiordland earthquake (New Zealand), by the M_W6.6 Northridge earthquake (California) and by the M_W5.6 Rotoehu earthquake (New Zealand). Then we compare landslide and aftershock distance distributions with

ground motion observations (Peak Ground Acceleration, Peak Ground Velocity and Peak Ground Displacement) and consider the role of static stress changes in landslide triggering.

In conclusion, we discuss the present limitations of landslide databases and suggest potential improvements. Finally, we synthesize the various results and interpretations in this thesis and propose future research perspectives.

Chapter 1

Landslide triggering

Catastrophic landslides and rockfalls are mainly triggered by large ($M > 4$) nearby earthquakes (for a review see Keefer, 2002) or heavy rain (for references see De Vita et al., 1998). Those are the only two triggering factors which can produce daily large clusters of individual landslides (Crozier, 1996). Other processes known to influence slope stability are freeze-thaw cycles (Matsuoka and Sakai, 1999; Frayssines and Hantz, 2006), snow-melt episodes (Sandersen et al., 1996; Frayssines and Hantz, 2006; Gruner, 2008), anthropic works (Stark et al., 2005; Smyth and Royle, 2000), glacial and fluvial downcutting (Wieczorek, 2002), neotectonic stresses (Ai and Miao, 1987; Julian and Anthony, 1996), and deglaciation (Wieczorek, 2002; Holm et al., 2004). The time-scales of these forcings range from a few seconds for seismic pulses to more than 10,000 years for deglaciation cycles. For some of the longest time-scale forcings, no transient trigger is identified when the landslide occurs, and those types of landslides are described as spontaneous, gravitational failures (McSaveney, 2002; Wieczorek, 2002; Cox and Allen, 2009). For giant, catastrophic slope collapses, other mechanisms are put forward by Kilburn and Petley (2003) such as self-accelerating rock fracture, readily catalysed by circulating fluids. Landslide failures are also controlled by a combination of the following factors: inherited tectonic history (Molnar et al., 2007), geology, soil engineering, chemical and mineralogical properties, geomorphology, hydrology (for a review of these different factors see Sidle and Ochiai, 2006),

vegetation cover (e.g. Fuchu et al., 1999; Reid and Page, 2002), land use and associated drainage/seepage patterns (e.g. Crosta, 1998; Fuchu et al., 1999; Basile et al., 2003). The combination of heterogeneous forcings and slope conditions leads to the complexity of landslide triggering. In this chapter, we focus solely on the external perturbations leading to landslide failure. The combination of these forcings is more likely to trigger landslides than a single one but for clarity we review each process individually.

1.1 Triggering of landslides by increase of slope angle

Increase in slope angles can be driven by anthropogenic processes, such as road cutting steepening hillslopes or other urbanization works as reported for landsliding in urban area of Rio de Janeiro, Brazil (Smyth and Royle, 2000). As another example, Stark et al. (2005) analyzed the influence of excavation of a cutslope toe, which contributed to triggering a landslide by exposing geologic structures on the cutslope (such as shear zones, faults, and folds) and by unloading the toe of the slope. Basile et al. (2003) showed, through numerical modelling, that the presence of a road cut could result in an increase of more than 30% in soil water storage with respect to the same section of undisturbed slope/ This can cause an overloading which can bring the slope to failure. Natural processes such as erosion of the hillslope toe by fluvial or glacial action can also change the slope inclination. Holm et al. (2004) demonstrated the influence of glacier retreat on landslide triggering in British Columbia. Wieczorek (2002), after a study of landsliding in the Sierra Nevada, California, noted that glaciated topography had oversteepened slopes, prone to rockfalls and rockslides. He also pointed out that fluvial and glacial downcutting and lack of lateral confinement cause stresses in oversteepened valley walls which induces the formation of exfoliation sheets and the dilation of joints which in turn produce rockfalls. McSaveney (2002) studied rockfalls in the Southern Alps of New Zealand. He pointed out the mechanical action of still present glaciers, scouring and plucking their headwalls, steepening the bottom of the slopes. He also mentioned that glacier thinning could induce rockfalls by unloading the toe of structurally defective rock slopes.

It is noticeable that a change of slope can also result from an earthquake, but it remains difficult with available data to test whether the landslides are triggered by geometrical effects independently of the shaking due to seismic waves.

1.2 Triggering of landslides by increase of load applied to the slope

An increase in the weight of the landslide may be due to erosion processes or rainfall. For instance, Chigira and Yokoyama (2005) showed the influence of weight increase by water for landslides in non-welded ignimbrite (Kyushu, Japan). The weathering profile shows permeability variations, with layers of low permeability allowing for rain water to build up, increasing the weight of the weathered material and decreasing the suction within the material. The latter was the final trigger for this shallow landsliding case study. Basile et al. (2003) showed that an increase of water storage resulted in overloading of the slope, which produced the same values of soil tangential stress as those of peak strength and consequently brought the slope to failure.

1.3 Triggering of landslides by rise in groundwater level and pore water pressure

Ground water level and pore pressure changes result from the infiltration from surface (rainfall, snowmelt, leaking pipe...), or exfiltration from bedrock, preferential flow and convergent flow leading to water accumulation. This in turn leads to increased pore water pressure which reduces the soil strength and increases stress (Ray and Jacobs, 2007). Caine (1980) first proposed, after a study of 73 worldwide natural slope failures, that rainfall intensities and durations associated with shallow landsliding and debris-flow activity suggested a limiting threshold for this type of slope instability, the limit having the general form:

$$I = 14.82\ D^{-0.39}$$

where I is the intensity of rainfall (mm/hr) to be overcome for triggering landslides, and D the duration of the rainfall (hrs; Fig. 1.1). Sidle and Ochiai (2006) developed these results and proposed two empirical relationships between the amount of rainfall and landsliding, depending on the antecedent water status of the soil. The first relationship is for soil that has endured more than 20 mm of rain on the two previous days before failure:

$$I = 12.64\ D^{-0.39}$$

while the other relationship is applicable for dry soils (less than 20 mm of rain on the antecedent two days):

$$I = 19.99\ D^{-0.58}$$

For a better estimate of regional triggering of landslides by rainfall, other studies include more parameters such as antecedent water soil conditions (Crozier, 1999; Glade, 2000), regolith hydrological behaviour and depth (Brooks et al., 2004), and the combined influence of mean and maximum hourly intensity, duration and total amount of rainstorms (Dhakal and Sidle, 2004). Triggering thresholds are found to be variable in space, depending on the susceptibility of a given landscape (existing physical conditions) to landslide-triggering rainfall (Glade, 2000; Brooks et al., 2004) and to be variable in time, depending on the rainfall duration (Guzzetti et al., 2007) and on the geomorphological stage of the slope (Brooks et al., 2002; Hufschmidt and Crozier, 2008). Hufschmidt and Crozier (2008) showed that the relationship between magnitudes of rainfall and magnitudes of landslide events is weak, suggesting that a given "Critical Water Content" (antecedent soil water status and rainfall on the day) does not produce similar magnitudes of landsliding. Flageollet et al. (1999), from analysis of rainfall triggered landslides in two basins of the Southern French Alps,

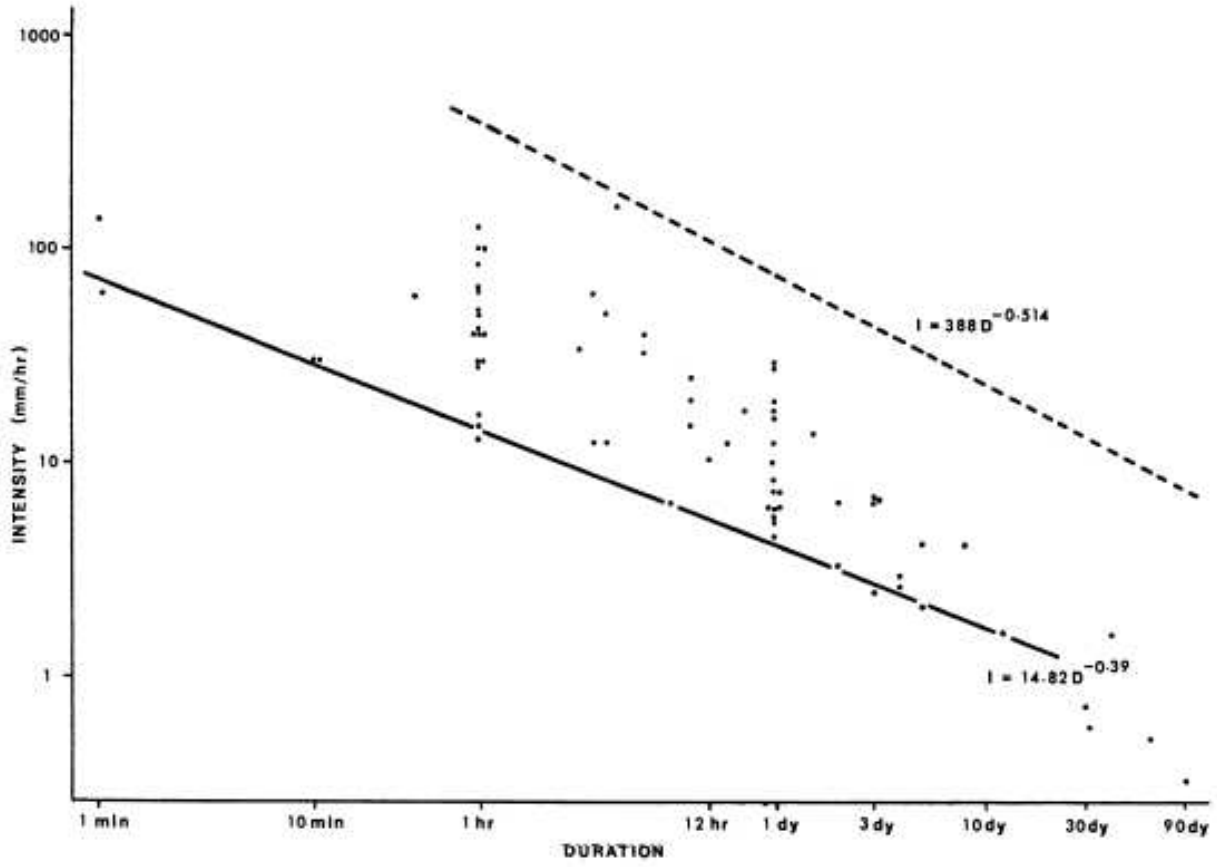

Figure 1.1: Rainfall intensities and durations associated with slope failures. The lower curve is the threshold: I = 14.82 $D^{-0.39}$ with I = rainfall intensity ($mm\ hr^{-1}$) and D = rainfall duration (hr). The upper curve presents the global maximum precipitation intensities I = 388 $D^{-0.514}$. From Caine (1980).

argue that the complexity of relations between landslides and climatic conditions makes it difficult to define universal laws. They suggest that further investigation is needed for defining such laws for given areas, taking into account types of landslide, their generation (triggering or reactivation), the season they occur and, finally, the resulting initial degree of slope stability.

For deep, slow-moving landslide case studies, no triggering threshold, based on rainfall properties, was demonstrated. Terlien (1998) showed that, in the case of deep landslides triggered by a slow accumulation of water at hydraulic boundaries (such as the soil-bedrock contact), no simple correlations between landslide occurrence and rainfall could be established. In these cases, the author suggests that the determination of real-time failure probabilities should be done using hydrological catchment models in combination with the infinite slope model as a rainfall-based threshold approach is irrelevant. Macfarlane (2009) showed that, in the case of a slow-moving landslide in schist (Clyde Dam Reservoir, New Zealand), a threshold approach, based on piezometer level, was relevant, as he found that displacement was initiated every time one of the piezometer levels increased from 280.9 to 281 m (Fig. 1.2).

1.4 Triggering of landslides by frost weathering processes

Frost weathering processes are not associated with daily clustered rockfall crisis, which makes this triggering mechanism more difficult to recognize, in comparison to rainfall or earthquake triggering. Nevertheless, the role of frost weathering as a rockfall trigger has been demonstrated in several studies. In Norway, Sandersen et al. (1996) showed that the distribution of rockfalls through the year presented two maxima, in early spring and late autumn. These two periods not only correspond to the time of the highest rate of snowmelt for the former and of the highest precipitation for the latter, they also coincide with the

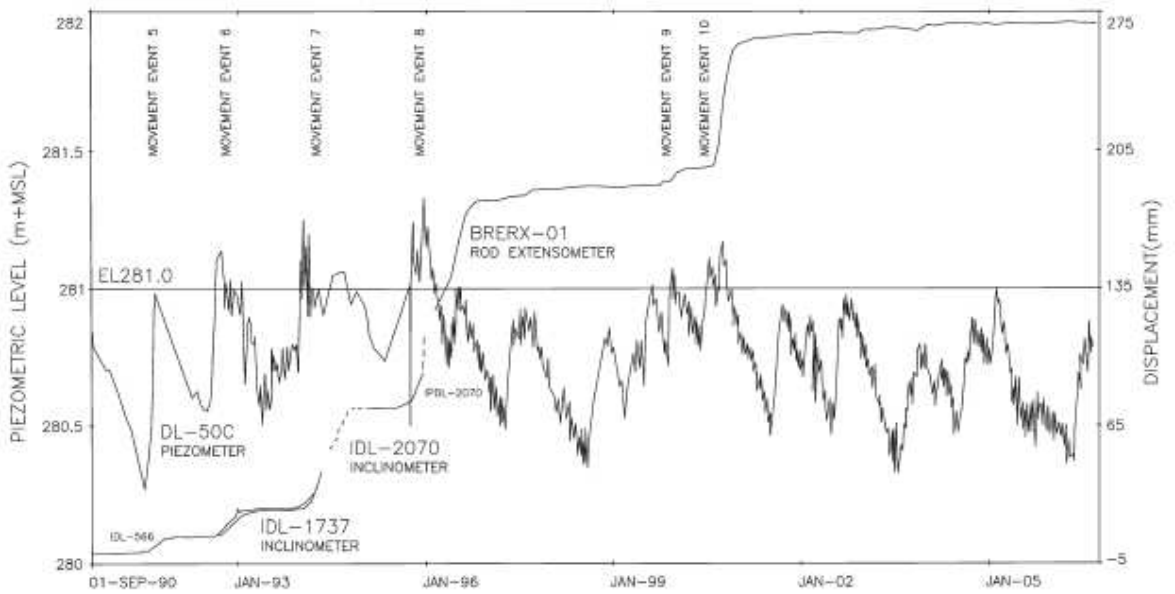

Figure 1.2: Movement history of the Brewery Creek Slide (New Zealand) since 1990 versus piezometer DL 50C water height. Discrete movement events are triggered when the piezometer level rises from EL280.9 to EL281 m. From Macfarlane (2009).

periods of most frequent variations of temperature around the freezing point (Fig. 1.3). Matsuoka and Sakai (1999) analysed rockfall activity in the Hosozawa Cirque, Japan, and concluded that intense rockfall activity does not reflect precipitation events but is primarily controlled by seasonal frost weathering. Frayssines and Hantz (2006) showed that the rockfalls in the French Alps were correlated with freeze-thaw cycles, suggesting that ice jacking could be the main physical process leading to failure by causing microcrack propagation. Hales and Roering (2005, 2007) found that the scree deposits (corresponding to frequent, small magnitude - *i.e.* $< 100\ m^3$ - rock-fall events) in a 80 by 40 km transect in the Southern Alps of New Zealand were mostly influenced by altitude and not by lithology, seismicity or glaciation history (Fig. 1.4). Nearly 70% of the scree deposits were found to be confined in the 1200-1600 m elevation range, just below the altitude corresponding to the frost-cracking window (-3 to -8° C) where ice segregation processes are most efficient.

The frost weathering processes which can lead to rockfall are volume expansion and ice

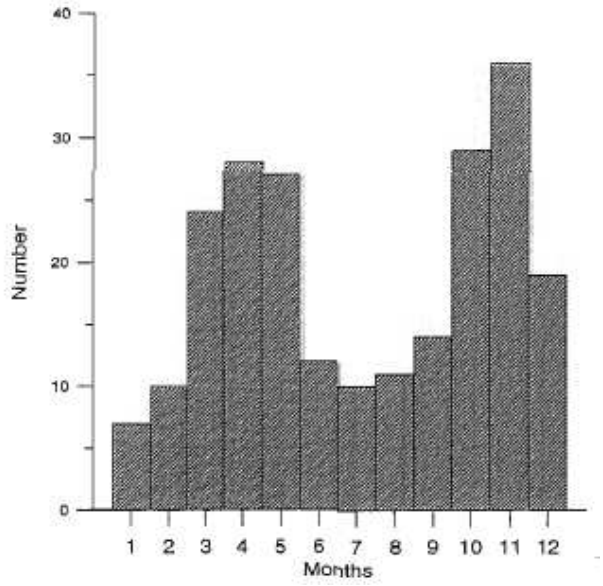

Figure 1.3: Distribution of rockfall over the months in Norway, showing two maximae, in early spring and late autumn, which both coincide with the periods of frequent variations of temperature around the freezing point. From Sandersen et al. (1996).

segregation. The first process corresponds to the 9% volumetric expansion which occurs as water turns to ice. The conditions required for such a process are nevertheless unusual: the rock must be water-saturated or nearly so and must freeze rapidly from all sides, so that water is frozen *in situ*. The ice-induced stress is enough to fracture any rock, eventually leading to rockfall. In addition, rapid freezing of saturated rock can break up rocks by hydrofracture (Matsuoka and Murton, 2008). The second process corresponds to progressive micro-cracking due to the growth of ice lenses during ice segregation. The conditions required for this process are slow rates of freezing or sustained subzero temperatures in moist, porous, fine-grained rocks, which are common in natural bedrock (Matsuoka and Murton, 2008).

1.5 Triggering of landslides by earthquake loading

Earthquake triggering of landslides is very common but not quantitatively understood. Keefer (1984, 2002) observed from a worldwide catalogue of landslides and earthquakes,

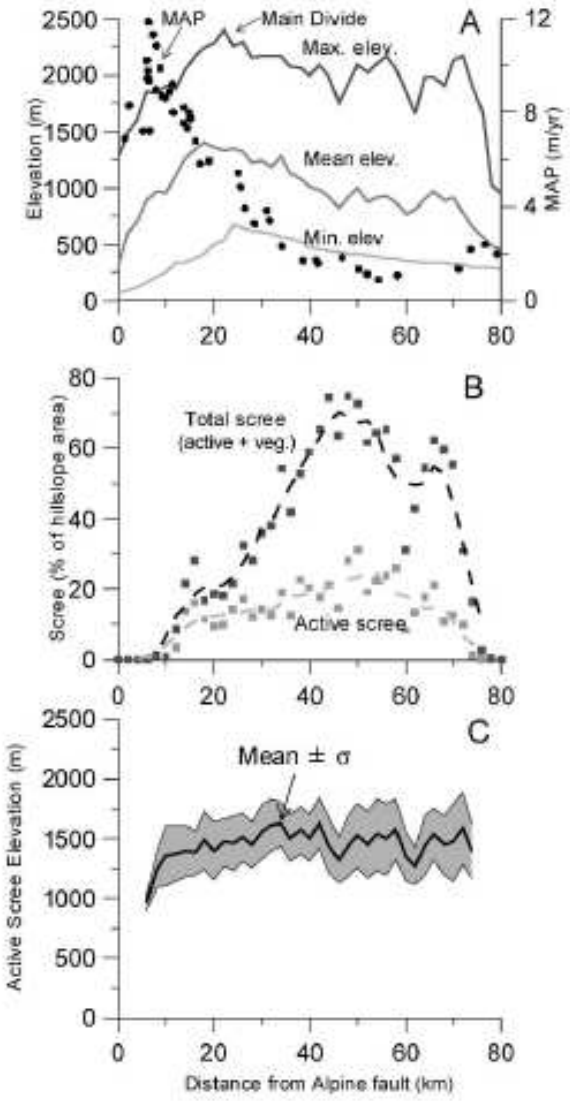

Figure 1.4: a) minimum (light gray), mean (dark gray), and maximum (black) elevations calculated for 2 km swaths across studied transect (South Island, New Zealand). Black squares represent mean annual precipitation (MAP). b) minimum (light gray squares) and maximum (dark gray squares) estimates of fraction of hillslopes mantled by scree across the transect. c) variation in elevation of active scree deposits. Solid black line and shaded region represent mean and standard deviation of elevation of scree slopes. From Hales and Roering, 2005.

that the minimum magnitude for an earthquake to trigger a landslide was M=4, and that the area where landslides occurred increases with magnitude M: from A=0 km^2 for M=4 to A=250 km^2 for M=5.4 and A=500,000 km^2 for M=9.2 (Figs 1.5 and 1.6). The relationship between the potential area A affected by landslides (in km^2) and M is given by Keefer and Wilson (1989):

Log10 A = M - c with c=3.46 $\pm$ 0.47.

Malamud et al. (2004) found, from a worldwide inventory, that the minimum magnitude to trigger a landslide was M=4.3$\pm$0.4. They introduced the landslide - event magnitude M_L=log (N_{lt}) where N_{lt} is the total number of landslides associated with the earthquake event (Fig. 1.7). Meunier et al. (2007) acknowledged that landslide densities, for $M >$ 7 earthquakes on thrust faults (California, Taiwan and Papua New Guinea) are shown to correlate linearly with peak ground acceleration and to decay with distance from the epicentre (Fig. 1.8). The density of landslides in space seems to be fully described by an expression similar to a classical law for seismic wave attenuation.

The effect of low magnitude earthquakes ($M < 5$) on landsliding has been less reported and studied than the effect of larger earthquakes. Miller (1931) first stated that a "slight" earthquake was followed by a notable acceleration of the Point Firmin creeping landslide (California), lasting about two months. Del Gaudio et al. (2000) studied the influence of a low-magnitude (maximum $M_L = 3.6$) earthquake sequence on a nearby (less than 20 km away) landslide in Vadoncello (Southern Italy). They found that it was dubious whether the seismic accelerations generated within the landslide were sufficient to activate mass movements and if the effect of repeated shocks on hydrogeological conditions could explain the time delay observed between seismic and landslide accelerations. Sassa et al. (2007) argued that the $M_s = 2.6$ earthquake which occurred on the same day as the 22 km distant Leyte landslide (Philippines) was the cause of the landslide failure, which also occurred five days after a heavy rainfall. Walter and Joswig (2008) found that it was possible that local (10 km distant) earthquakes of $M_L > 2.0$ caused stress relief within the sliding body

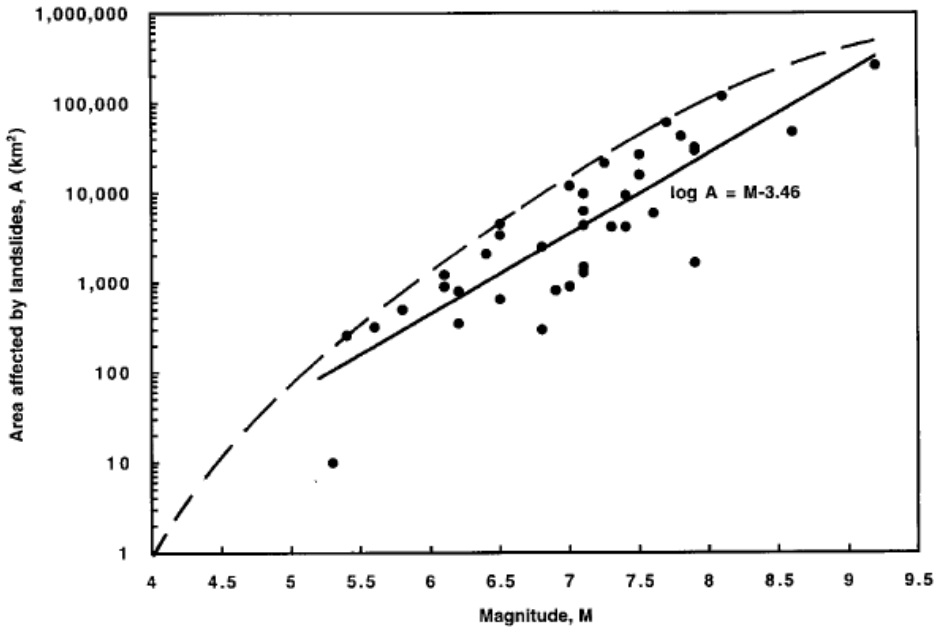

Figure 1.5: Relations between area affected by landslides and earthquake magnitude. Circles are data from earthquakes discussed by Keefer (1984) and Keefer and Wilson (1989). Dashed line is approximate upper bound from Keefer (1984), curved to approach A=0 at M=4. Solid line is least-squares linear regression mean from Keefer and Wilson (1989). Magnitude determinations for individual earthquakes are given in Keefer (1984) and Keefer and Wilson (1989); most magnitudes smaller than 7.5 are Richter surface-wave magnitudes (M_S), and most magnitudes of 7.5 or larger are moment magnitudes (M). From Keefer (2002).

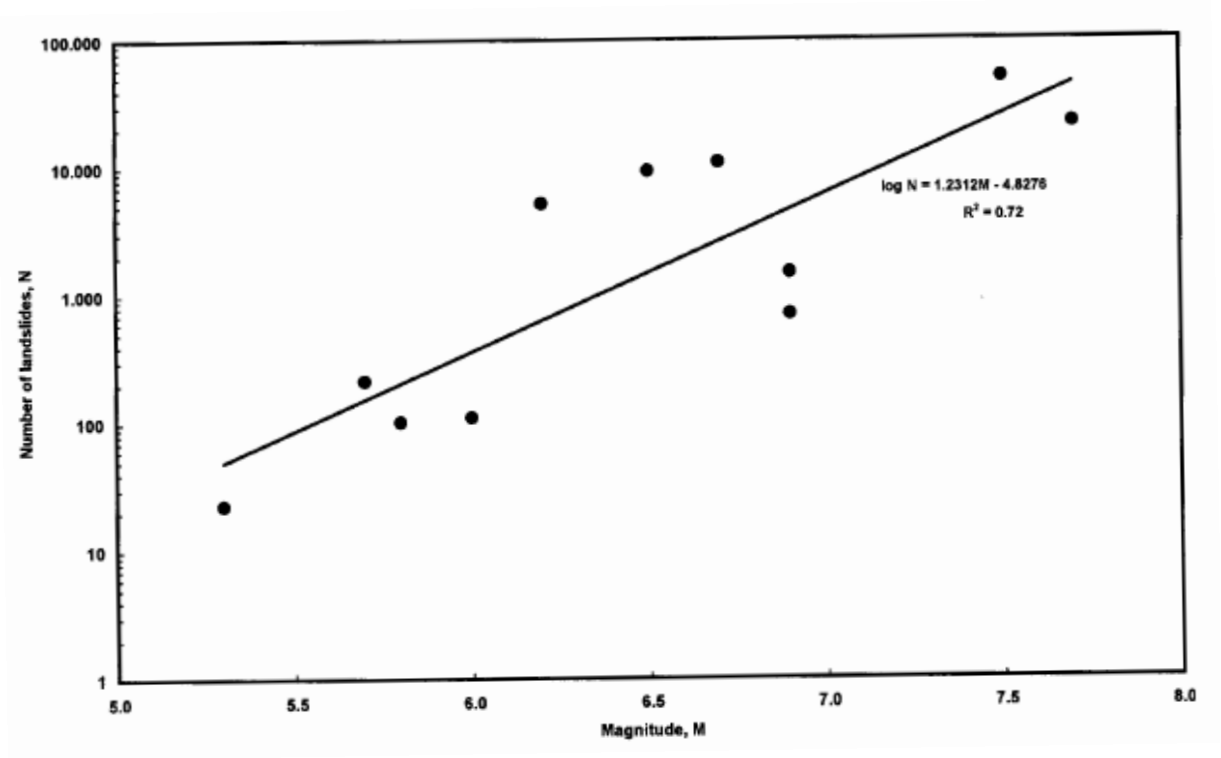

Figure 1.6: Relationship between total number of reported landslides and earthquake magnitude. Data are from earthquakes listed in Table 3 of Keefer (2002). The solid line is the least-squares linear regression mean with R^2 being the square of the correlation coefficient. From Keefer (2002).

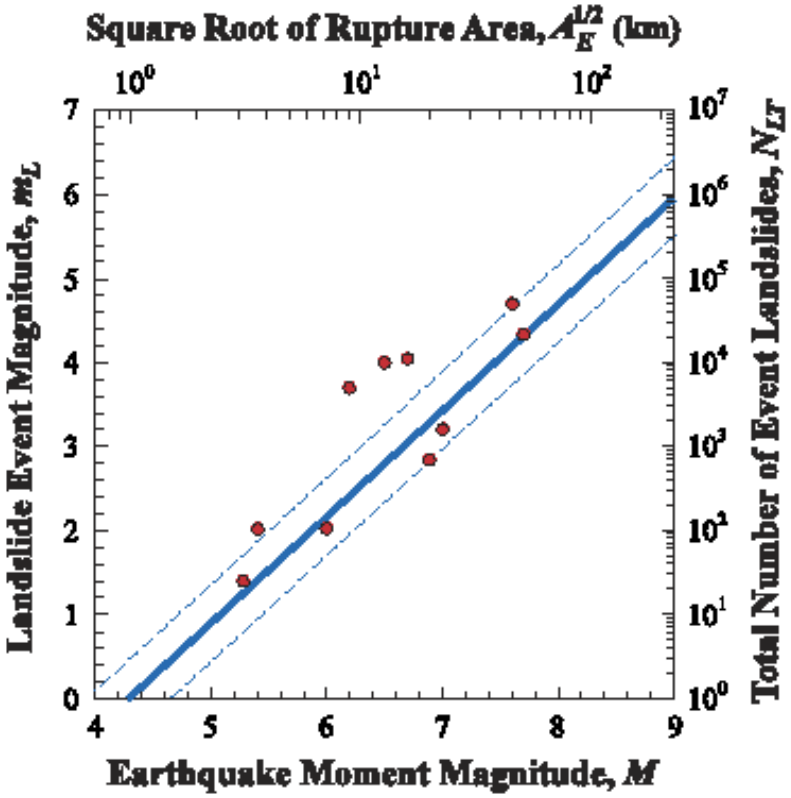

Figure 1.7: Dependence of landslide-event magnitude m_L and total number of landslides N_{LT} on earthquake moment magnitude M. Also given is the square root of the equivalent rupture area $A_E^{1/2}$. The solid line is the correlation from $m_L = 1.27M - 5.45(\pm 0.46) = logN_{LT}$, and the dashed lines are the corresponding error bounds. Also given are observational data for 11 earthquakes. From Malamud et al. (2004).

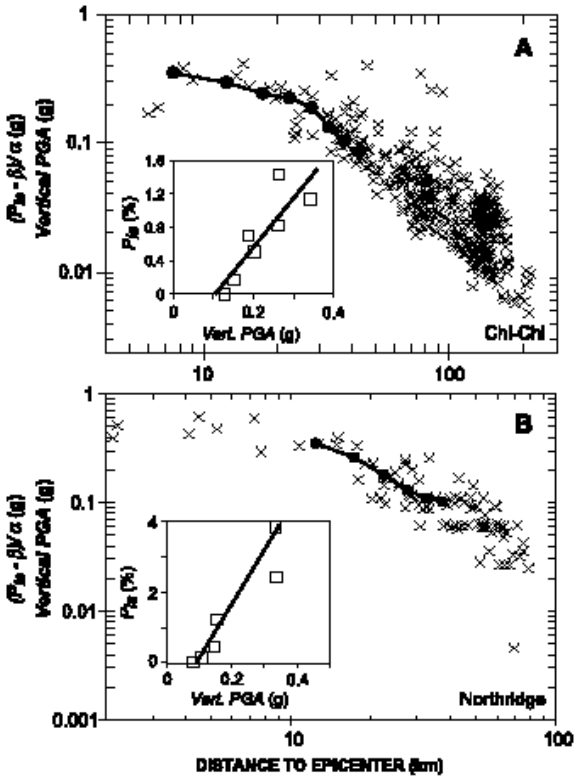

Figure 1.8: Landslide density (filled circles) and vertical PGA (crosses) plotted against distance from the epicenter for a) the Chi-Chi earthquake and b) the Northridge earthquake. For comparison with PGA, landslide densities were scaled linearly with help of trends shown in inset graphs. Inset graphs show average landslide density plotted against average vertical PGA for 5 km windows parallel to the fault trend with least squares linear regressions. From Meunier et al. (2007).

and triggered fracture initiation and/or growth within the Heumoes slope, Voralberg Alps, Austria.

Many factors related to earthquakes and the settings in which they propagate can influence the number, size and type of landslides. Factors related to the intrinsic properties of earthquakes include earthquake magnitude, focal depth, direction of seismic wave propagation, seismic wave attenuation, and aftershock distribution in space and time (Sidle and Ochiai, 2006). Factors related to the environment in which earthquakes occur include inherent stability of the potential failure sites, existence of old or dormant landslides, vegetation and land use, orientation or previously existing faults with respect to the direction of seismic wave propagation, regolith wetness, and slope gradient and other topographic factors suggested by Sidle and Ochiai (2006). In addition, two phenomena are known to enhance failure during earthquakes: site effects and liquefaction.

Site effects correspond to the amplification of seismic waves induced by local resonance due to the shear-wave velocity contrast between the landsliding material and the stable material. Sepúlveda et al. (2005) showed that the observed extensive rock sliding and falling at Pacoima Canyon, triggered by the 1994 M_W=6.6 Northridge earthquake, would not have been possible without amplified seismic conditions. Meunier et al. (2008) also demonstrated by numerical modelling significant amplification of peak ground acceleration at or near ridge crests and at convex knick points within ridge flanks (Fig. 1.9).

Liquefaction corresponds to soil behaving as a fluid under shaking and depends on the soils involved. It was highlighted by Harp et al. (2003) after the 2003 Denali M=7.9 earthquake, Alaska, during which liquefaction occurred for several hundreds of kilometers along the Tanana River.

It is noticeable that delayed initiation or reactivation of landslide(s) after an earthquake can happen and is a direct consequence of the physical - geometric modification of the slope which changes the hydrologic conditions of the slope (Keefer, 2002). Furthermore, Lin et al. (2006, 2008a) pointed out that earthquakes can greatly disturb surface strata around their epicentral area, increasing the slopes' susceptibility. This, in turn, leads to significant

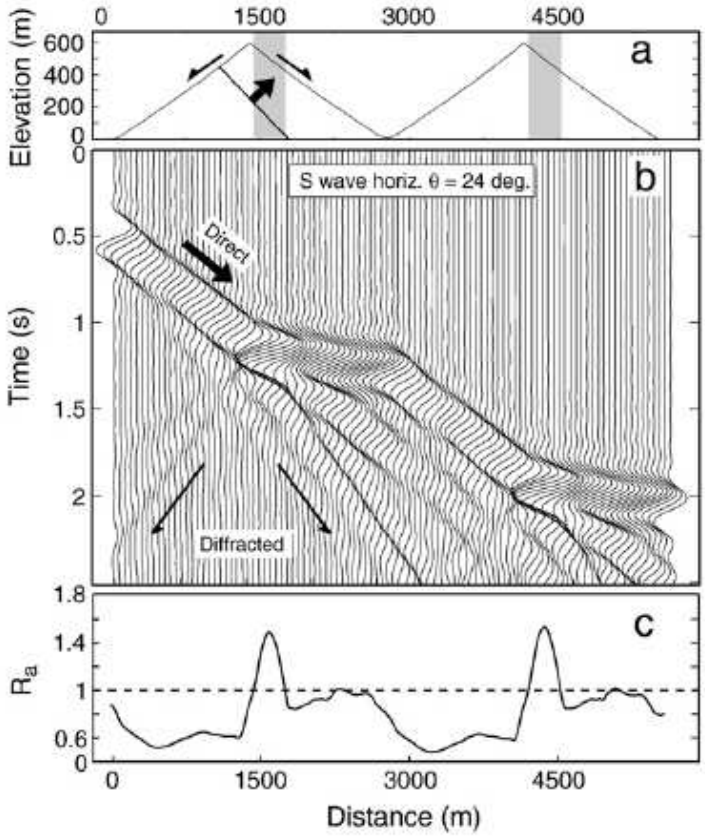

Figure 1.9: a) Topographic profile consisting of two adjacent mountain ridges. b) Synthetic accelerogram (ground acceleration recorded along the surface with time) generated along the topographic profile. This accelerogram is for the horizontal component of an S wave delta pulse (0-6 Hz) arriving from the left at an angle of 24° to the vertical. The associated PGA ratio R_a is shown in c). The direct wave interferes constructively with the diffracted wave generated at the ridge crest, causing amplification of the PGA on the ridge flank facing away from the wave source. From Meunier et al. (2008).

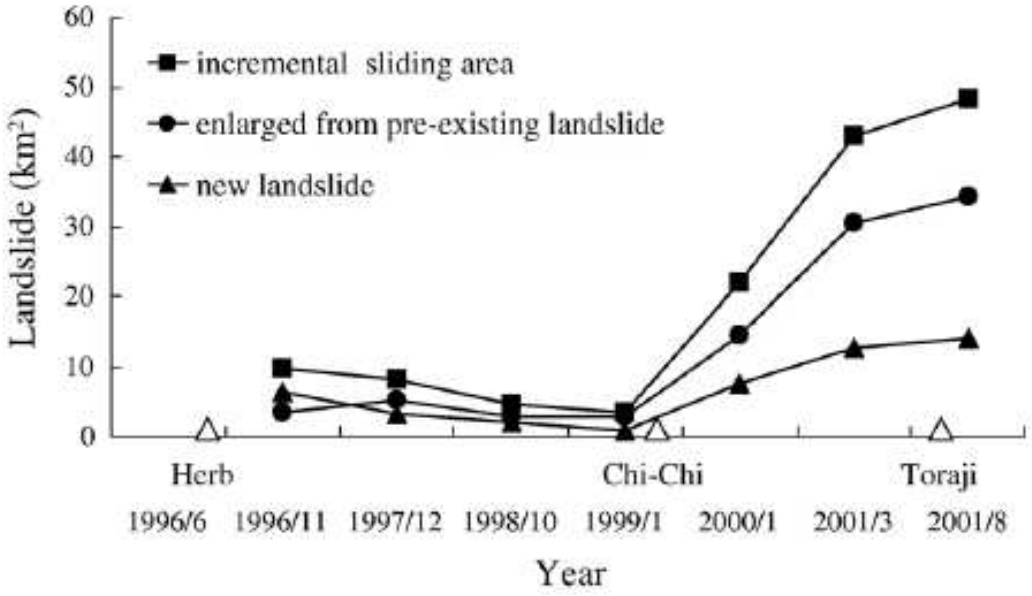

Figure 1.10: Plot of incremental sliding area (new landslides plus landslides enlarged from pre-existing ones) for 5 SPOT images taken before the Chi-Chi earthquake and 3 SPOT images taken after. The higher landsliding increment is due to the large slope disturbance caused by the Chi-Chi earthquake, as typhoon Herb (1996) brought more precipitation than typhoon Toraji (2001). From Lin et al. (2006).

increase in the density of rainfall-induced landslides in the following months to years (Fig. 1.10).

Chapter 2

Interaction among landslides, seismicity and climate in New Zealand

Submitted to Journal of Geophysical Research – Earth Surface.

Tatard, L., Grasso, J.R., Helmstetter, A., Dellow, G. and Garambois, S.

2.1 Abstract

Catastrophic landslides are reported worldwide to increase following heavy rain and nearby $M > 4 - 5$ earthquakes. To better quantify interactions between landslides and their triggers, we analyse the daily rate patterns of the 1996-2004 New Zealand landslide catalogue. The fluctuations of New Zealand landslide daily rates appear erratic and are much larger than the earthquake and rainfall rate fluctuations. The largest fluctuations in landslide daily rates correspond to four landslide crises for which the daily landsliding rates are 150 times larger than the averaged landsliding rate. Other than these four crises, we find that landslide occurrences in time are non-random. The distribution of the landslide waiting times follow a power-law for landslide waiting times longer than 9 days, suggesting

a correlation between landslide events. This time clustering of landslide occurrences is robust when tested against sub-catalogues selected on space, time, volume and dynamic criteria. For daily rates larger than 1 event/day a power-law distribution is also significant for the distribution of landslide daily rate values. For daily rates larger than 10 events/day the distribution tail displays a second trend, larger than the one expected from the power-law at smaller rates, where 10 events/day and more than 100 events/day rates belong to the same distribution. The time correlation is driven by neither the earthquake/landslide nor the landslide/landslide interactions. The climate/landslide interaction is considered the more likely cause of the observed correlations. The climate signal is the most visible one in the New Zealand landslide catalogue and drives (non-linearly) most New Zealand landsliding activity.

2.2 Introduction

Catastrophic failure of landslides increases following heavy rain (for references see De Vita et al., 1998) and large ($M > 4$) nearby earthquakes (for a review see Keefer, 2002). Other processes known to influence the slope stability are frost weathering processes (for a review see Matsuoka and Murton, 2008), snow melt episodes (e.g. Sandersen et al., 1996; Guzzetti et al., 2002), anthropomorphic works (e.g. Stark et al., 2005; Smyth and Royle, 2000), neo-tectonic stresses (e.g. Ai and Miao, 1987; Julian and Anthony, 1996) and deglaciation (e.g. Holm et al., 2004). Time-scales of these forcings range from a few seconds for seismic pulses to 10,000 years for deglaciation cycles. The influence of these perturbations on landslide development and triggering is not accurately known. For a better understanding of interactions between landslides and their potential triggers, we study the time and space patterns within the 1996-2004 New Zealand landslide catalogue. This database is one of the most detailed worldwide. New Zealand's geological and geographical setting has high seismicity rates and extreme rainfall events.

Previous studies on New Zealand landslides include i) case studies of single failed landslides (e.g. Wright, 1998; McSaveney, 2002; Hancox et al., 2005; Smith et al., 2006; Hancox,

2008; Cox and Allen, 2009) or ongoing landslides (e.g. Macfarlane, 2009); ii) a global conceptual study of landslide activity in New Zealand from 1970 to 2004 (Crozier, 2005), where New Zealand landsliding was characterised as multiple-occurrence landslide events mainly triggered by rainfall but also by earthquakes; iii) regional inventory studies, establishing large rock avalanche and landslide frequency (Whitehouse and Griffiths, 1983; Korup, 2005, respectively); iv) several studies performed using back analysis on a group of landslides and rock-falls, triggered either by heavy rainfall, $M > 4$ earthquakes and frost weathering processes. For rainfall triggering, the strategy (designed for real-time warning of rainfall-triggered landslides) is to extract, from daily rainfall records, empirical climatic thresholds above which at least one landslide occurs (Glade, 1998). Other studies use daily rainfall coupled to other parameters such as antecedent soil water conditions (Crozier, 1999; Glade, 2000), or antecedent soil water conditions and regolith hydrological behaviour and depth (Brooks et al., 2004), in order to understand and predict an increase in the probability of landslide occurrences. Two pieces of information emerge from these analyses. First, triggering thresholds are found to be variable in space and time (Glade, 1998; Glade, 2000; Brooks et al., 2002; Hufschmidt and Crozier, 2008). Second the rainfall-landslide interaction is complex and non-linear (Hufschmidt and Crozier, 2008). The results found for New Zealand landslides are in agreement with results found from rainfall-triggered landslide analyses worldwide, where empirical thresholds were established for both wet and dry soil conditions (e.g. Caine, 1980; Sidle and Ochiai, 2006).

For earthquake triggering, Hancox et al. (2002) studied 22 historical earthquakes from 1848 to 1995 and reported that the minimum magnitude for triggering landslides in New Zealand using this dataset is $M = 4.9$ and the minimum Modified Mercalli shaking intensity is MMI VI. For worldwide events, the magnitude threshold for which landslides are triggered is $M = 4$ (Keefer, 2002). Hancox et al. (2002) also established an empirical relationship linking the magnitude of the triggering event to the area affected by landslides. This area is generally smaller than the corresponding one estimated from worldwide data (Keefer, 2002).

For frost weathering processes, Hales and Roering (2005, 2007) found that the scree

deposits (corresponding to frequent, small magnitude - *i.e.* $< 100\ m^3$ - rock-fall events) in a 80 by 40 km transect in the Southern Alps of New Zealand were most influenced by altitude and not by lithology, seismicity or glaciation history. Nearly 70% of the scree deposits were found to be confined in the 1200-1600 m elevation range, just below the altitude corresponding to the frost-cracking window (-3 to -8° C) where ice segregation processes are most efficient. Other worldwide studies confirm the influence of frost weathering processes for triggering landslides (Matsuoka and Murton, 2008). Pirulli (in press) particularly brought to light the triggering effect of permafrost melting, in the context of global climate change, on the 18^{th} of September 2004, $3x10^6\ m^3$ Thurwieser rock avalanche, Italian Central Alps.

In this study we analyse a landslide catalogue containing 1943 landslides reported from throughout New Zealand during the period 1996 to 2004, in order to characterize New Zealand landslide occurrences in time and space and to study their relationship with landslide triggering processes. First, we describe the New Zealand catalogue. Second, we apply, for the first time on a landslide database, methods which have been successful in characterising the clustering of earthquake sequences, volcano eruptions and tsunami occurrences. We show that the distributions of the landslide waiting (*i.e.* inter-event) times and daily rates are both more clustered than random processes. The robustness of this clustering is tested by analysing sub-catalogues in space and time domains. Finally we study and discuss the processes that may drive the observed time clustering, such as landslide/landslide, earthquake/landslide and climate/landslide interactions.

2.3 Data and methods

2.3.1 The New Zealand 1996-2004 landslide catalogue

GNS Science Ltd has compiled a landslide catalogue (http://www.geonet.org.nz) of 2100 events for the 1996-2004 period. Data in the catalogue were obtained from a variety

of sources, such as media reports, aerial surveys and ground inspection. For each landslide, the available parameters include: date, location, type of material, type of movement, trigger mechanism, size, impact and references. Time accuracy varies from one day to one year, with a mean value of 1.77 ± 0.95 day for the whole catalogue. Landslide location accuracy ranges from a few metres for GPS-located landslides to a few kilometres for events remotely located using news reports, e.g. the distance to the nearest village. Volumes were roughly estimated from aerial photographs or from visual ground surveys, without any quantifying tool. Information on the trigger of a given landslide is provided for more than 90% of the landslides. The trigger mechanism relates to any nearby triggering event (intense rainfall, >M4 earthquake, etc), on the basis of a one to two days correlation in time with the landslide occurrence.

By imposing known location and time accuracy within two days, we extract 1943 landslides from the catalogue (Fig. 2.1a). Landslide volumes are given for 12% of the 1943 landslides, the largest event being $Vmax = 24 * 10^6\ m^3$. 98% of the 1943 landslide volumes are sorted in three volume classes (1 to 3) corresponding to 1) $V < 10^3\ m^3$, 2) $10^3 m^3 < V < 10^6\ m^3$ and 3) $V > 10^6\ m^3$. The 3 classes containing 1775, 118 and 26 landslides respectively. The material type and the landslide type are unknown for 58% and 91% of events, respectively. 65% of the landslides are reported as rainfall-triggered on 142 different days, 30% were earthquake-triggered on 4 different days, 7% had no reported trigger on 105 different days and 2% were triggered by other mechanisms (flooding, anthropic works, etc.) on 19 different days. In the first instance, we use all the 1943 landslides from the catalogue, independently of their reported trigger, for an overview of landslide behaviour in New Zealand. Then, we check how the *a priori* classification for triggered landslides may influence the results.

The landslide catalogue can be split into two different periods, before and after July 2001, for which the sampling methods and accuracies were different. July 2001 corresponds to the first use of more sensitive data sampling techniques which resulted in an increase of the average daily rate in the July 2001-2004 period compared to the 1996-June 2001 period.

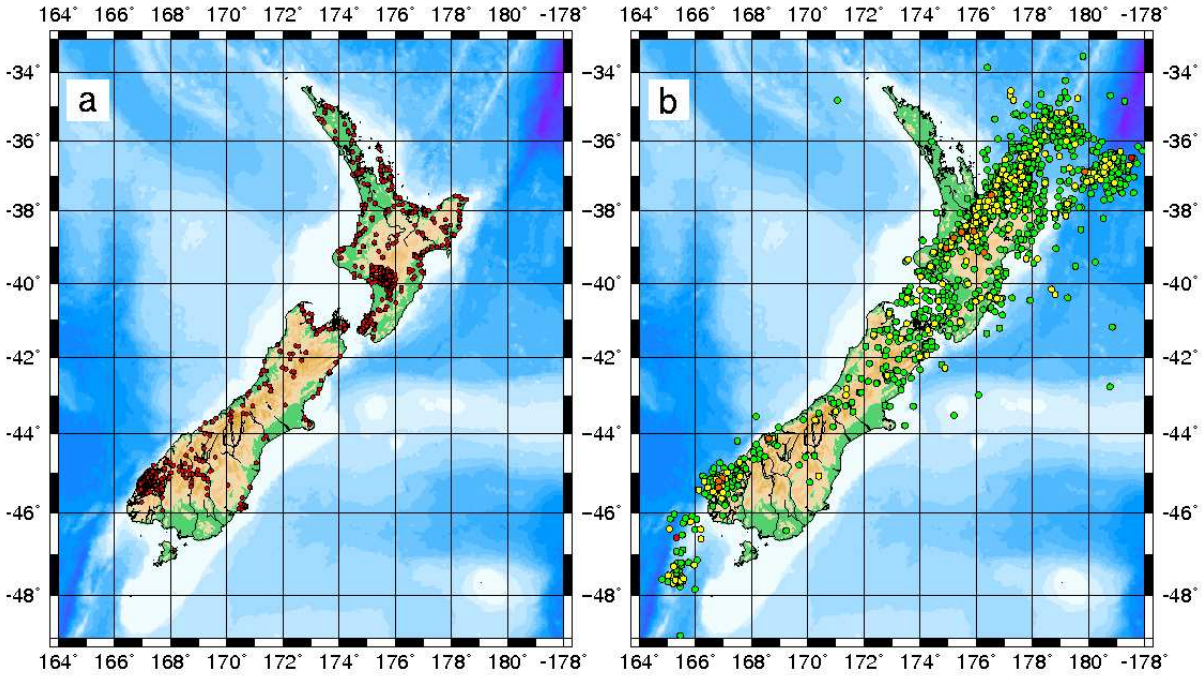

Figure 2.1: a) 1943 New Zealand landslides with known time and location which occurred in the 1996-2004 period, red dots. b) 1943 largest earthquakes, from 1996 to 2004 (green dots: $4 < M < 5$, yellow dots: $5 < M < 6$, orange dots: $6 < M < 7$, red dots: $M > 7$). Key for color shading on the map is elevation; ranging from green, 0 m elevation above sea level, to dark brown, 4000 m elevation a.s.l..

For this study, we analyse the 1943 New Zealand landslide catalogue and different sub-catalogues, to test the robustness of the results. The sub-catalogues were selected over i) space (North and South Island sub-catalogues), ii) time (1996 to June 2001 and July 2001 to 2004 sub-catalogues), iii) volume and iv) rate dynamics (binary sub-catalogue where the daily rate is set to 1 if at least one event occurred on that day or to 0 if no event was recorded on that day).

2.3.2 Methods

We test landslide time-series data in order to characterize any departure from randomness and the thresholds from which a given distribution emerges, if any. To accept or reject the null hypothesis of randomness *i.e.* independent events, we test the time and

volume data for exponential (*i.e.* the time distribution of random processes) or power-law distributions, which often emerge for natural processes.

To test and quantify for randomness, we use the reduced chi-square χ_r^2 test (e.g. Dussauge et al., 2003, for application to rock-fall volumes) and the η test (e.g. Marzocchi and Zaccarelli, 2006). The χ^2 value is a measure of the difference between the observed histogram and a histogram obtained by sampling the hypothesized distribution function (e.g. Press et al., 1992) and the χ_r^2 value is a normalised value of the χ^2 value (e.g. Dussauge et al., 2003). A $\chi_r^2 >> 1$ rejects the tested distribution as a possible description of the observed data. The $\eta = \sigma/\mu$ ratio, where μ and σ are the average and standard deviation of the inter-event times, respectively, allows us to characterize any clustering against random processes. For a Poisson process (*i.e.* random distribution) $\eta = 1$, while $\eta > 1$ characterizes statistical distributions more clustered than an exponential one, and $\eta < 1$ is typical for more "regular" time occurrences (see e.g. Marzocchi and Zaccarelli, 2006 for an application to volcano processes).

Power-law tests were performed using the Kolmogorov-Smirnoff (KS) test (e.g. Press et al., 1992) associated with the Maximum Likelihood Method (Aki, 1965) which allows an estimate of the exponent b of the power-law. The KS test consists of minimizing the distance between the empirical data and the synthetic power-law (e.g. Press et al., 1992).

Estimations of the power-law parameters and power-law goodness of fit are worked through using the algorithm proposed by Clauset et al. (2009) and are as follows: 1) setting series of lower cut-off and exponent b (via the Maximum Likelihood method) combinations of power-law models which describe the distribution; 2) selecting the combination giving the best power-law fit, using the Kolmogorov-Smirnoff statistic; 3) estimating the standard deviation of the lower cut-off and exponent b via a non-parametric bootstrap method. It consists in generating 2500 synthetic datasets with a similar distribution to the original one by randomly drawing a new sequence of points from the original data. Then, estimation of the best exponent b and lower cut-off pair for each of the 2500 datasets is performed. The

standard deviation of both the 2500 exponent b and lower cut-off values gives the standard deviation of the estimated parameters of the power-law describing the empirical data.

The validity of the power-law to describe the frequency-volume distribution is tested using a goodness-of-fit test. It consists of generating 2500 power-law distributed synthetic datasets with the exponent b and lower cut-off equal to those of the distribution that best fits the observed data. Then a fit of each synthetic dataset is performed and the KS statistics are computed for each synthetic distribution relative to its own model. The fraction of times where the resulting statistic is larger than the value obtained from the empirical data is the p-value. Following Clauset et al. (2009) we take $p > 0.1$ for the power-law to be accepted.

2.3.3 Landslide catalogue completeness

Catalogues for natural phenomena are always incomplete at the smallest event sizes. Due to the resolution of the measurement technique, not all events below a given size (V_0) can be recorded. V_0 depends on the space and time sampling accuracies, which are notably influenced by population distribution, official awareness of landslide hazard (e.g. Glade, 1998, Stark and Hovius, 2001, Dussauge et al., 2003, Malamud et al., 2004) and also on surface morphology (Guzzetti et al., 2002).

To estimate V_0, one usually measures the minimum volume for which the landslide volume distribution follows a power-law (e.g. Dussauge et al., 2003). For volumes smaller than V_0 there is a "roll-over" which is due to a lack of reporting of small events as discussed above. Following Clauset et al. (2009), we compute the probability p that the distribution follows a power-law with corresponding values of b exponent and lower cut-off V_0 (see section 2.3.2 above).

For the New Zealand landslide volume distribution, we found $V_0 = 45 \pm 2,700\ m^3$, $b = 1.36 \pm 0.06$ and p=0 (Table 2.1, Fig. 2.2); the power-law is therefore rejected. It is also rejected for the North and South Island sub-catalogues. It is accepted for the 1996-June

Table 2.1: Frequency volume distribution of landslides: power-law exponent b, lower cut-off V_0 and associated probability p that the distribution follow the best power-law fit. $p > 0.1$ - in bold in the Table - accepts the power-law as a possible description of the data.

Catalogue name	Number of landslides with known volume	b	V_0 (m^3)	p
New Zealand	245	1.36 ± 0.06	$45 \pm 2,700$	0
North Island	214	1.41 ± 0.07	$45 \pm 1,460$	0
South Island	31	1.25 ± 0.52	$80 \pm 34,000$	0.03
1996-June 2001	34	1.76 ± 0.68	$8,000 \pm 4,000$	**0.89**
July 2001-2004	211	1.36 ± 0.04	$150 \pm 1,407$	**0.26**

2001 and July 2001-2004 sub-catalogues, with $b = 1.76 \pm 0.68$, $V_0 = 8,000 \pm 4,000\ m^3$, and $b = 1.36 \pm 0.04$, $V_0 = 150 \pm 1,400\ m^3$, respectively (Table 2.1, Fig. 2.2). V_0 standard deviations show large variations, perhaps because less than 15% of the landslides from the catalogue were associated with a volume, which was generally roughly estimated. The exponent values of the volume distributions are of the same order of magnitude as the exponent values found for rock-fall volumes on sub-vertical cliffs (1.5 ± 0.2), and are smaller than the 2.2 ± 0.3 value reported for mixed landslide types (see references of Table 3 of Dussauge et al., 2003).

The power-law exponent of the New Zealand landslide volume distribution is equal to that of the July 2001-2004 sub-catalogue even though the power-law is rejected for the former catalogue. This result implies that the combination of two different power-laws (the ones from the 1996-June 2001 and July 2001-2004 sub-catalogues) does not necessarily result in a power-law. The acceptance of the power-law for the 1996-June 2001 and July 2001-2004 sub-catalogues emphasises the importance of the sampling method and accuracy for a coherent dataset. Therefore we add a last sub-catalogue on which we test the robustness of our results: the $V \geq 150\ m^3$, July 2001 to 2004 landslide sub-catalogue. This sub-catalogue is considered as complete for volumes larger than $150\ m^3$, over the July 2001-2004 period and also provide a subset catalogue independent of small landslides.

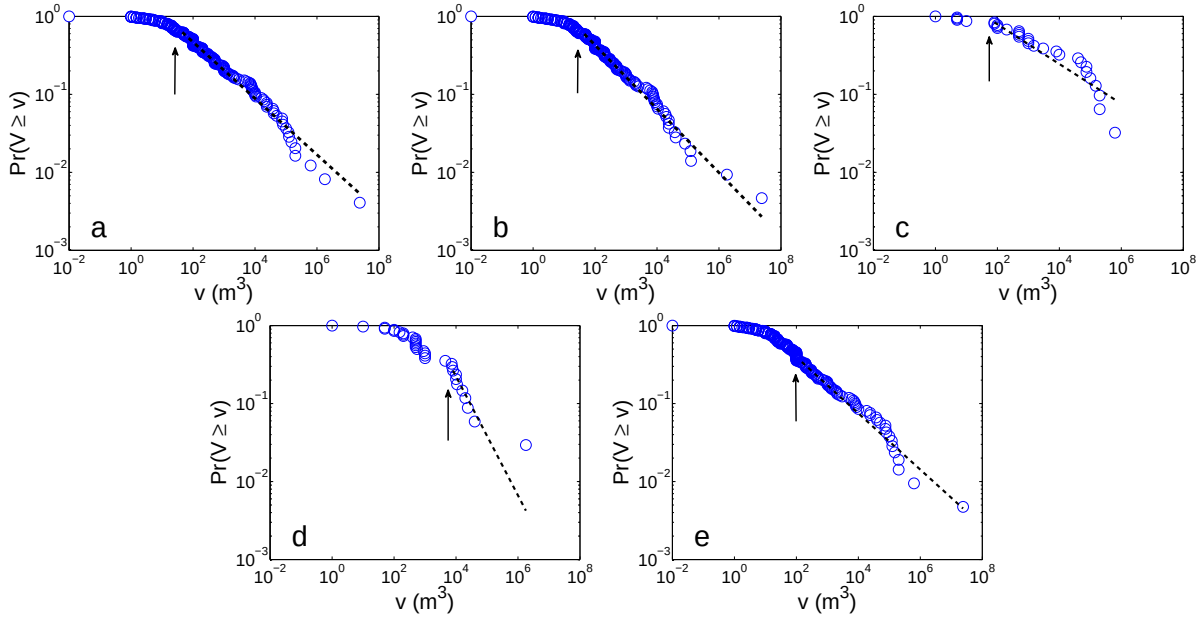

Figure 2.2: Cumulative distribution of volumes of New Zealand landslides (blue circles) and their best Kolmogorov-Smirnoff power-law fit (black dashed line). a) New Zealand landslides; b) New Zealand North Island landslides; c) New Zealand South Island lanslides; d) 1996-June 2001 landslides and e) July 2001-2004 landslides. Arrows indicate V_0. Values of exponents b and lower cut-offs V_0 are given in Table 2.1. Note that the exponent of the cumulative distribution (CDF) function is equal to $b-1$ (e.g. Bonnet et al., 2001).

2.3.4 Earthquake and weather catalogues

Shallow (less than 50 km deep) earthquake data are from the 1996-2004 GeoNet earthquake catalogue compiled and maintained by GNS Science Ltd, New Zealand. The magnitude of completude of the catalogue, $M_c = 3.0 \pm 0.03$, is estimated using the method of Ogata and Katsura (1993). We also use an earthquake catalogue as a counterpart to the landslide catalogue. To this end, we gathered the 1943 largest earthquakes - with $M = 4.3 - 7.1$ - from the complete catalogue, with a daily accuracy. Choices were made to prevent any biases due to scale, number of events or time accuracy effects when comparing the earthquake data to landslide data. Figure 2.1b gives the locations of the 1943 earthquakes.

The rainfall and temperature data for the 1996 to 2004 period are from the National Institute of Water and Atmospheric Research (NIWA), in New Zealand. They consist of i) New Zealand averaged rainfall depth per month ii) New Zealand averaged number of rain days per month iii) New Zealand averaged minimum and maximum temperatures per month. Since the data are New Zealand-averaged, only the global trend will be analysed. Figure 2.3a and b give the mean annual rainfall and temperature of New Zealand from 1971 to 2000, respectively. The North Island is globally warmer than the more mountainous South Island and its mean annual rainfall presents smaller minima and maxima and less spatial variability than the South Island. The South Island presents two different rainfall regimes: the West Coast is extremely wet with mean rainfall from 4,000 to 10,000 mm/year whereas the East Coast is drier with mean rainfall ranging from less than 500 to 1,250 mm/year. These different characteristics emphasise the use of two separate sub-catalogues for the North and the South Island and the need to pay special attention to the South Island when studying the climate - landslide interactions.

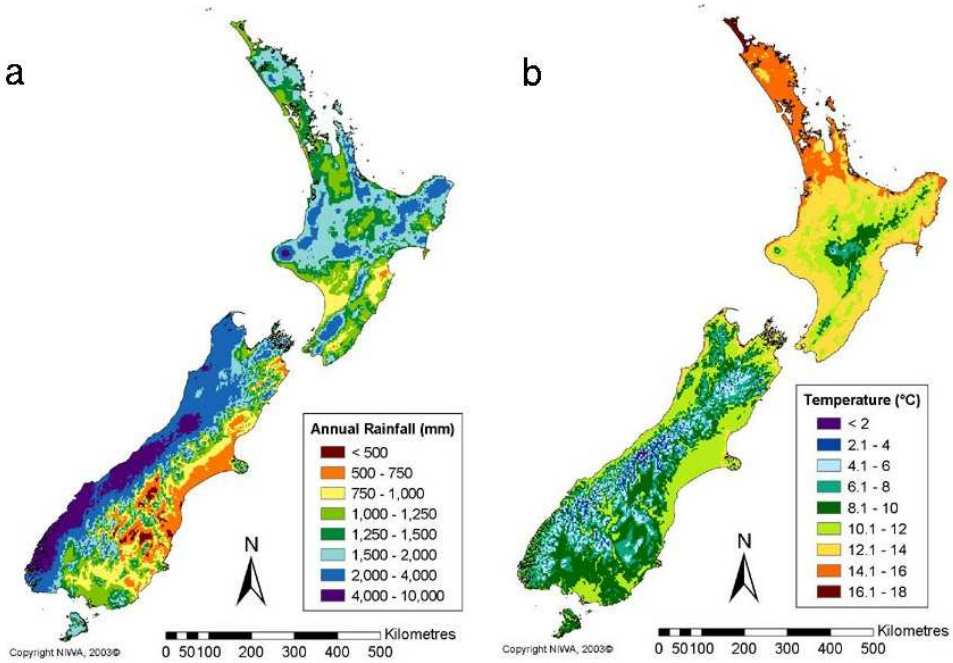

Figure 2.3: a) New Zealand mean annual rainfall in millimeters from 1971 to 2000 (image courtesy: NIWA). b) New Zealand mean annual temperature in Celsius degrees from 1971 to 2000 (image courtesy: NIWA).

2.4 Correlation between landslide occurrences

2.4.1 Landslide daily patterns

During the 1996-2004 period, the New Zealand landslide time series - or catalogue - (Fig. 2.4) shows 4 spikes in the daily landsliding rate that are more than 150 times larger than the mean landsliding rate ($\lambda \sim 0.63$ events/day) for this period. The four peaks in daily landsliding rates correspond to landslide clusters triggered by two rainfalls and two earthquakes ($M = 5.1, 7.0$). This pattern agrees with Crozier (2005) who reviewed the 1970-2004 New Zealand landslide patterns and found they are dominated by large daily occurrences of landslides, mostly triggered by rainstorms but also by earthquakes.

During the 1996-2004 period, the fluctuations in earthquake and rainfall rates are smaller than the fluctuations reported for landslide rates (see Fig. 2.4). The fluctuations in landslide rates are observed for both the North and South Island sub-catalogues (Fig. 2.4) and for the binary catalogue (Fig. 2.4). The change in rate after July 2001, corresponding to the change in landslide recording, can be seen in the 1943 events catalogue (Fig. 2.4) and the binary catalogue (Fig. 2.4).

Excluding the 4 event crises with daily landsliding rates 150 times larger than the background rate, we looked for any departure from randomness at lower rates. We used the reduced chi-square χ^2_r test (e.g. Dussauge et al., 2003) to test if the uniform distribution could be rejected, and to what degree, in the different datasets: the time series of the 1943 largest earthquakes, the $V \geq 150\ m^3$, July 2001-2004 landslides, the North and South Island landslides, the binary landslide catalogue, and the binary catalogues from 1996 to June 2001 and from July 2001 to 2004. The uniform distribution is rejected at a 100% confidence level for all the catalogues. A progressive decrease in χ^2_r value emerges when analysing the whole catalogue of landslides, the $V \geq 150\ m^3$ July 2001-2004 landslides, and the binary catalogues, respectively (Table 2.2). A deviation from the uniform time distribution is still detectable after excluding the crisis periods, *i.e.* by using the binary catalogue. It confirms that the correlated part of the landslides time series is not simply

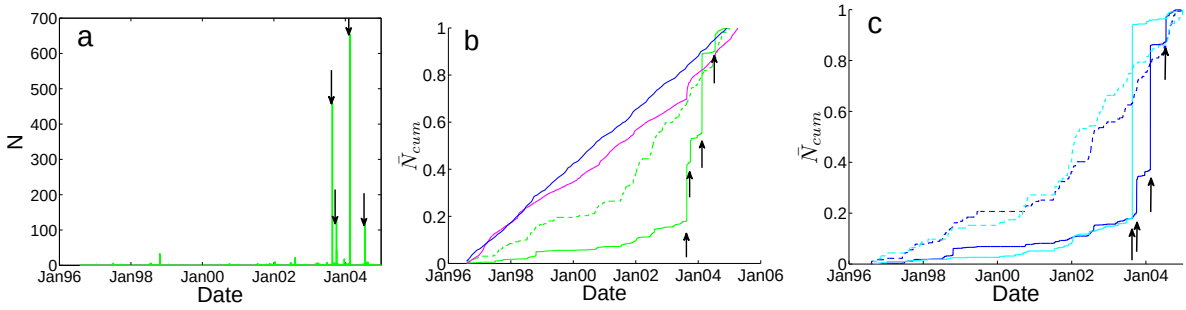

Figure 2.4: Time series of the New Zealand landslides a) discrete daily rate b) normalised, cumulative daily rate (green line), binary catalogue (green dashed line), New Zealand earthquakes (magenta line) and rainfall (blue line). c) normalised, cumulative daily rate for North Island (blue line) and its binary occurrence counterpart (blue dashed line), South Island landslides (cyan line) and its binary occurrence counterpart (cyan dashed line). Left to right, the first arrow corresponds to the M_L7 Fiordland earthquake, the second and the third arrows correspond to 2 rainfalls and the fourth arrow corresponds to the $M_L5.1$ Rotoehu earthquake.

driven by "one day" crises, *i.e.* the strong rainfall and earthquake forcings. For the binary catalogues, the landslide time distribution remains more clustered than its earthquake counterpart.

We further confirm the clustering in time by using the η test (see section 2.3.2). For all the landslide catalogues, we find $\eta >> 1$ and $\eta_{landslides} > \eta_{earthquakes}$ (Table 2.2). Landslide rates are more clustered than large earthquakes (known to be non-random, e.g. Utsu, 1961).

2.4.2 Distributions of landslide waiting (inter-event) times

The correlation observed between landslide occurrences using daily landsliding rates in the previous section, can be quantified by analysing the frequency distribution of the landslide inter-event times, *i.e.* the waiting time between two landslides. We use the binary catalogues, excluding dt=0 days waiting times, to quantify the correlation beyond the daily correlation. We use the method of Clauset et al. (2009) (detailed in section 2.3.2) to estimate the exponent b and the lower cut-off dt_0 of the most probable power-law as well as the probability p that the empirical data follow this most probable power-law (see

Table 2.2: Landslide rate distribution against uniform law: $\chi_r^2 >> 1$ or $\eta >> 1$ reject the uniform law as a good description of the data.

Catalogue	χ_r^2	η
New Zealand landslides	354	5.87
New Zealand $V \geq 150\ m^3$ July 01-04 landslides	15	2.92
New Zealand binary landslide	5.39	1.94
North Island landslides	360	7.26
North Island binary landslides	5.7	2.49
South Island landslides	354	4.75
South Island binary landslides	4.14	1.61
New Zealand binary 96-June 01 landslides	3.47	1.46
New Zealand binary July 01-04 landslides	3.67	1.47
1943 New Zealand largest earthquakes	55.32	1.44
1943 New Zealand binary largest earthquakes	1.89	0.90

Table 2.3 for values). This analysis shows that all binary catalogue and sub-catalogues accept the power-law hypothesis over one order of magnitude, with lower cut-offs dt_0 in the 9-38 days range (Fig. 2.5). The visual fits for the 1996-June 2001 and July 2001-2004 sub-catalogues are close to the exponential distribution although it is rejected (Table 2.2, note that these two catalogues are the ones associated with the lowest χ^2 and η values). Note that the lower cut-off values (37-38 days) for the two island sub-catalogues are larger than for the whole New Zealand catalogue (9 days) (Table 2.3). As seen in Table 2.3 it is not an artefact due to the number of events in each catalogue. This result suggests that the correlation between landslide occurrences, as seen by the power-law distribution of waiting times, is detectable for waiting times larger than 9 days only when considering landslides occurring on both islands. This result implies i) the mechanism(s) driving the correlation occur on both islands, despite their different weathering, geologic and tectonic settings and ii) there is a dependency on space for the time correlation.

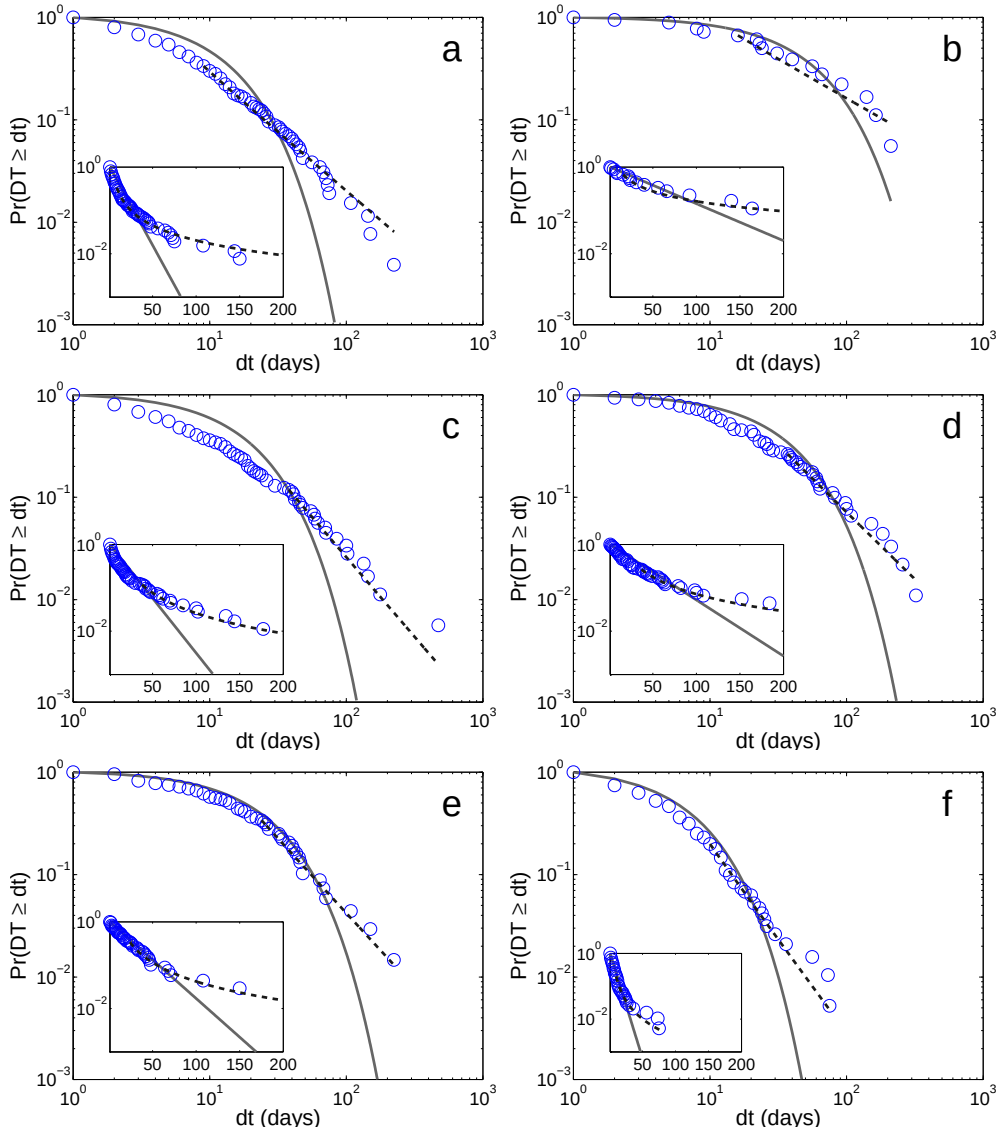

Figure 2.5: Cumulative distribution of the New Zealand landslide waiting times (blue circles) for the binary catalogue and sub-catalogues and their best Kolmogoroff-Smirnoff power-law fit (black dashed line). a) New Zealand landslide waiting times; b) $V \geq 150\ m^3$, July 2001-2004 landslide waiting times; c) North Island landslide waiting times; d) South Island landslide waiting times; e) 1996-June 2001 landslide waiting times; f) July 2001-2004 landslide waiting times. Grey line: exponential distribution. Values of exponents b and lower cut-offs dt_0 are given in Table 2.3. Note that the exponent of the cumulative distribution function (CDF) is equal to $b - 1$ (e.g. Bonnet et al., 2001). Insets: same in log linear axes.

Table 2.3: Distribution of landslide waiting times (for the binary catalogues): power-law exponent b, lower cut-off dt_0 and associated probability p that distribution of the landslide inter-event time follow the best power-law fit. $p > 0.1$ - in bold in the Table - accepts power-law as a possible description of the data.

Binary catalogue name	Number of days with at least one landslide	Exponent b	dt_0 (days)	p
New Zealand	261	2.14 ± 0.23	9 ± 5	**0.41**
New Zealand North Island	179	2.55 ± 0.29	38 ± 8	**0.90**
New Zealand South Island	92	2.30 ± 0.35	37 ± 13	**0.48**
New Zealand 1996-June 2001	69	2.44 ± 0.44	24 ± 8	**0.31**
New Zealand $V \geq 150\ m^3$ July 2001-2004	19	1.76 ± 0.39	16 ± 13	**0.54**
New Zealand July 2001-2004	192	2.81 ± 0.35	10 ± 3	**0.62**

2.4.3 Distribution of landslide daily rate

While the power-law distribution of waiting times between landslides argues for a correlation between landslide occurrences, the distribution of daily landsliding rates allows depiction of the intensity of the interaction between landslides. We therefore analyse the cumulative distribution function of the number of landslides per day for the whole New Zealand catalogue and all the sub-catalogues (Fig. 2.6). The New Zealand, New Zealand North Island, New Zealand 1996-June 2001 and New Zealand July 2001-2004 daily rates accept a power-law distribution (Table 2.4). The estimated lower cut-off is equal to 1 event/day in all four cases. For the New Zealand, New Zealand North Island and New Zealand July 2001-2004 catalogues, there is a change in slope for rates greater than 10 events per day: the frequencies of the empirical data are larger than that expected from the power-law, even though the power-law is accepted. The power-law acceptance for daily rates implies that the triggering of hundreds of landslides on the same day is not an extreme event but holds within the same distribution as the 10 events/day rate. Besides, the power-law distribution of daily rates confirms the correlated landslide time occurrences (see e.g. Kagan and Jackson, 1991 for the same analysis on earthquake rate).

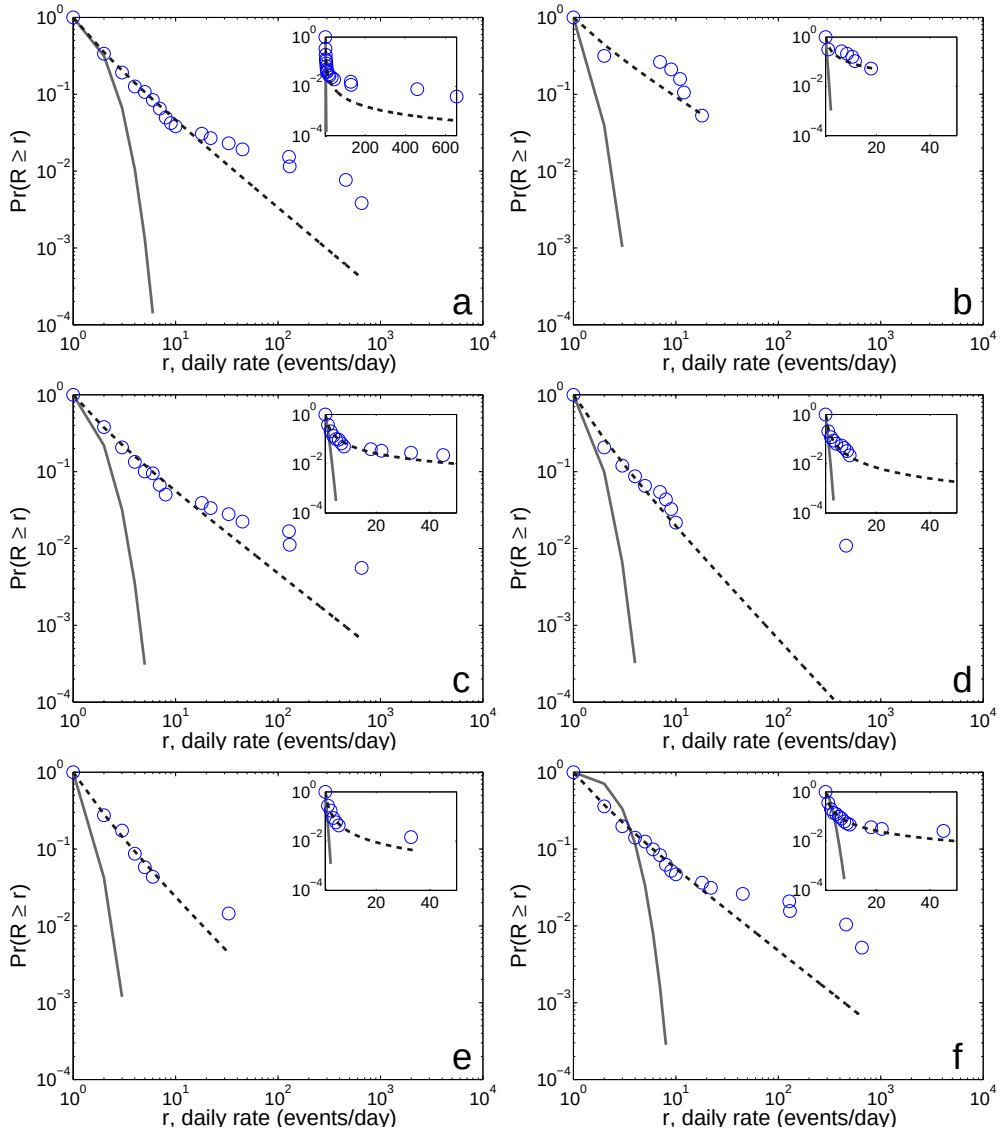

Figure 2.6: Cumulative distribution of New Zealand landslide daily rates (blue circles) for all catalogue and sub-catalogues, and their best Kolmogorov-Smirnoff power-law fit (black dashed line). a) New Zealand landslides; b) $V \geq 150\ m^3$, July 2001-2004 landslides; c) North Island landslides; d) South Island landslides; e) 1996-June 2001 landslides; f) July 2001-2004 landslides. Grey line: exponential distribution. Values of exponent b and lower cut-offs are given in Table 2.4. Note that i) the fit is slightly curved for daily rates lower than 6 events/day, which is inherent to the definition of a discrete power-law (e.g. Clauset et al., 2009) and ii) the exponent of the cumulative distribution function (CDF) is equal to $b - 1$ (e.g. Bonnet et al., 2001). Insets: same in log linear axes.

Table 2.4: Daily rate distributions of New Zealand landslides: power-law exponent b, lower cut-off and associated probability p that the distributions follow the best power-law fit. $p > 0.1$ - in bold in the Table - accepts power-law as a possible description of the data.

Catalogue name	Number of landslides	Exponent of PL b	Lower cut-off	p
New Zealand	1943	2.12 ± 0.09	1	**0.74**
New Zealand $V \geq 150$ m^3 July 2001-2004	72	1.86 ± 0.5	1 ± 2	0.03
New Zealand North Island	1339	2.05 ± 0.11	1	**0.53**
New Zealand South Island	604	2.46 ± 0.24	1	0.03
New Zealand 1996-June 2001	140	2.37 ± 0.21	1	**0.51**
New Zealand July 2001-2004	1803	2.05 ± 0.09	1	**0.42**

2.5 Possible processes for landslide clustering in time

2.5.1 Earthquake-landslide interaction

The New Zealand landslide catalogue reports earthquake-triggered landslides without unequivocal documentation of the relationship between the time of the earthquake and the triggered landslide. Because of the time delay (24 hours to a few days) between the main-shock occurrence and the landslide reconnaissance, landslides are reported as triggered by the main-shock, and the possible effects of aftershocks are not considered. This kind of analysis implicitly focuses on the deterministic aspect of earthquake triggering for landslides, *i.e.* the large $M > 5-6$ shocks. We analyse the possible effect of small $M < 5$ earthquakes on landslide triggering, with the aim of increasing the signal-to-noise ratio by stacking time series of landslides relatively to the earthquake time. To that end, we use the entire New Zealand earthquake catalogue (http://www.geonet.org.nz) from 1996 to 2004, with depths less than 50 km. We condition the time on each earthquake occurrence time t_0 and stack time series of landslides relative to the earthquake time. Because of the larger number of small-magnitude shocks, the signal is dominated by the small-magnitude earthquakes. Fol-

lowing Lemarchand and Grasso (2007), who applied the technique on earthquake-volcano interactions, we normalise the distance Δ between landslide and earthquake by the earthquake fault length size L using the Wells and Coppersmith (1994) relationship between L and the magnitude.

For the 1943 New Zealand landslides two peaks of occurrences at t=0 and t=1 day are found, with a maximum signal to noise ratio obtained for $\Delta/L < 1$ (Fig. 2.7). This result indicates a correlation between earthquakes and landslides. The landslide signal at t=0 and t=1 day correspond to landslides triggered by four earthquakes (Table 2.5) ranging from M_L=4.1 to M_L=7.0. The landslides were reported on the day and the day after the main-shock occurrence.

We apply the same technique to the binary catalogue and to the *a priori* unknown-trigger landslide catalogue. The latter catalogue includes the landslides for which there were no associated triggers in the database. In addition, applying the test to this catalogue allows us to test the effect of small-magnitude earthquakes, which possibly triggered some landslides, but were not *a priori* identified as such, owing to their low ($M < 4$) magnitude. For the binary catalogue, landslide signal at t=0 is only due to the 4 earthquakes already known as landslide triggering earthquakes whereas no signal is found at t=0 for the unknown trigger landslides.

From this study, it can be inferred that earthquakes in New Zealand between 1996 and 2004 triggered landslides only on the four different days mentioned in Table 2.5. Landslides occurring on those four days were *a priori* labelled as earthquake-triggered in the New Zealand landslide catalogue. The influence of $\Delta/L < 10$, $M < 4$ earthquakes on landsliding seems to be weak if any. The four days on which earthquake-triggered landslides occurred are more than 400 days apart. Accordingly they cannot drive the observed non-randomness for landslide inter-event times longer than 9 days observed in figure 2.5. The landslide daily rates for earthquake-triggered events range from a few hundred events to one. They match the power-law that describes the New Zealand daily rate distribution, the larger rates (relative to the background rate) and are not outliers from the distribution.

Table 2.5: The 4 landslide triggering earthquakes. M_w magnitudes are from the Harvard catalogue and M_l magnitude is from the New Zealand (GNS) catalogue.

Reported date of landslide(s)	Area	Magnitude	Number of reported landslides	Min-max quake-slide distances
November, 1^{st} 2000	Thomson Sound	M_W=6.1	1	∼15 km
February, 2^{nd} 2002	Haast area	M_L=4.1	1	∼4 km
July, 18^{th} 2004	Lake Rotoehu	M_W=5.4	127	1 - 10 km
August, 22^{nd} 2003	Fiordland	M_W=7.2	459	15 - 200 km

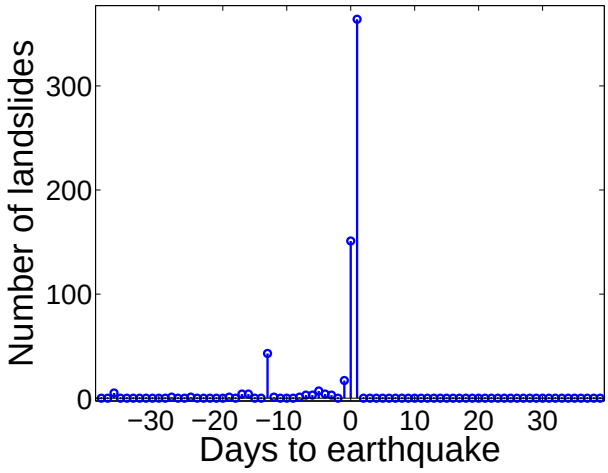

Figure 2.7: Stacked time series of landslides relative to earthquake time for the New Zealand landslide catalogue. The best signal to noise ratio is obtained for $\Delta/L < 1$.

2.5.2 Landslide-landslide interaction

To analyse the possible impact of landslide-landslide interactions on the waiting times and daily rates of New Zealand landslides, we analyse the distribution of the inter-event distances as a function of the inter-event time. A landslide may trigger another landslide by 1) changing the stresses and the geometry of the slope or 2) by generating a seismic wave (e.g. the V=$11.8 \pm 2.4 * 10^6$ m^3 Mount Cook (New Zealand) rock-fall of December, 14^{th} 1991, was equivalent to a $M_L = 3.9$ tectonic earthquake, McSaveney, 2002). For landslides occurring on the same day, we find that more than 75% of the inter-event distances are smaller than 100 kilometres (Fig. 2.8). There is no means to discriminate whether the landslides were triggered by the primary trigger or by an adjacent landslide. We then analysed the distribution of the inter-event distances (between all events) for inter-event times less than 30 days for the entire catalogue and the binary catalogue (Fig. 2.9). For the latter catalogue, landslides happening on the same day are conceptualized as a single event, whose coordinates are the coordinates of the barycenter of the landslides occurring on this day. We find a positive correlation for the New Zealand catalogue at dt=0 and dt=1 day, up to 200 km distances, but the large number of landslides occurring on the same day (1682 events out of 1943) may skew the signal at dt=1. We find no correlation at dt=1 for the binary catalogue, but the coordinates of the barycenter are only partially representative of the landslides which occurred on the same day since the mean distances between all these landslides varies from 0 to 600 km (Fig. 2.8). Therefore the interaction of landslides at dt=1 day cannot be resolved with this catalogue. The seismic wave generated by any rock-fall is reported in the national seismicity catalogue used in section 2.5.1, and we show in the previous section that $M < 4$ seismic signal had no effect on 1996-2004 New Zealand landsliding. We conclude that no landslide - landslide interaction is evidenced in the 1996-2004 period. More precise landslide timing is necessary in order to study landslide - landslide interaction.

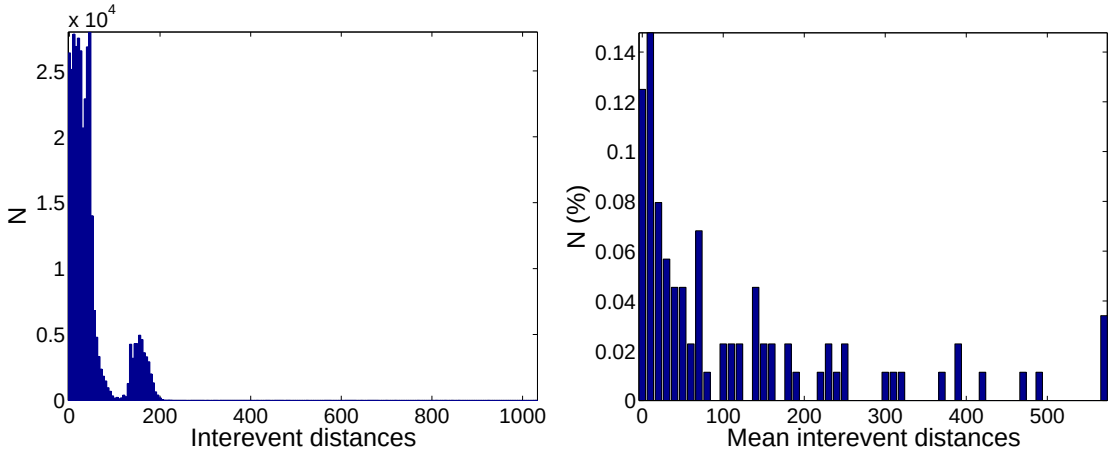

Figure 2.8: Histograms of inter-event distances between landslides, for landslides occurring on the same day (dt=0). a) histogram of all inter-event distances between every landslide; b) histogram of the mean inter-event distance between every landslide. There are 88 days with more than one landslide per day.

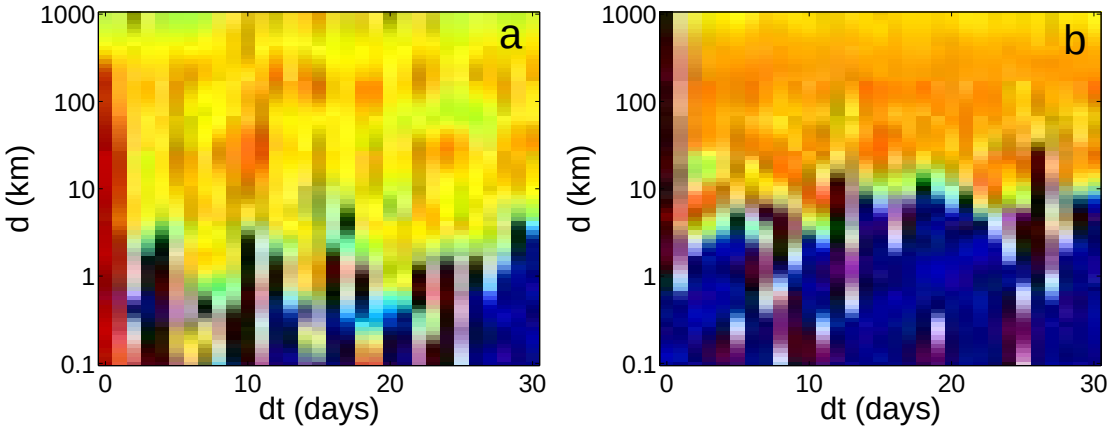

Figure 2.9: Probability Density Function (PDF) of the inter-event distances, for each inter-event time. a) for the New Zealand landslide catalogue b) for the binary catalogue, where landslides occurring on the same day are conceptualized by a single landslide, whose coordinates are relative to the barycenter of all landslides occurring on this day. The PDFs were computed using a log binning and then convolved with a Gaussian kernel, e.g. Izenman (1991) and normalised by the maximum number of events. For each inter-event time dt, color scale varies from blue, no event, to dark red, maximum of events for the considered inter-event time.

2.5.3 Climate-landslide interaction

The last process investigated as a possible basis for the observed correlation in landslide time series is the climate-landslide interaction. Figures 2.10 and 2.11 plot weather variables averaged over all of New Zealand (monthly rainfall, monthly number of rain days, monthly minimum and maximum temperatures) against the number of landslides per month. We quantify any possible correlation using the linear correlation coefficient r (e.g. Press et al., 1992) between the monthly landslide rate and the weather variables. The r value theoretically ranges between -1 and 1, inclusive, with r=1 for perfectly correlated datasets and r=-1 for perfectly anti-correlated datasets. We find a better correlation when using the binary number of landslides rather than the total number of landslides. r is equal to 0.29, 0.37, -0.26 and -0.30 for the correlation between the monthly binary landslide rate and the monthly rainfall depth, the monthly number of rain days, the minimum temperatures and the maximum temperatures, respectively. All correlations are significant *i.e.* the probability of getting a correlation as large as the computed value by random chance, when true correlation is zero, is less then 0.01%.

We then test seasonal patterns by analysing the different variables stacked per month, over the 9 years of the 1996-2004 catalogue. The binary landslide rate is highest from June to October and reaches a maximum in July (Fig. 2.12a). The rainfall depth and the number of rainy days both reach a maximum in October (Fig. 2.12a), with a wetter period from May to December. Monthly landslide rate and rainfall rate both present their maxima during the same season although there is no simple linear correlation between the two. Temperatures reach a minimum in July and the minima are lower than 5° C from May to September (Fig. 2.12b). This also coincides with the maximum of activity of New Zealand landslides.

The binary rainfall-triggered landslide rate reaches a maximum in September, which is one month before the maximum of rainfall in New Zealand. The binary unknown-trigger landslide rate reaches a maximum in July (Fig. 2.13a) and behaves globally in a manner similar to the rainfall-triggered landslides. This implies that rainfall has an influence on

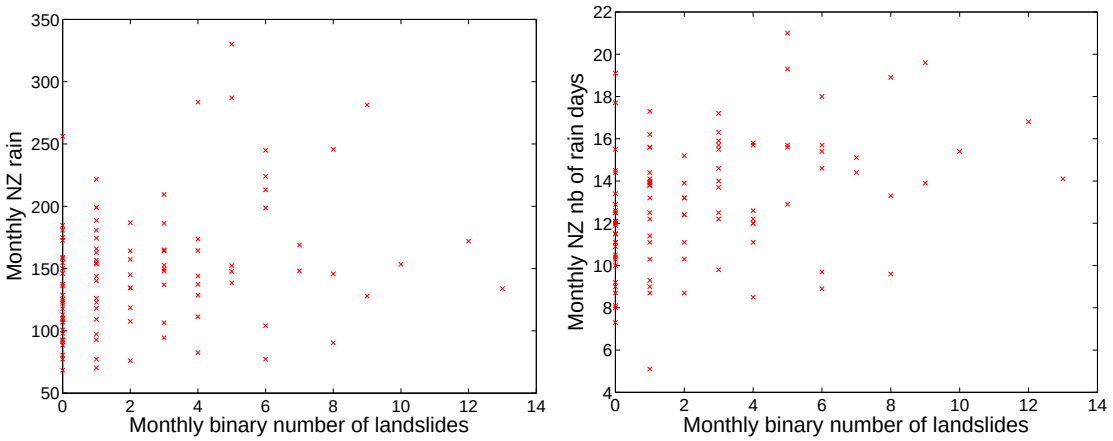

Figure 2.10: a) Monthly number of landslides from the binary catalogue versus the New Zealand, monthly averaged rainfall depth (coefficient of correlation r=0.29). b) same with the New Zealand, monthly averaged number of rain days (r=0.37).

the landslides whose triggers were not reported.

The North and South island binary landslide rates present similar behaviours including maxima in July and August, respectively (Fig. 2.13b).

2.5.4 Discussion

The relative fluctuations of the New Zealand landslide rate in the 1996-2004 period appear larger than those estimated for earthquake and rainfall rates, respectively. It suggests a stronger volatility for landslides than for earthquake and rainfall events, implying complex climate-landslide and earthquake-landslide interactions, as suggested by Hufschmidt and Crozier (2008).

A change in the landslide rate before and after July 2001, is apparent in both the 1943 events catalogue and the binary catalogue (Fig. 2.4). The estimated average rates increase from 0.08 landslides/day (0.04 "at least one landslide"/day) during the 1996-June 2001 period to 1.41 landslides/day (0.15 "at least one landslide"/day), during the July 2001-2004 period. We tested for any increase in rainfall, temperature or $M > 4$ seismicity after July 2001 which could account for the landslide rate increase as well. We find no increase of rainfall, a 7% decrease of the lowest temperatures and a 22% increase in $M > 4$ seismicity.

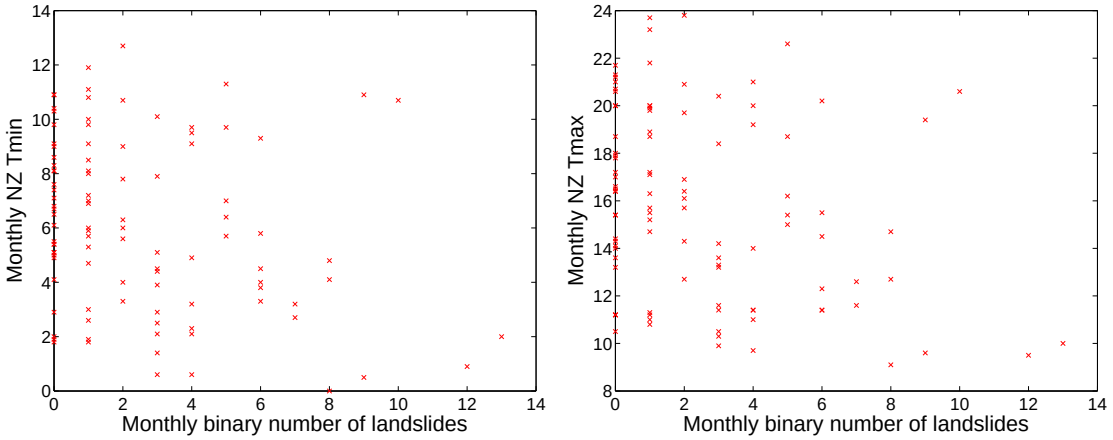

Figure 2.11: a) Monthly number of landslides from the binary catalogue versus the New Zealand, monthly averaged lowest temperatures (coefficient of correlation r=-0.26. b) same with the New Zealand, monthly averaged highest temperatures (r=-0.30).

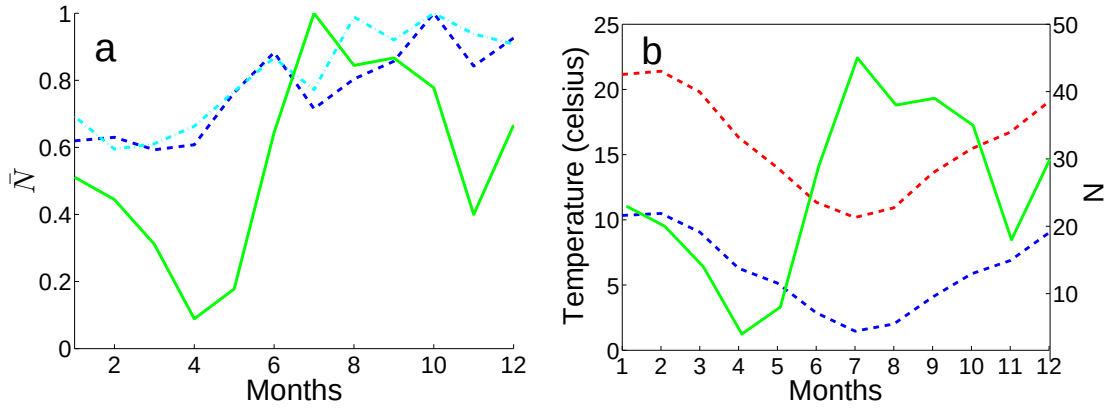

Figure 2.12: Monthly landslide rate and weather variables. a) Normalised number of landslides, from the binary catalogue (green line), normalised, New Zealand averaged, rainfall depth (blue dashed line) and normalised, New Zealand averaged, number of rain days (cyan dash dot line). b) Number of landslides, from the binary catalogue (green line), New Zealand averaged maximum temperature (red dashed line) and New Zealand averaged minimum temperature (blue dashed line).

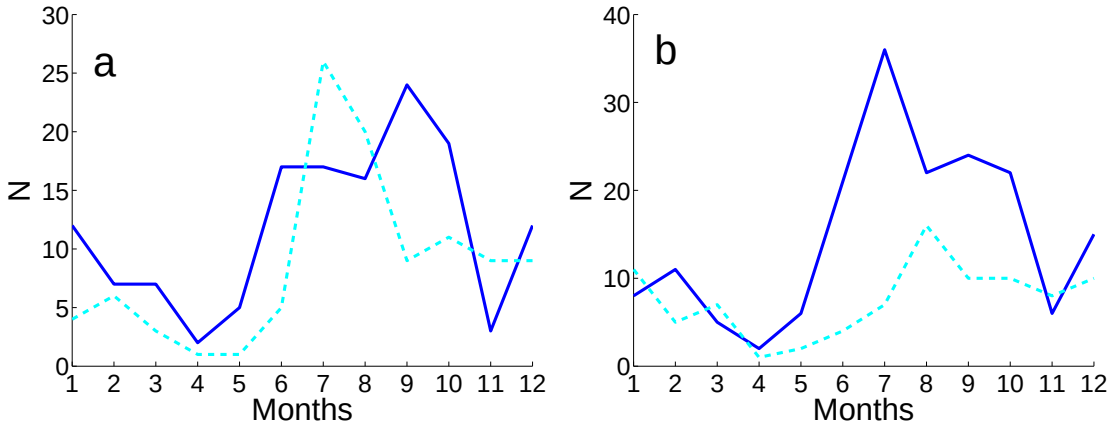

Figure 2.13: a) Number of rainfall-triggered (blue line) and unreported trigger (cyan dashed line) landslides per month, with a maximum of one event per day. b) North (blue line) and South Island (cyan dashed line) landslides per month, with a maximum of one event per day.

The July 2001 rate change also corresponds to an improvement in the methodologies used to compile the New Zealand landslide catalogue. The two environmental factors (temperature decrease and increased seismicity) could potentially increase landslide triggering. However the improvement in data collection post-July 2001 precludes attributing the July 2001 change in landsliding rate to these environmental forcings.

Four landslide crises (multiple-landslide events), with landsliding rates more than 150 times the ~ 0.63 averaged background rate, occurred during the 1996-2004 period. These crises correspond to landslide clusters triggered by two rainstorms and two earthquakes ($M_L = 5.1$ & 7.0). Excluding these four crises, we found that the landslide occurrences still remain non-random. The coefficient of variation (Table 2.2) quantifies the correlation between landslide occurrences and this is found to be as least as strong as the corresponding one between earthquakes. Further, we have shown that the uniform distribution is rejected as a good description for all the distributions of landslide waiting times (New Zealand catalogue and sub-catalogues) whereas a power-law distribution is accepted to fit the observations (Table 2.3). The best power-law fit, for landslide waiting times for the whole New Zealand catalogue, exhibits an exponent equal to 2.14 ± 0.23 with a waiting time cut-off dt_0 equal to 9 ± 5 days. The waiting time cut-offs for the North and South

Island catalogues are larger than 35 days, suggesting that the correlation is dependent on the size of the studied area. The correlation may be volume-dependent as the $V \geq 150\ m^3$ July 2001 - 2004 sub-catalogue presents a correlation between its landslide waiting times, having a lower cut-off equal to 16 days whereas that of the July 2001 - 2004 sub-catalogue is equal to 10 days. The question of randomness over short time-scales (less than 9 days) remains open. The lack of correlation below 10 days may be caused by either the low time accuracies of the landslide catalogue or by overlaps in time of sequences of triggered events independent in space (see e.g. Touati et al., 2009 for an application on earthquake aftershock sequences).

Distributions of daily landslide rates are not random and accept a power-law for rates larger than 1 event/day for the New Zealand, New Zealand North Island, New Zealand 1996-June 2001 and July 2001-2004 catalogues. Daily landslide rates with more than 10 events per day have frequencies that are larger than expected from the power-law distribution although they still hold within the same distribution. These results imply that the large crises with several hundred of landslides per day are not outliers in the rate distribution but remain in the same tail as the "smaller" crises. It raises questions about whether these daily rate distributions are driven by either the susceptibility of the upper crust to forcing or alternatively the forcing intensities themselves.

We tested the landslide - earthquake, landslide - landslide and climate - landslide interactions because they are potential candidate causes for the time correlation between landslide occurrences and the power-law distributed daily landslide rate.

For the 1996-2004 New Zealand catalogue, the landslide - earthquake interactions do not build correlations beyond the one-day waiting time since only four earthquakes triggered landslides in New Zealand during this period, and those earthquakes occurred more than 400 days apart. Since only a single landslide survey is performed after an earthquake, it is not yet possible to determine if aftershocks also trigger landslides. The effect of $M < 4$ earthquakes on landsliding in New Zealand is negligible, if present at all. This result is in agreement with the literature where few effects of $M < 4$ earthquakes on landsliding have been demonstrated. In his review of landslides triggered by earthquakes,

Keefer (2002) found no landslide triggered by $M < 4$ earthquakes. Miller (1931) found a correlation between the acceleration of a creeping landslide in California and what is called a "slight" earthquake. Del Gaudio et al. (2000), after studying the effect of a $M < 3.6$ earthquake sequence which happened simultaneously with a landslide in Italy, were not able to establish the role of the seismic action in triggering this mass movement. Last, we found that a M_L=4.1 earthquake triggered a landslide on February 2, 2002, in the Haast area, New Zealand, which decreases to M=4.1 the previous M=4.9 threshold suggested by Hancox et al. (2002).

No landslide - landslide interactions were demonstrated to cause correlation in the 1996-2004 New Zealand catalogue. If some correlations are found between landslides occurring on the same day, the catalogue is not precise enough to discriminate whether the correlation is linked to the trigger or to the landslide - landslide interaction. For inter-event time equal to one day the correlation is not resolved because of several biases of the data and method. For further study of the landslide - landslide interaction, as well as the earthquake - landslide interaction, more precise landslide occurrence times are needed.

The landslide - climate interaction is the last possible candidate for the observed correlation in the 10-100 days range. We found correlations between landslide activity and monthly rainfall depth, number of rain days per month and mean monthly temperature. The strongest correlation is found between landslide activity and the number of rain days per month. This reinforces the role of antecedent soil moisture content on landsliding, which confirms the results of Crozier (1999). We also found that the landslide rate is larger during winter time (Fig. 2.12) with the highest landslide occurrences in July. This is correlated with the lowest temperatures, having a minimum in July, and the wettest months, having a maximum in October. The role of rainfall, increasing pore pressure, and temperature, through frost weathering processes are well documented in the literature (see Sidle and Ochiai, 2006 and Matsuoka and Murton, 2008 for reviews, respectively). Nevertheless, Matsuoka and Murton (2008) stated that rock-falls prevailed during seasonal thawing *i.e.* spring, which is not the case for New Zealand. Moreover, altitudes of individual landslides are needed to test the hypothesis of Hales and Roering (2005, 2007)

who correlated altitude of landsliding with the efficiency of ice segregation processes. We suggest another mechanism linked to low temperatures and rainfall which can have an influence on landslide triggering: the reduction of evapotranspiration leading to wetter slopes that are more prone to landslides.

The binary rainfall-triggered landslide rate reaches a maximum in September, which is one month before the maximum of rainfall in New Zealand. Landslide activity also decreases after October whereas rainfall remains high until December. These differences can be explained either by the "event resistance phenomenon", which postulates that the first rainfalls remove the susceptible ground, leaving a stronger more stable residual surface (Crozier, 2005) which therefore will not fail later in the year. Alternatively there is a shift of time occurrences of the localised extreme events, which are the events that are most efficient in triggering landslides (see for example Pasuto and Silvano, 1998), compared to the averaged New Zealand precipitation. Better rainfall and landslide catalogues are needed to confirm or refute this suggestion.

Landslides with an unknown trigger (*a priori* classified 7% landslides from New Zealand catalogue and 35% from binary catalogue) share the same seasonal trend (*i.e.* a higher rate in winter) as the rainfall-triggered landslides (*a priori* classified 65% of landslides from New Zealand catalogue and 50% from binary catalogue), as indicated by Fig. 2.13. This suggests a rainfall control on those unknown trigger landslides and enhances rainfall as the primary mechanism driving landslide activity in New Zealand.

The North and South island binary landslide rates present similar monthly behaviours, including landslide rate maxima in July and August, respectively (Fig. 2.13b). Nevertheless, North Island landsliding is more rainfall-driven than the South Island landsliding. One third of the South Island (the West Coast) receives more than one and a half times the rainfall of the North Island, but the North Island has three times as many rainfall-triggered landslides (normalised by aerial extent) as the West Coast of the South Island. This extends the space variability of the rainfall triggering thresholds from a regional scale, as pointed out by Glade (1998, 2000) to a larger scale (the two islands).

Two candidates are proposed for driving the difference in landslide responses to rainfall

between the two islands. The first explanation may be a difference in geology. The geology of the West Coast of the South Island (with a relatively low rainfall-triggered landslide rate) is mainly schist, granite (strong rocks) in the mountains, with minor Tertiary age sediments (weak rocks). The geology of the North Island hill country (with a relatively high rainfall triggered landslide rate) is dominated by Tertiary age sediments (weak rocks) with minor greywacke and volcanic rocks (strong rock). Geomorphologically, this corresponds to steeper slopes for the West Coast of the South Island than those of the North Island. The second explanation may be a difference in rainfall regime. The West Coast has very high precipitation all year long ($\sim$200 mm per month) whereas over the North Island the wetter season lasts $\sim$6 months. We suggest that not only is the forcing important on the triggering of landslides but also how the forcing is applied. A continuous forcing, like intense rainfall on the West Coast of the South Island, is less effective. In this case it suggests the landscape is in equilibrium with the weather. A discontinuous forcing, *i.e.* heavy rainfall for only six months in the North Island, and its alternation with a dryer season could be responsible for the greater weakening of slopes leading to shorter landslide cycles. One of the possible implications is that the time interval between successive landslides at the same site is on average shorter in the North Island than it is on the West Coast of the South Island.

Nevertheless, this difference in behaviour still needs to be confirmed, as alternative hypotheses to the two outlined previously are also possible. For example, the influence of anthropic factors varies between the two islands. It is possible that the influence of rainfall may be greater on the North Island because of the greater deforestation that has taken place and/or the better observation opportunity in the North Island, which is more densely inhabited than the South Island.

We observed a correlation of landslide waiting times for waiting times longer than 9 days and we reviewed the possible mechanisms to drive such a correlation between landslides. Note that the lack of power-law correlation below nine days may be caused by the low time accuracies of landslide occurrences. This latter induces randomness in the landslide waiting times. It may suggest that the *a priori* 2-day estimate time accuracy of the New Zealand

landslide occurrences could be closer to 10 days. Another possibility is the randomness induced by overlapping in time of sequences of landslides which occurred independently in space. This process was modelled by Touati et al. (2009) to reproduce a decrease in correlation for aftershock sequences.

First, both landslides and rainfall are correlated in time, possibly by cyclonic weather system transit times across New Zealand. Second, there might be a delay between rainfall and landsliding for some landslides. As a possible mechanism, circulating fluids can catalyze sudden failure, as stated by Kilburn and Petley (2003) after revisiting the deep-seated landslide of Vajont, North Italy. Keefer (2002) also stated that a change in groundwater regime, caused by co-seismic tectonic deformation, can lead to delayed initiation and reactivation of landslides. We suggest that a change in groundwater regime following rainfall could also lead to a delayed effect of the rainfall on slope stability. These two examples explain the observation that landslides with an unknown trigger occurred predominantly during the wettest months but were not reported as rainfall triggered since there was no consistent 1-2 days delay between rainfall occurrences and the occurrence of landslides with an unknown reported trigger. Last we suggest an increase in susceptibility of the slopes from June to October, due to an increase of pore-water pressure and a decrease in temperature. Slopes are therefore more prone to landsliding, independent of the trigger. For example, Dellow and Hancox (2006) show that the M_L=5.1 Lake Rotoehu earthquake of July 18, 2004, triggered numerous landslides and suggest that this was because it had rained in the days immediately prior to the earthquake. An earlier earthquake (Edgecumbe earthquake of March, 2^{nd} 1987; $M_s = 6.6$) produced similar shaking intensities in the same area around Lakes Rotoehu and Rotoma but did not trigger any landslides. Dellow and Hancox (2006) attribute the difference observed between the landslide densities near Lakes Rotoehu and Rotoma, after the two earthquakes to the difference in rainfall totals immediately prior to the earthquake (*c.f.* 10-day rainfall totals at nearby sites in the range 3-10 mm for the 1987 Edgecumbe earthquake versus 3-day rainfall totals at the same rainfall gauges in the range of 223-312 mm). Similar cases were reported worldwide by Keefer (2002).

2.5.5 Conclusion

The daily landslide rates in New Zealand attest to the large volatility of landslide occurrences. Fluctuations of landslide rates during the 1996-2004 period are larger than those for earthquake and rainfall rates. This demonstrates the efficiency of external forcings, *i.e.* earthquakes and rainfalls, in triggering landslides in New Zealand, compared to the long term gravity loading.

Excluding the four crises with more than 150 times the average background landslide rate, triggered by 2 rainstorms and 2 earthquakes, analyses of waiting times and daily rate distributions argue for a correlation between landslide events. Power-law behaviour is accepted as a good description for these distributions, with cut-offs equal to 9 days for the waiting time distribution and 1 event per day for the daily rate distribution. When using the North and South Island sub-catalogues, the waiting time cut-off appears to be dependent on the space scale of the catalogue. Daily landslide rates with more than 10 events per day have frequencies that are larger than expected from the power-law which emerges for the smaller rates.

Within the daily accuracy of the landslide catalogue we do not resolve any evidence for the time correlation to be driven by either earthquake/landslide or landslide/landslide interactions. The significant correlation in time between rainfall depth, daily rate of rainy days and landslide rate, suggests the correlation between landslide occurrences to be driven by climate-landslide interactions, for most of the New Zealand landslide catalogue.

Chapter 3

Characterization and comparison of landslide dynamics in different tectonic and climatic settings

Submitted to Journal of Geophysical Research – Earth Surface.

Tatard, L., Grasso, J.R., Helmstetter, A. and Garambois, S.

3.1 Abstract

We aim to identify and characterize landslide triggering patterns in time, space and rate, using six global landslide inventories: 2001 - 2004 New Zealand, 1980-2004 Yosemite cliffs (California, USA), 1982 - 2005 Grenoble cliffs (Isère, French Alps), 1954 - 1975 Val d'Arly cliffs (Haute-Savoie, French Alps), 1996 - 2007 Australia and 1988 - 2000 Wollongong (New South Wales, Australia) landslide catalogues. Landslides are resolved as correlated in time for all catalogues. The New Zealand, Yosemite, Australia and Wollongong landslide daily rates are well fitted by a power law for rates between 1 and 1000 events per day: there is no characteristic scale for daily rate values. This result suggests that the same mechanism(s) are driving both the large landslide daily crises and the single events. We

then constrain the space pattern of the landslide crises and propose some minimum length scales corresponding to a measure of the combined effect of the trigger intensity and of the slope susceptibility. We show that earthquakes trigger landslides for the New Zealand, Yosemite and Australia areas to distances up to ten times the ruptured fault length. The influence of $M < 4$ earthquakes on landsliding is found to be weak, if present at all, for all catalogues. We find that the New Zealand, Val d'Arly, Australia and Wollongong landslide monthly rates correlate with both the monthly rainfall depth and the monthly number of rainy days. The New Zealand and Grenoble landslide monthly rates are anti-correlated to monthly temperatures. The Yosemite landslides display no correlation to any of the monthly weather variables.

The joint analysis of the six catalogues permits us to derive parameters that describe the relative landslide dynamics of each of the six areas. Landslide dynamics include here both the slope susceptibilities and the applied forcings for a given area. From the most re-active landslide area (New Zealand) to the least re-active area (Grenoble), the global trends of the different parameters are: i) decreasing departure from randomness; ii) decreasing maximum daily rates and area over which the trigger operates; iii) decreasing landslide triggering for landslides occurring one day apart; iv) decreasing global interaction to earthquake, rainfall and temperature.

3.2 Introduction

Our study focuses on the behaviour in time and space of landslides in different tectonic, climatic and weathering conditions. The term "landslide" used in this study denotes all mass movement characterized by an episode of movement between quiet periods. For the two main landslide triggers - heavy rainfall and large nearby earthquakes - most past studies confirmed the existence of thresholds above which landslides were triggered. For rainfall-triggered landslides, Sidle and Ochiai (2006, modified from Caine, 1980) and Crozier (1999) found empirical relationships between the amount of rainfall and landsliding, depending on the antecedent water status of the soil. Glade (1998) established thresholds, ranging from

120 mm to 300 mm of daily rainfall, for which there is a probability of 100% to trigger a landslide in 3 parts of the North Island of New Zealand. Rainfall-triggered landslide analyses show first that the parameters/thresholds are variable in space, depending on the susceptibility of a given landscape (existing physical conditions) to landslide-triggering rainfall (Glade, 2000; Brooks et al., 2004). Second, the parameters/thresholds for triggering seem to be variable in time, depending on the rainfall duration (Guzzetti et al., 2007) and dependent on the geomorphological stage of the slope (Brooks et al., 2002; Hufschmidt and Crozier, 2008). All these studies emphasise the complexity of the rainfall - landslide interactions (Hufschmidt and Crozier, 2008).

Sandersen et al. (1996) studied the seasonal occurrence of landslides in Norway and found that the yearly distribution of rock falls exhibits two maxima, one in early spring and one in late autumn. Both periods coincide with frequent fluctuations of temperature around the freezing point. The first maximum also coincides with the time of highest rate of snowmelt, while the second one coincides with the months of largest rainfall. Gruner (2008) and Frayssines and Hantz (2006) noticed an increase of rockfall events in the Alps during spring times, which underlines the influence of meteorological conditions such as frequent freeze-thaw cycles and snowmelt.

From a review of worldwide case studies of earthquake triggered landslides, Keefer (1984, 2002) reported that the minimum magnitude of a triggering earthquake was 4, and that the area A affected by landslides increases with magnitude M was $Log_{10}A = M - c$ with $c = 3.46 \pm 0.47$, with $A = 0\ km^2$ for $M \sim 4$ to $A = 500,000\ km^2$ for $M = 9.2$. The effect of low $M < 5$ magnitude earthquakes on landsliding has been less reported and studied than the effect of $M > 5$ magnitude earthquakes. Miller (1931) first stated that a "slight" earthquake was followed by a notable acceleration of the Point Firmin creeping landslide (California), lasting about two months. Del Gaudio et al. (2000) studied the influence of a low magnitude (maximum $M_L = 3.6$) earthquake sequence on a nearby (less than 20 km away) landslide in Vadoncello (Southern Italy). They found that it was dubious whether the seismic accelerations generated within the landslide were sufficient to activate mass movements and whether the effect of repeated shocks on hydrogeological conditions

could explain the time delay observed between seismic and landslide accelerations. Sassa et al. (2007) argued that the $M_s = 2.6$ earthquake which occurred on the same day as the 22 km distant Leyte landslide (Philippines), was the cause of the landslide failure, which also occurred five days after a heavy rainfall. Walter and Joswig (2008) suggested that local (10 km distant) earthquakes of $M_L > 2.0$ may have caused stress relief within the sliding body and triggered fracture initiation and/or growth within the Heumoes slope, Voralberg Alps, Austria.

In the present study, we use the time series of landsliding occurrences in different tectonic and climatic settings to better understand landslide triggering. We analyse landslides from New Zealand, 2001-2004 period; Yosemite (California, USA), 1980-2004; Chartreuse-Vercors cliffs (French Alps), 1982-2005; Val d'Arly cliffs (French Alps), 1954-1975; Australia, 1996-2007 and Wollongong (New South Wales, Australia), 1988-1999. After a description of the characteristics of these databases, we analyse the time, daily rate and space patterns of landsliding in these six areas. We then quantify the possible interactions between landslides and i) landslides, ii) earthquakes and iii) climate for the six databases. Finally, we use these results to compare the relative landslide susceptibility and reactivity as deduced from the six studied areas.

3.3 Databases

3.3.1 Landslide databases

We extract six landslide catalogues from six heterogeneous databases: in time, they range from nine years to more than one hundred years, while in space, they range from a ten kilometres roadcut to thousands of square kilometres (Table 3.1). The six databases are the following: 1996 - 2004 New Zealand; 1857 - 2004 100 km-long Yosemite cliffs (California, USA); 1890 - 2005 100 km-long Chartreuse and Vercors cliffs in the vicinity of Grenoble (Isère, French Alps); 1948 - 2000 16 km-long Val d'Arly cliffs (Haute-Savoie, French Alps); 1842 - 2007 Australia database and 1890 - 2004 50 km long Illawarra escarpment in the

vicinity of Wollongong (New South Wales, Australia). Figure 3.1 illustrates the temporal evolution of the landslide rates and compares them with rainfall and with seismicity in each area. In order to remove the influence of the largest crisis of landslide activity, we introduce the "binary catalogue", which is defined as all days for which one or more events have occurred. The binary rate is either equal to 1 (at least one event in the catalogue for this day) or 0 (see Fig. 3.1). The location of an event in the binary catalogue is defined as the barycenter of all events that occurred during that day.

Four possible candidates causes for the observed long-term fluctuations of daily rates are: i) changes in data collection, e.g. in July 2001 for the New Zealand database (Tatard et al., Submitted) and in 1988 for the Wollongong database (Flentje et al., 2007); ii) changes in the forcing intensities, e.g. an accentuation of rainfall from 1988 to 1992 for the Wollongong database (Flentje et al., 2007); iii) changes in the slope susceptibilities via natural processes, e.g. an increase of the landsliding rate over a five years period after the Chi-Chi earthquake (Lin et al., 2008b) or a decrease in the rate of rainfall-triggered landslides in New Zealand after the 1970s peak of rainfall-triggered landslides (Hufschmidt and Crozier, 2008); iv) changes in the slope susceptibilities due to anthropogenic processes, e.g. stabilization works in 1976 for the Val d'Arly database (Dussauge et al., 2002), deforestation (Brooks et al., 2002) and intensive urbanization (Smyth and Royle, 2000).

The Yosemite, Grenoble and Australia databases display significant rate fluctuations, which cannot be related to any particular phenomenon. It appears difficult to distinguish anthropogenic signals from natural ones due to the lack of available information on the anthropogenic biases in the compiled databases (evolution of the database recording techniques, evolution of land-use and of human actions on the studied area). As the rainfall and seismicity rates are relatively constant in time for all databases (Fig. 3.1), it is more probable that the unidentified major changes observed in long term (at least several years) landsliding rates are due to anthropogenic causes. For this reason, five out of the six catalogues were restricted to the more recent period, for which the most roughly constant binary landslide rates are observed (Table 3.2). These periods are July 2001 - 2004 for New Zealand, 1980-2004 for Yosemite, 1982 - 2005 for Grenoble, 1996 - 2007 for Australia

and 1988 - 2000 for Wollongong. For the Val d'Arly catalogue the 1954 - 1975 time period was chosen as stabilization works took place on the site after 1976.

The reduced landslide databases were further sub-sampled in order to keep only landslides presenting a date known to within 2 days' accuracy and a known location (Table 3.2, Fig. 3.3). Other available information for landslides in the databases includes volume (13% of the database events for New Zealand, 32% for Yosemite, 35% for Grenoble, 74% for Val d'Arly, 9% for Australia) and reported trigger (for New Zealand, Yosemite, Australia and Wollongong). The trigger mechanism relates to any nearby triggering event (intense rainfall, >M4 earthquake), on the basis of a one to two days correlation in time with the landslide occurrence.

Table 3.2 summarizes possible parameters that can be used to compare landslide dynamics such as mean landslide daily rate, landslide density (number of landslides per year and per square kilometre) and maximum erosion (maximum volume of landslide per year and per square kilometre). All these values must be treated with caution since they were not corrected from their catalogue resolution. Indeed, volume estimates for most catalogues are too inaccurate (Table 3.1).

3.3.2 Earthquake databases and tectonic settings

Earthquake data are extracted from national catalogues (Table 3.3). Their magnitudes of completude, estimated using the Ogata and Katsura (1993) method, range from 1.9 to 3.0 (Table 3.3). The earthquake data represent different tectonic settings. Local seismicity was defined as seismicity located within the area covered by landslide catalogue for New Zealand and Australia and, for other catalogues, as seismicity located within a 5x5 degrees square centered on the landsliding zone. New Zealand presents the strongest seismicity rate with on average 1 local $M \geq 7$ earthquake every year and 100 $M \geq 5$ earthquakes/year. It is followed by the Yosemite Park with on average 2 regional $M \geq 5$ earthquakes per year (albeit the local seismicity in the Yosemite Park is weak, compared to the strong seismogenic California). Due to intraplate tectonics, Australia experiences 3 local $M \geq 5$

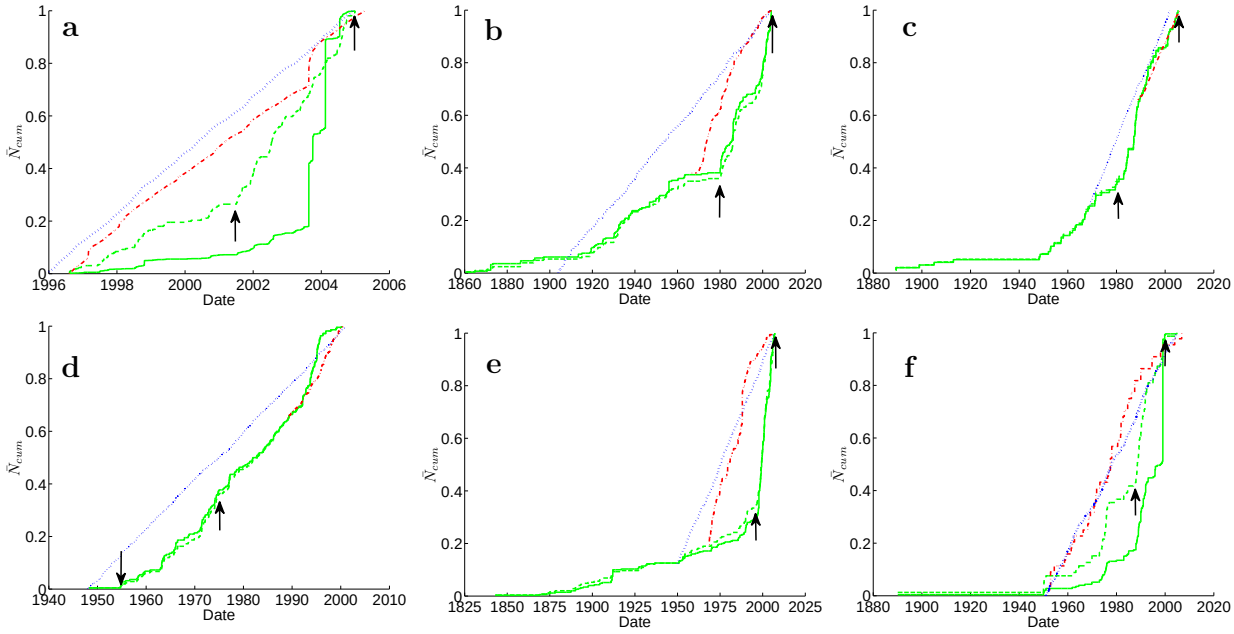

Figure 3.1: Normalised daily landslide rate, rainfall rate and earthquake rate for the 6 databases: Entire (green line) and binary (green dashed line) landslide time series; rainfall (blue dot line) and local seismicity (red dot line). a) New Zealand; b) Yosemite; c) Grenoble; d) Val d'Arly; e) Australia; f) Wollongong. Arrows indicate beginning and end of the catalogues extracted for this study.

Table 3.1: *Landslide databases.*

	New Zealand[a]	Yosemite[b]	Grenoble[c]	Val d'Arly[d]	Australia[e]	Wollongong[f]
Date	1996-2004	1857-2004	1890-2005	1948-2000	1842-2007	1890-2004
Nevent	2100	519	144	221	965	487
Surface (km^2)	270,000	3000	3700	16	7,700,000	550
Geology	hetero-geneous	granite	limestone	micashist	hetero-geneous	sandstone, mudstone
Type of movement	hetero-geneous	rockfalls, rockslides	rockfalls	rockfalls	hetero-geneous	hetero-geneous
Elevation (m)	0-3800	1000-2300	250-1600	1000-1200	0-2200	300-500
Landslide with volume (%)	13	32	35	74	9	no data

[a]Database online at http://www.geonet.org.nz, characteristics of database from Tatard et al., Submitted.

[b]Database online at http://pubs.usgs.gov/of/2003/of03-491/, characteristics of database from Dussauge et al., 2003.

[c]Characteristics of database from Dussauge et al., 2003.

[d]Characteristics of database from Dussauge et al., 2002.

[e]Database online at http://www.ga.gov, characteristics of database from Michael-Leiba et al., 1997.

[f]Database online at http://www.ga.gov, characteristics of database from Flentje and Chowdhury, 2005; Flentje et al., 2007.

Table 3.2: *Selected landslide catalogues.*

	New Zealand	Yosemite	Grenoble	Val d'Arly	Australia	Wollongong
Date	July 2001-2004	1980-2004	1982-2005	1954-1975	1996-2007	1988-1999
N (events)	1788	172	63	83	247	207
$\langle N \rangle$ (event/day)	1.4	2×10^{-2}	0.8×10^{-2}	1×10^{-2}	5.6×10^{-2}	44×10^{-2}
Density (event/yr/km^2)	1.9×10^{-3}	2.3×10^{-3}	7.0×10^{-4}	2.4×10^{-1}	2.7×10^{-6}	2.9×10^{-2}
V_{max} (m^3)	2.4×10^{7}	6×10^{5}	2×10^{4}	4×10^{3}	2×10^{3}	no data
Maximum erosion rate[a] ($m^3/yr/km^2$)	22	8	2.3×10^{-1}	11	2.7×10^{-5}	no data

[a]The maximum erosion rate is equal to the landslide maximum volume V_{max} divided by the number of years of the catalogue duration, divided by the spatial extent of the catalogue.

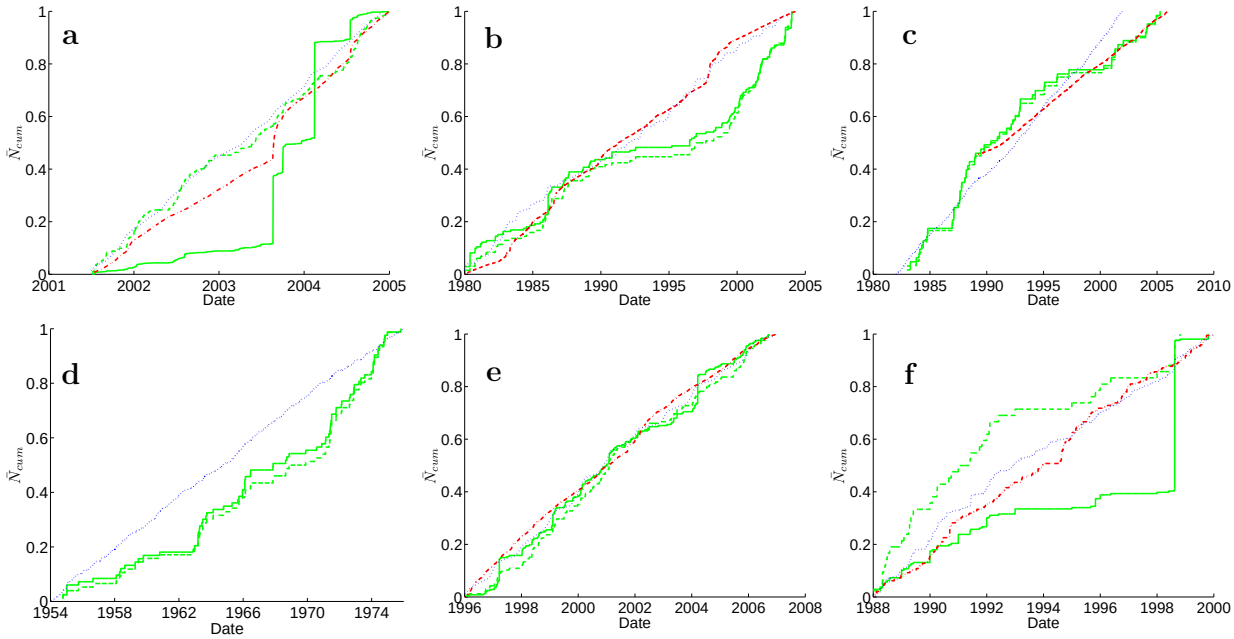

Figure 3.2: Normalised daily landslide rate, rainfall rate and earthquake rate for the 6 catalogues: Entire (green line) and binary (green dashed line) landslide time series; rainfall (blue dot line) and local seismicity (red dot line). a) New Zealand; b) Yosemite; c) Grenoble; d) Val d'Arly (no local seismicity data available); e) Australia; f) Wollongong.

earthquakes per year and Wollongong area 0.14 regional $M \geq 5$ earthquake per year. The French Alps experiences 0.05 $M \geq 5$ earthquake per year and 1 regional $M \geq 4$ earthquake every 2 years. Figure 3.5 presents seismicity maps compiled over the analysed time periods, with $M > 4$ earthquakes for New Zealand and Australia and $M > 3$ earthquakes for Yosemite, Grenoble, Val d'Arly and Wollongong.

The contemporary tectonic uplift rate is the highest for New Zealand, ranging from 1 to 10 mm per year (Fitzsimons and Veit, 2001). The South Island uplift is mainly localized along the Southern Alps whereas the uplift in the North Island appears more diffuse, spreading and partitioning along dozens of major faults. The second highest uplift rate is found for the French Alps with 1 to 2 mm of uplift per year (Fitzsimons and Veit, 2001). The Sierra Nevada block, of which Yosemite is part has uplift less than 1 mm/yr (Dixon et al., 2000). Finally, there is no contemporary uplift in Australia and in Wollongong (Miner et al., 2008).

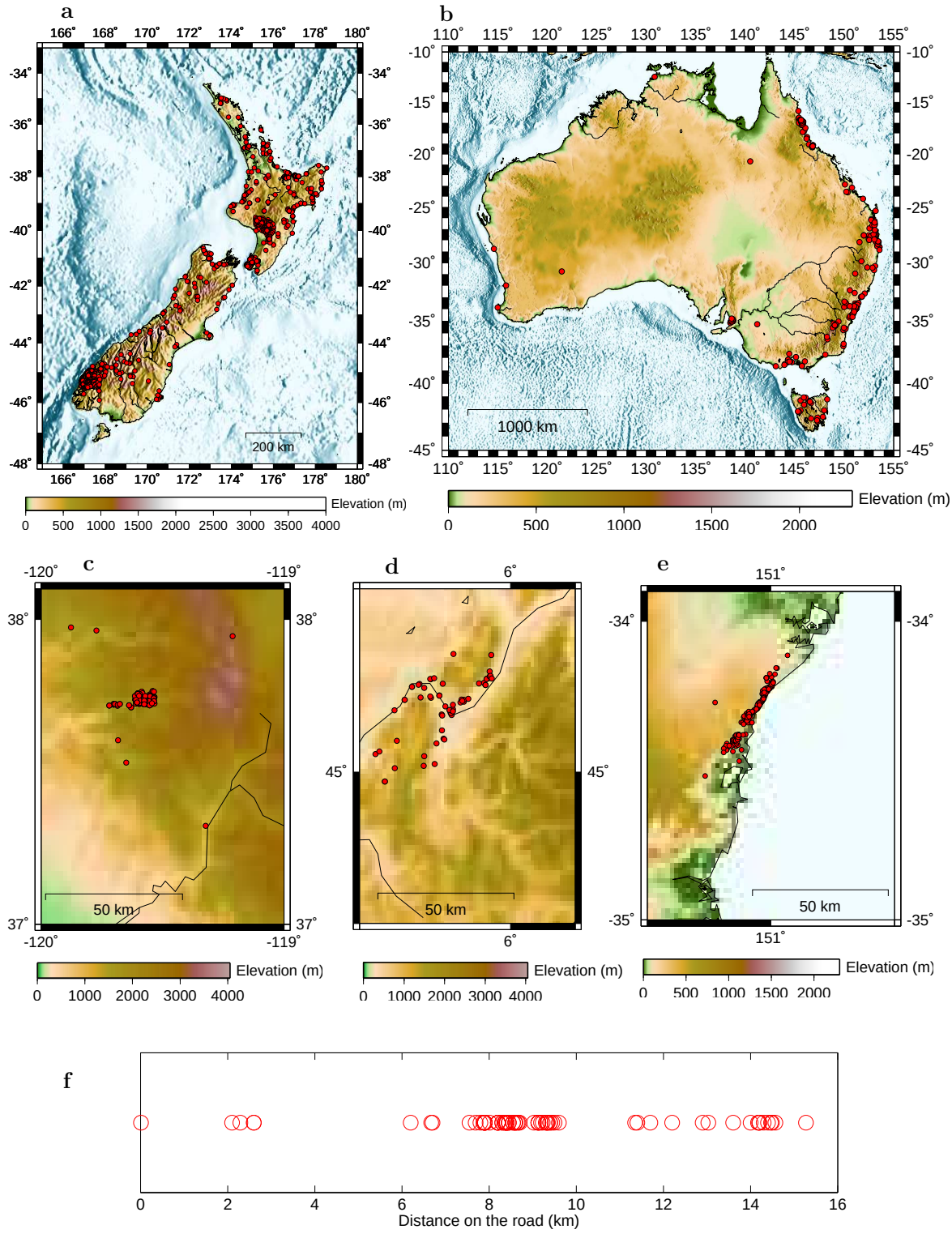

Figure 3.3: Landslide locations (red dots) and associated topography. a) 1788 New Zealand landslides; b) 247 Australia landslides; c) 172 Yosemite landslides; d) 63 Grenoble landslides; e) 207 Wollongong landslides; f) 83 Val d'Arly landslides.

Table 3.3: *Earthquake catalogues.*

	New Zealand[1]	Yosemite[2]	Alps[3]	Australia[4]	Wollongong[4]
Date	1996-2004	1965-2004	1989-2005	1950-2006	1950-2000
Mc	3.0 ± 0.03	1.9 ± 0.01	2.2 ± 0.1	2.5 ± 0.05	2.5 ± 0.05
Seismicity[5]	M_{max} = 7.1, local	M_{max} = 7.0, regional	M_{max} = 4.8, local	M_{max} = 6.9, local	M_{max} = 5.8, local
$M > 5$/yr	12	2	0.05	3	0.14

[a]Database online at http://magma.geonet.org.nz
[b]Database online at http://www.ncedc.org
[c]Database from F. Thouvenot, personal communication 2008
[d]Database from Leonard, 2008
[e]Figures are given for the earthquake database of the whole country for New Zealand and Australia and for 5x5 degrees area centered over the studied area for Yosemite, Grenoble, Val d'Arly and Wollongong areas

3.3.3 Weather databases and climatic settings

As the landslide catalogues are analysed as a whole, with no account taken of the local tectonic, geologic or climatic settings, we use global weather data, corresponding to the same area as that where landslides were recorded. We are aware that for New Zealand and Australia such strategy implies averaging data which has large fluctuations but this choice is coherent with the global analysis used for landslide databases.

New Zealand's climate varies from warm subtropical conditions in the far north to cool temperate climates in the far south, with severe alpine conditions in the mountainous areas. Mountain chains extending the length of New Zealand provide a barrier to the prevailing westerly winds, dividing the country into distinct climate regions (see Whipple, 2009 for a discussion on the interaction between climate and tectonics in New Zealand). The West Coast of the South Island is the wettest area of New Zealand, whereas the area to the east of the mountains (100 km away) is the driest. Most areas of New Zealand record between 600 and 1600 mm of rainfall spread throughout the year. Over the northern and central

areas of New Zealand more rain falls in winter than in summer, whereas for much of the southern part of New Zealand, winter is the season of least rainfall (NIWA, 2009).

Australia is a large island continent with different climate zones, varying from tropical in the north through the arid expanses of the interior to temperate regions in the south. Seasonal fluctuations can be large, with temperatures ranging from above 50° C to well below zero. Minimum temperatures are moderated by the lack of mountains and by the influence of surrounding oceans. Australia is relatively arid, with 80% of the land recording less than 600 millimetres rain per year and 50% having less than 300 mm (Bureau of Meteorology, 2009). Rainfall is highly seasonal and occurs mainly during summer.

The climatic conditions of the Chartreuse and Vercors areas, near Grenoble, in the French Alps foothills, are characterized by wet spring (up to 90 mm/month) and fall (up to 110 mm/month) seasons. Val d'Arly area, located in the more central part of the French Alps, has wet summers with rainfall depth up to 240 mm/month. The climatic conditions of the Yosemite Park are a dry April - October period and wet October - April period (up to 180 mm/month). These three areas have cold winters with minimum monthly temperatures below 0° Celsius.

The New Zealand and Australia weather databases used in this study are averaged from hundred of gauges spread over the whole countries. The Yosemite, Grenoble and Wollongong gauges are located within the three studied areas, whereas the Val d'Arly gauge is located 30 km to the North. The selection of the gauges was made on availability and completeness criteria for both rainfall and temperature data. For these local catalogues, the gauges give a robust estimate of local rainfall, whereas the estimate of temperature may be biased due to elevation differences between available gauges and landslides (largest offsets for Yosemite, Grenoble, Val d'Arly and Wollongong gauges are 1100 m, 1300 m, 200 m and 400 m, respectively).

The New Zealand, Grenoble, Val d'Arly and Wollongong weather catalogues all show 10-15 rain days per month. The monthly rainfall depth is the key parameter that drives the differences between the six areas. New Zealand presents the largest amount of rainfall per

Table 3.4: *Rainfall and temperature for the 6 studied areas.*

	New Zealand[1]	Yosemite[2]	Grenoble[3]	Val d'Arly[3]	Australia[4]	Wollongong[4]
Monthly min–max rainfall[5] (mm)	90 – 220	0 – 180	65 – 105	75 – 145	15 – 100	65 – 160
Mean monthly rainfall (mm)	150	80	85	105	45	115
Raindays per month[5]	10 – 16	no data	10 – 16	10 – 15	no data	8 – 15
Monthly[5] min–max T (° C)	1 – 22	-2 – 32	-1 – 29	-8 – 22	15 – 28	8 – 26

[a]Database from National Institute of Water and Atmospheric research - NIWA, New Zealand
[b]Database from National Climatic Data Center, USA
[c]Database from Météofrance
[d]Database online at http://www.bom.gov.au/
[e]Monthly minimae and maximae were obtained by averaging, per month, over the time period of the corresponding landslide catalogue, monthly weather variables, in order to get the yearly climatic trend of the studied area.

month, up to 220 mm, followed by Yosemite and Wollongong, while Australia presents the smallest annual mean. Yosemite presents the greatest contrast between the minimum and maximum monthly rainfall depth (180 mm), while Grenoble presents the smallest contrast (40 mm) (see Table 3.4 for yearly data and Fig. 3.4 for times series of rainfall).

3.4 Correlation between landslide occurrences

3.4.1 Evidences for complex inter-relationship between landslide patterns, and rainfall and seismicity forcings

In a first attempt to characterize landsliding patterns in the six studied areas, we work with space-time diagrams (figures 3.4 and 3.5). All catalogues show clusters of landslides in time and space. These clusters display different intensities, as measured by the number of landslides per cluster, and different spatial extents, as measured by the cluster size. These clusters are either associated with earthquakes (New Zealand), or large rainfalls (New Zealand, Yosemite, Australia, Wollongong) or with neither earthquake nor large rainfall. No linear interaction for either landslide - rainfall or landslide - earthquake can be deduced from these figures since responses to similar amplitude triggers appear as heterogeneous. For example, earthquakes in New Zealand, near latitude -45°and longitude 168°, sometimes trigger landslides and sometimes do not. In Australia, near latitude -23°and longitude 154°and near latitude -37°and longitude 146°some landslides occurred several years after a sequence of $M = 4.4 - 4.8$ earthquakes. We may wonder i) why they were not directly triggered by the earthquake sequence and ii) if they are related to these shocks. In Wollongong, similar monthly rainfall depths do not trigger the same number of landslides, if indeed they trigger any.

To understand these observations, we first characterize, for each catalogue i) the time patterns of landslides, ii) the daily rate patterns and iii) the time-space correlation, if any. In a second step, we quantitatively assess the landslides-landslides, landslides-earthquakes and landslides-climate interactions.

3.4.2 Landslide daily patterns

The landsliding rates of the New Zealand, Yosemite, Australia and Wollongong catalogues show a larger variability than both their rainfall and seismicity counterparts (Fig. 3.1). The peak value of daily landslide rates varies over two orders of magnitude: from

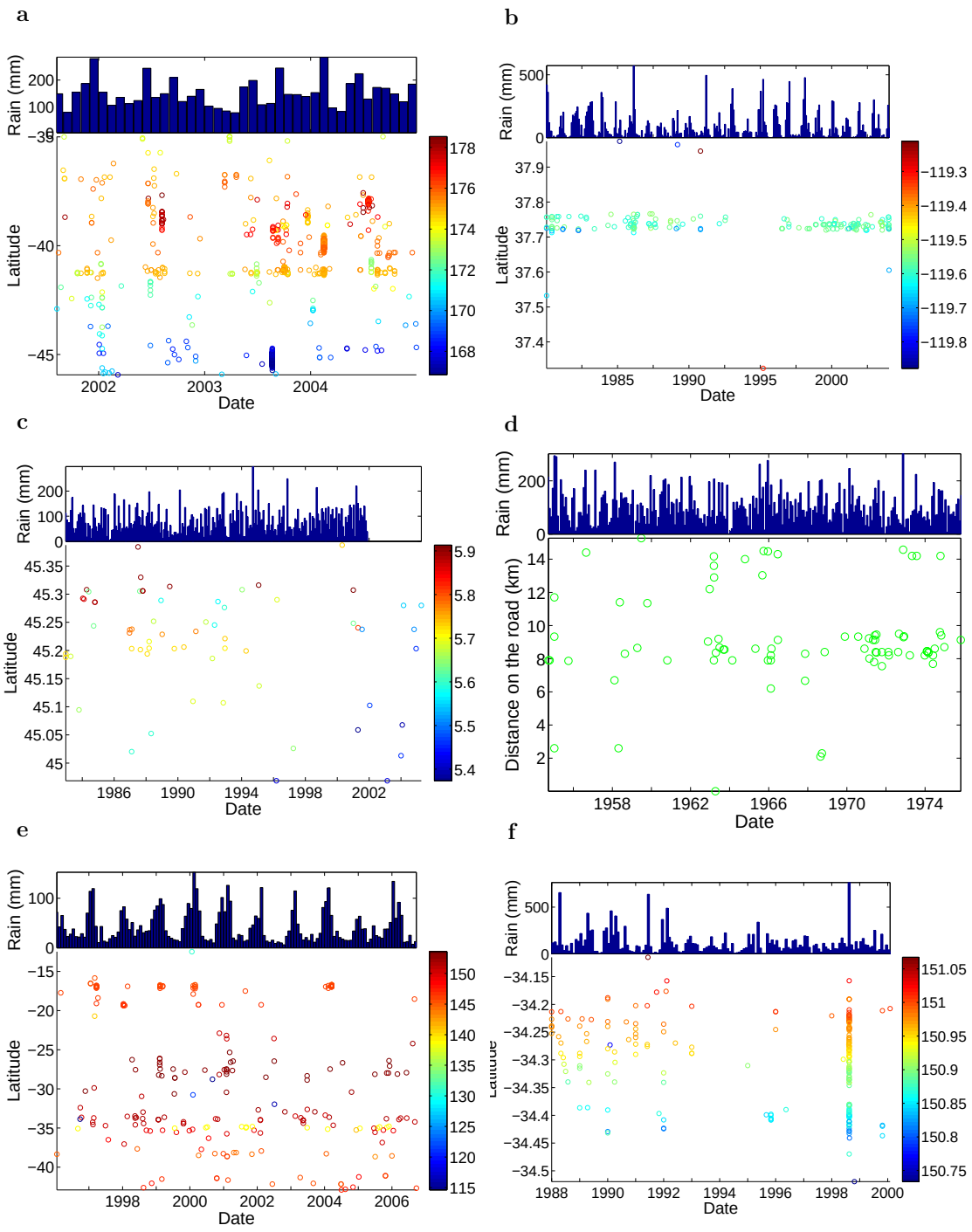

Figure 3.4: Space-time diagrams for landslide activity: landslides (circles) as a function of space (y axis for latitude and color for longitude) and time. The upper blue histogram gives monthly rain falls (mm). a) New Zealand; b) Yosemite; c) Grenoble; d) Val d'Arly; e) Australia; f) Wollongong. For d) y axis corresponds to distances (km) along the roadcut.

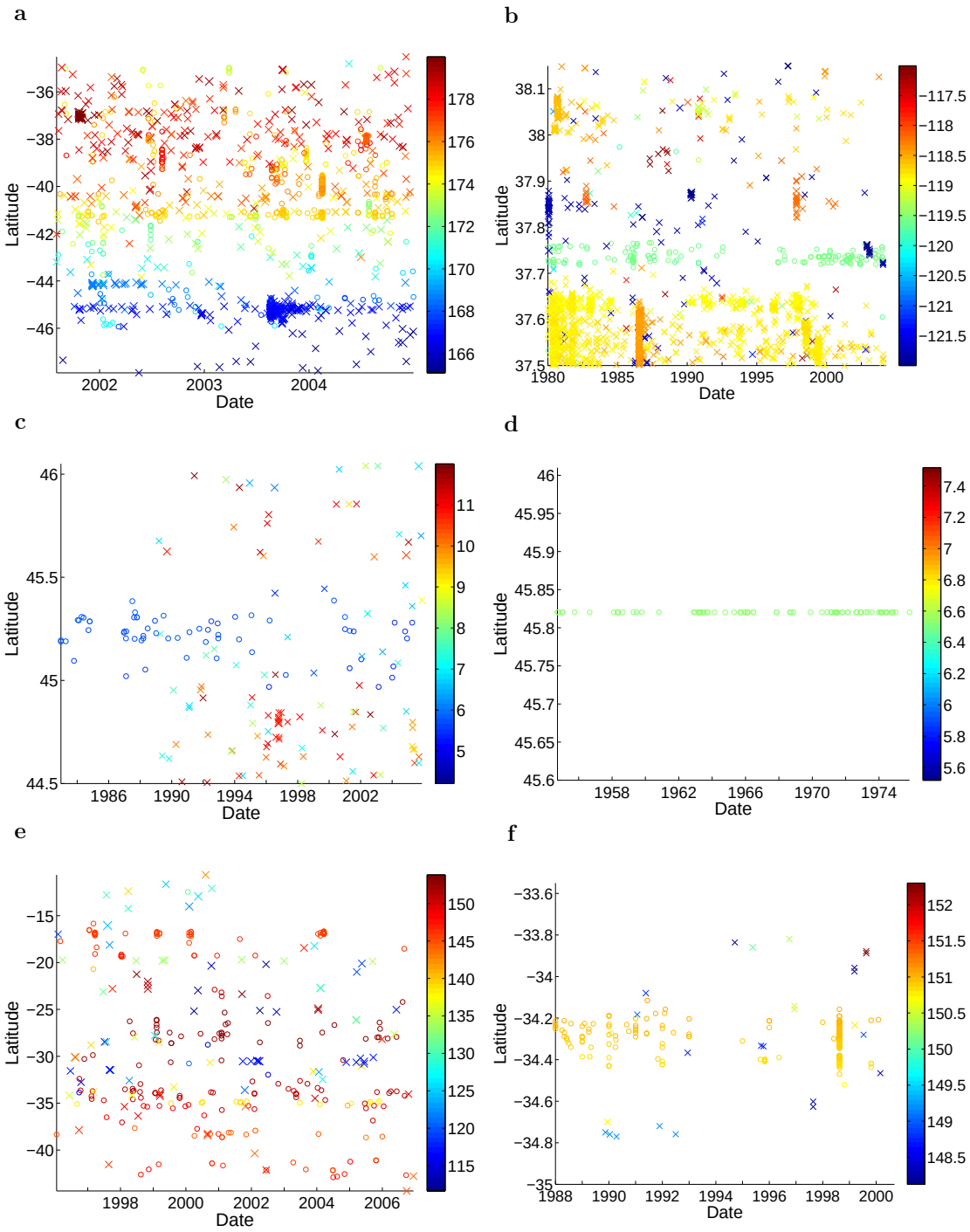

Figure 3.5: Space-time diagrams for landslides and earthquakes: Landslides (circles) and earthquakes (crosses) as a function of space (y axis for latitude and color for longitude) and time. Size of the earthquake marker increases with increasing magnitude ($M > 4$ for New Zealand and Australia and $M > 3$ for other catalogues). a) New Zealand; b) Yosemite; c) Grenoble; d) Val d'Arly; e) Australia; f) Wollongong.

1 and 3 landslides per day for Grenoble and Val d'Arly, up to 10 landslides per day for Yosemite and Australia and more than 100 landslides per day for New Zealand and Wollongong catalogues. For all catalogues, daily rates larger than three events per day correspond in the databases to landslides reported as either rain-triggered (New Zealand, Wollongong, Australia, Yosemite) or earthquake-triggered (New Zealand, Yosemite).

The mean daily rates range between 0.01 events per day for Grenoble and 1.4 events per day for New Zealand (Table 3.2). The landslide densities span five orders of magnitude, from 2.7 10^{-6} events/year/km^2 for Australia to 2.4 10^{-1} events/year/km^2 for Val d'Arly. The largest and smallest landslide daily rates do not correspond to the largest and smallest landslide densities, respectively.

These patterns emphasize the scale effect inherent to our choice of catalogues. As an example, Val d'Arly is an active cliff extending over a 10 km scale, while New Zealand is an active mountain range extending over a 1000 km scale. Landslide recording is therefore very different between one catalogue and another and the landslide rates and densities should be normalised by the resolution of each landslide catalogue (as performed for earthquake catalogues, e.g. Traversa and Grasso, 2009). The detection threshold V_0 is usually defined by fitting a power-law distribution to the cumulative volume distribution, and looking at the deviation from a power-law for small volumes (e.g. Dussauge et al., 2003). Because discrete volume estimates are reported for less than 40% of events for most of the catalogues (Table 3.1), we cannot calculate V_0 values for all catalogues and therefore cannot correct the landslide rate and density values from the catalogue resolution (see also Appendix A). Accordingly, landslide rates and densities in Table 3.2 must not be overinterpreted.

These results underline the difficulty of establishing accurate indices from available catalogues, in the absence of better volume estimates, which inhibit comparisons between different landslide catalogues.

3.4.3 Distribution of landslide times and waiting times

Using the ratio η between the mean inter-event time dt and the inter-event time standard deviation, we characterize clustering of landslides occurrence in time (e.g. Marzocchi and Zaccarelli, 2006). For a Poisson process, *i.e.* a uniform distribution in time, $\eta = 1$, and the distribution of inter-event times obeys an exponential distribution. $\eta > 1$ characterizes events that are more clustered than a Poisson process, and $\eta < 1$ is typical for more "regular" occurrence times. The assumption that occurrence times obey a Poisson process is rejected for all areas, for both the full and binary catalogues, using the η test (Table 3.4.3). The entire Grenoble and Val d'Arly catalogues are characterized by the smallest η values and therefore are the less clustered in time, whereas the entire New Zealand catalogue appears to be the most clustered. To further investigate clustering of landslide in time, we analyse the waiting time distributions for the six catalogues (Fig. 3.6). For each catalogue, there is a threshold time (t_r) above which large inter-event times are more frequent than expected from an exponential distribution (Fig. 3.6). t_r ranges between 30 and 250 days (Table 3.4.3). This deviation from a Poisson process for $t > t_r$ may be due to seasonal variations of climate, because landslides are less frequent during the dry season.

3.4.4 Distribution of landslide daily rates

To further constrain the dynamics of landslides, we analyse the distribution of daily rates. The heavy tail of the distributions suggests a fit of distributions of landslide rates to a power-law. We use the method of Clauset et al. (2009), based on the Maximum Likelihood Method (Aki, 1965) to evaluate the power-law exponent, along with the Kolmogorov-Smirnoff test (e.g. Press et al., 1992) to test the power-law goodness-of-fit. The New Zealand, Yosemite, Australia and Wollongong daily rates accept a power-law distribution (Table 3.6) for daily rates larger than 1 event/day in the four cases. This result implies that there is no characteristic scale for daily rate values. The Grenoble and Val d'Arly daily rates present only three and eight days with more than one landslide per day, respectively, and the power-law distribution is rejected (Table 3.6, Fig. 3.7). For New Zealand, Australia and

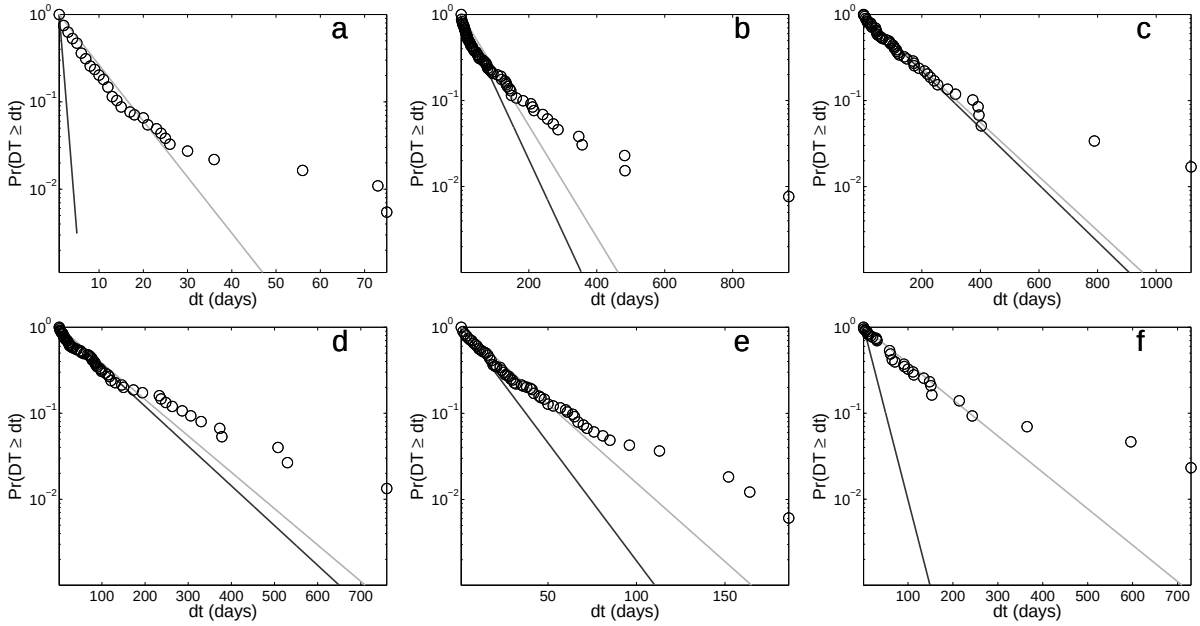

Figure 3.6: Cumulative distribution of landslide waiting times for $dt > 0$ (circles) along with exponential distributions, corresponding to uniformly distributed occurrence times, computed from the entire catalogue (dark grey line) and from the binary landslide catalogue (light grey line). a) New Zealand; b) Yosemite; c) Grenoble; d) Val d'Arly; e) Australia; f) Wollongong.

Table 3.5: η test and t_r values. $\eta > 1$ characterizes statistical distributions more clustered than a random one, $\eta = 1$ characterizes statistical distributions as a Poisson process and $\eta < 1$ characterizes statistical distributions as more "regular" than a random one. t_r is the inter-event time over which the inter-event time distribution departs from the random distribution. N is the number of landslides of the studied catalogue.

catalogue	N	η	t_r
New Zealand	1788	2.3	1
New Zealand binary	192	1.5	30
Yosemite	172	2.1	100
Yosemite binary	132	1.8	180
Grenoble	63	1.2	250
Grenoble binary	60	1.2	250
Val d'Arly	83	1.5	150
Val d'Arly binary	76	1.4	100
Australia	247	1.8	25
Australia binary	163	1.3	50
Wollongong	207	3.4	1
Wollongong binary	44	1.3	250

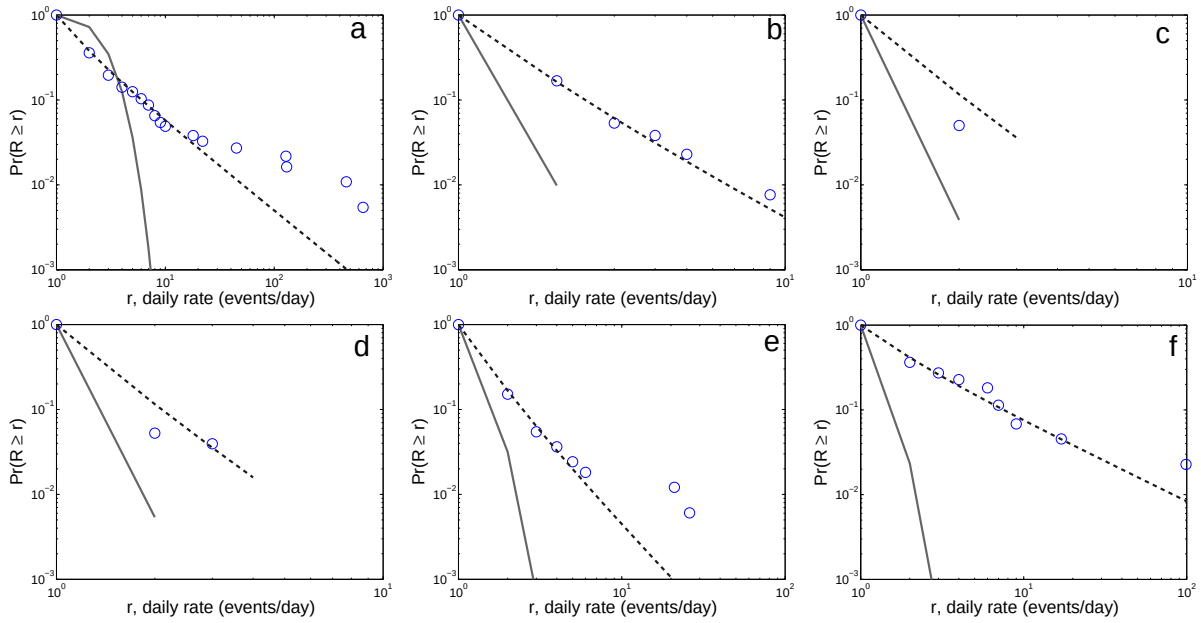

Figure 3.7: Cumulative Distribution Function (CDF) of landslide daily rates (blue circles); best Kolmogorov-Smirnoff power-law fit (black dashed line). a) New Zealand landslides; b) Yosemite landslides; c) Grenoble cliffs landslides; d) Val d'Arly cliff landslides; e) Australia landslides; f) Wollongong landslides. The grey line represents the poisson function which fit best the values. Values of exponent b and lower cutoffs are given in Table 3.6. Note that i) the fit is slightly curved for daily rates lower than 6 events/day, which is inherent in the definition of a discrete power-law (e.g. Clauset et al., 2009) and ii) the exponent of the CDF B is equal to $b-1$ (e.g. Bonnet et al., 2001).

possibly Wollongong daily rate distributions, there is a change in slope for rates greater than 10-20 events per day: the frequencies of the empirical daily rates are larger than expected from the best fit power-law (Fig. 3.7). This suggests a different origin or mechanism for the largest crises.

3.4.5 Distribution of landslide inter-event distances

After analyzing clustering of landslides in the time domain, we study clustering of landslides in space, and its evolution with time. We evaluate the distribution of landslide inter-event distances, using all couples of events in the catalogue, and then selecting only events occurring on the same day, or with an inter-event time dt of 1 day. All distributions are normalized by the maximum time lag between events, so that all curves would overlap

Table 3.6: Landslide daily rate distributions and associated power-laws. N denotes the number of landslides, b the power-law exponent and p the associated probability that the distribution follows the best power-law fit. $p > 0.1$ - in bold in the Table - accepts power-law as a possible description of the data. Standard deviation are calculated via a non parametric bootstrap method (see Clauset et al., 2009 for details).

catalogue name	N	Exponent b	Lower cut-off	p
New Zealand	1788	2.04 ± 0.11	1 ± 0.13	**0.26**
Yosemite	172	3.04 ± 0.21	1 ± 0.00	**0.93**
Grenoble	67			0.07
Val d'Arly	83			0
Australia	247	3.01 ± 0.21	1 ± 0.00	**0.42**
Wollongong	207	1.93 ± 0.20	1 ± 0.35	**0.37**

for a uniform distribution in space and time. The distributions were computed using a log binning and then convolved with a gaussian kernel, e.g. Izenman (1991). 0.01 km and 1 km location errors were added to Val d'Arly distances and to New Zealand, Yosemite, Grenoble, Australia and Wollongong distances, respectively.

Figure 3.8 compares the average inter-event distance distributions ($dt > 1$ day) to the $dt = 0$ inter-event distance distributions, for the entire catalogues. Figure 3.9 presents the same analysis for the binary catalogues, and comparing the case $dt = 1$ with $dt > 1$. The difference between the two curves in each plot gives (i) the intensity of landslide triggering for the studied dt and (ii) the distance range where landslides were triggered (Figs 3.8, 3.9).

We find significant triggering at $dt = 0$ day for all the entire catalogues (Fig. 3.8). For $dt = 1$ day, we find significant triggering only for New Zealand, Yosemite and Australia catalogues (Fig. 3.9). At $t = 0$ day, landslide triggering is maximum from 0 to 50 km and it extends up to 200 km for New Zealand. Landslide triggering is observed between 0 and 30 km for Australia, 2 and 3 km for Grenoble. It is equal to the size of the sampled area for Yosemite, Val d'Arly and Wollongong catalogues. It is noticeable that the values given for Grenoble and Val d'Arly are only indicative since the number of landslides occurring on the same day is small. We also checked the landslide triggering at $dt = 0$ not to be

driven only by the largest crises by performing the same test on landslide subcatalogues whose daily crises larger than one hundred landslides were withdrawn. For $dt = 1$ day, the spatial extent of landslide triggering is roughly similar to the size of the sampled area for New Zealand and Australia, whereas it is 10 km range for Yosemite.

3.5 Analysis of the possible processes for landslide triggering

3.5.1 Landslide - landslide interactions

The distribution of the inter-event distances as analysed in the previous section showed that there are more landslides than expected within the same day or the day following a landslide occurrence (Figs. 3.8 and 3.9). The inter-event distance distributions show that most of these landslides are within 50 km of each other. These distances are too large to result from landslide - landslide interactions. We suggest this correlation is driven by the primary trigger itself. For the weather trigger, the correlation can be due to the residence or transit time of the weather event. For the earthquake trigger, aftershocks are the best candidate to drive this time and space triggering (see also section 3.5.2).

We analyse variations of landslide rate before and after the 10 largest landslides of each catalogue. We stack landslide time-series relative to the time of each of these large events, a technique which allows us to increase the signal to noise ratio (e.g. Lemarchand and Grasso, 2007; Tatard et al., Submitted). We show, for the New Zealand, Grenoble, Val d'Arly and Australia landslide catalogues that there are more landslides in a 20-day period after the large landslide occurrence than in the 20-day period before it (Fig. 3.10). We test whether these average increases in landslide rates are significant against randomness by randomly selecting 10 landslides from the studied landslide catalogue and performing the same test. We find that there is less than 1, 17, 10 and 17 per cent chances of finding such a trend for the New Zealand, Grenoble, Val d'Arly and Australia landslide catalogues, respectively.

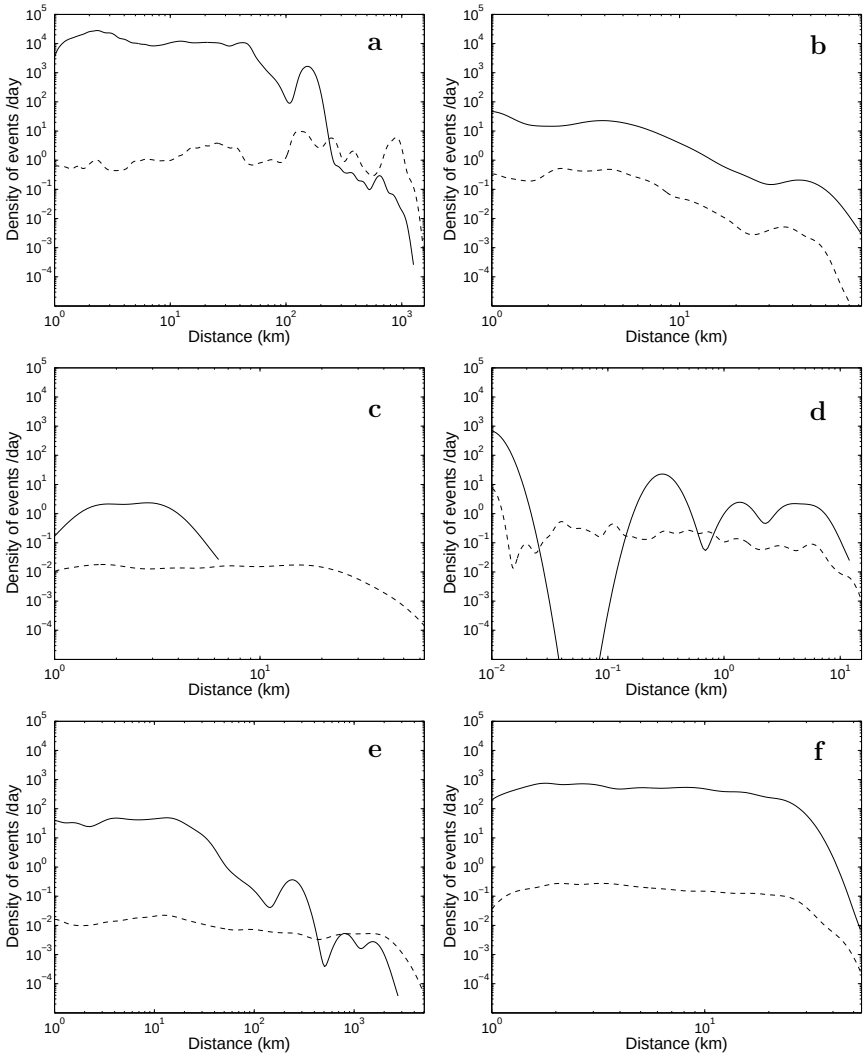

Figure 3.8: Distribution of inter-event distances for landslides occurring at $dt = 0$ day (plain line) and landslides occurring at $dt > 1$ day (dashed line). a) New Zealand; b) Yosemite; c) Grenoble; d) Val d'Arly; e) Australia; f) Wollongong. The distributions were computed using a log binning and then convolved with a gaussian kernel, e.g. Izenman (1991). A 0.01 km and a 1 km error were added to Val d'Arly distances and to New Zealand, Yosemite, Grenoble, Australia and Wollongong distances, respectively.

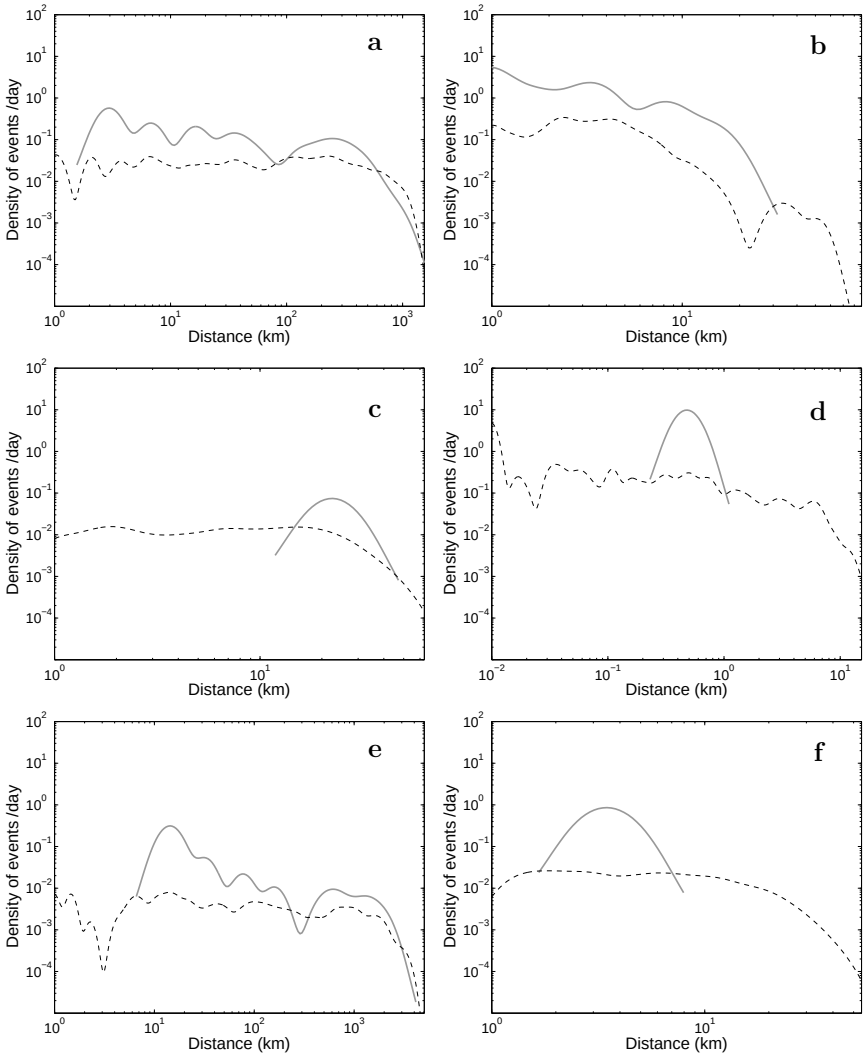

Figure 3.9: Same as Figure 3.8 but using the binary catalogues, and comparing $dt = 1$ (solid grey line) with $dt > 1$ (dashed line).

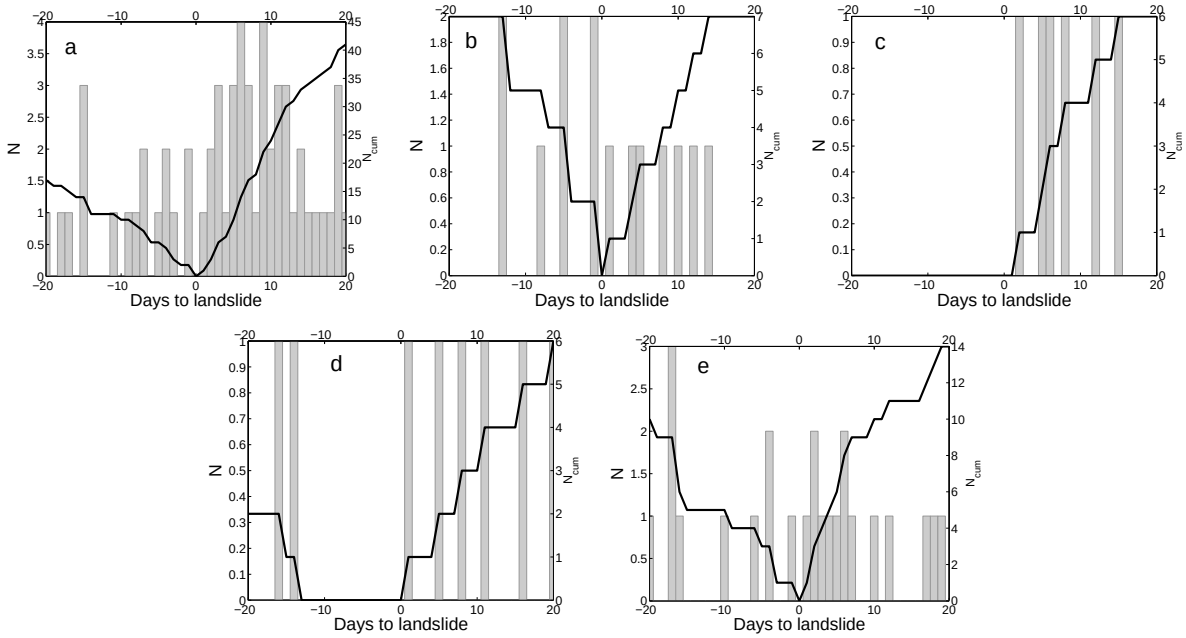

Figure 3.10: Stacked time series of binary landslide daily rates relative to the 10 largest landslide times. a) New Zealand; b) Yosemite; c) Grenoble; d) Val d'Arly and e) Australia. The black curves represent the cumulative number of events from t=0 to t=-20 day and from t=0 to t=20 days before/after the large landslide occurrences. There are no volume data for the Wollongong catalogue.

We looked at the distances between the largest landslides and the landslides occurring 20 days before or after the large landslides. We found that most of these events are located more than 1 km away from the large events (Fig. 3.11). Therefore, these landslides are probably not foreshocks or aftershocks of the large landslides. The average increase in landslide rates after large landslides can then be interpreted as the fingerprint of an external forcing, triggering first large landslides then smaller ones, or as a bias in observation after large event occurrences. The latter suggests that the community in charge of landslide observation is more sensitive to landslides during the few days to weeks following a large landslide.

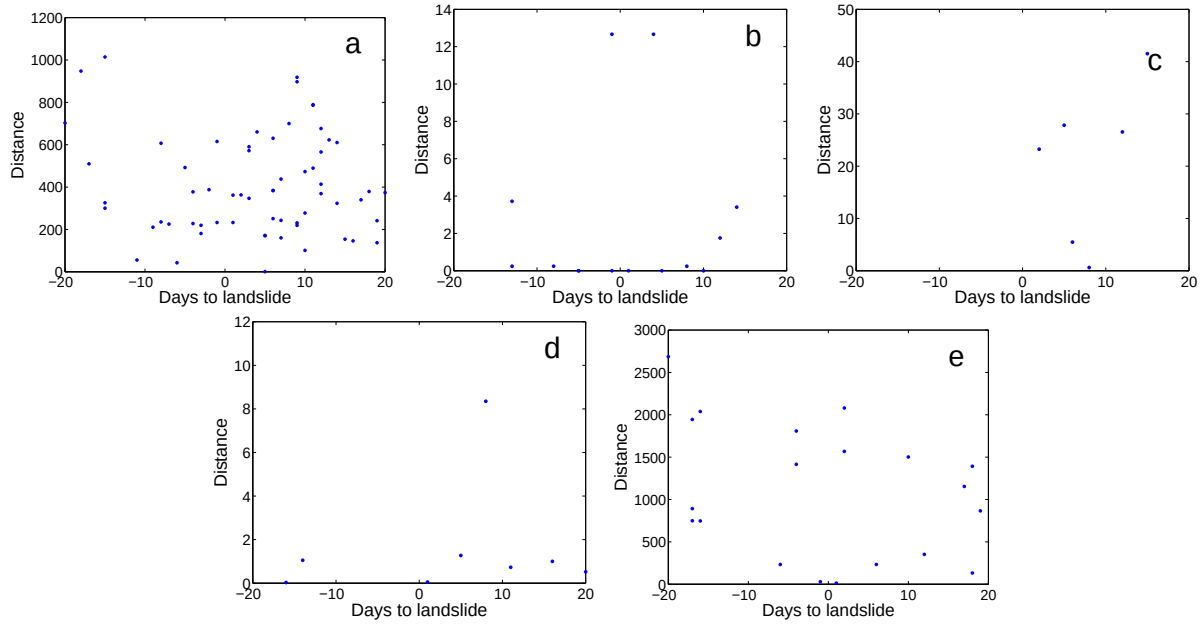

Figure 3.11: Distances between the ten largest landslides and the landslides occurring 20 days before and after them. a) New Zealand; b) Yosemite; c) Grenoble; d) Val d'Arly and e) Australia.

3.5.2 Earthquake - landslide interactions

We analyse the possible effect of seismicity on the triggering of landslides for the six catalogues by stacking time series of landslides relatively to each earthquake time, in order to increase the signal-to-noise ratio, as performed for landslide-landslide interaction studies (see section 3.5.1). The signal is dominated by small-magnitude earthquakes, since they are much more numerous than medium and large earthquakes (Gutenberg and Richter, 1956). Following Lemarchand and Grasso (2007), we select earthquakes with a given Δ/L ratio, to improve the signal-to-noise ratio, where Δ is the landslide-earthquake hypocenter distance and L is the fault length calculated from the earthquake magnitude (Wells and Coppersmith, 1994).

As we want to assess the effect of seismicity on the recorded landslides, we use the longest landslide databases (Table 3.1), selecting landslides with a known location and a known date (0 to 2 days time accuracy). We select from the local seismicity catalogues

earthquakes with magnitude $M > M_c$ and not deeper than 200 km (Table 3.3).

We find an increase of the number of landslides within 1 day from earthquake occurrences for the New Zealand, Yosemite and Australia catalogues, for Δ/L up to 100. In order to test whether the landslide signal for Δ/L up to 100 is significant, we perform the same test on 100 modified landslide catalogues. For these 100 catalogues, the landslide locations remain the same but the landslide occurrence dates are randomly drawn from a uniform distribution, while the landslide daily rate is kept similar to the power-law daily rate of the original landslide catalogue. In addition, we performed the tests with declustered earthquake catalogues, *i.e.* we removed the aftershocks occurring within two days and at distances less than 100 times the ruptured fault length of the $M > 4$ mainshocks. This process removes noise from the landslide signal, *i.e.* removes the landslide signal created by the correlation between landslides and aftershocks. We find significant signal for New Zealand landslides for Δ/L up to 10 (Fig. 3.12). For Yosemite and Australia landslides, the signal is found to be not significant for all Δ/L (Fig. 3.12). This result indicates that the Yosemite and Australia landslide-earthquake interactions are not strong: either the applied earthquake forcing is low or the slope susceptibility is low, compared to New Zealand.

We check the landslide and earthquake couples driving the signal around $t = 0$, for $\Delta/L \leq 10$. We restrict the study to $\Delta/L \leq 10$ as this corresponds to the average maximum distances at which mainshocks are found to trigger aftershocks (Felzer and Brodsky, 2006). New Zealand, Yosemite and Australia catalogues present 512, 14 and 2 earthquake-triggered landslides on 3, 3 and 2 different days, respectively (Table 3.7). The minimum magnitude earthquake found to correlate with a landslide is a M_L=5.1 event in New Zealand, whereas the maximum distance at which a landslide is found to be seismically correlated is 500 km (still in New Zealand). The two largest Δ/L ($\Delta/L \sim 10$) are associated with these two landslides. Accurate timing of these landslides or numerical modelling is needed to validate these landslides as earthquake-triggered.

Note that landslides are all spatially close to each other in the Yosemite catalogue;

Table 3.7: Landslide triggering earthquakes, with $\Delta/L \leq 10$. Δ is equal to the earthquake hypocenter - landslide distance and L is equal to the ruptured fault length.

Catalogue	Date of earthquake	M_L	Number of reported landslides	Δ_{min} - Δ_{max}	Min Δ/L
New Zealand	August, 22^{nd} 2003	7.0	459	25 - 205 km	5.1
	July, 18^{th} 2004	5.1	52	5 - 19 km	9.2
	November, 22^{nd} 2004	7.1	1	500 km	9.9
Yosemite	May, 25^{th} 1980	6.1	4	65 - 75 km	7.9
	May, 27^{th} 1980	6.2	5	70 - 75 km	6.7
	October, 24^{th} 1990	5.8	4	15 - 50 km	9
Grenoble	None				
Val d'Arly	None				
Australia	February, 28^{th} 1954	5.4	1	12 km	3.7
	December, 27^{th} 1989	5.7	1	14 km	2.7
Wollongong	None				

therefore, when an earthquake with a given Δ/L is effective on a landslide (as 3 nearby Yosemite earthquakes were, see Table 3.7), it is also potentially effective on all the slopes of the Yosemite area. The fact that most landslides were not triggered by the 3 nearby Yosemite earthquakes but triggered later on indicates that Δ/L alone (and more globally a given threshold) is not sufficient to predict whether a landslide will occur or not. We suggest that the geomorphological stage of the slope, *i.e.* its readiness for failure, has to be included as well for earthquake-triggered landslide prediction.

Last, we test the effect of the $M > 5$ earthquakes on the long-term landsliding rate (several hundred days before and after large earthquake occurrences) for the New Zealand, Yosemite and Australia catalogues. We find no robust evidence of an increase, or a decrease, of the landsliding rate after the large earthquake occurrences.

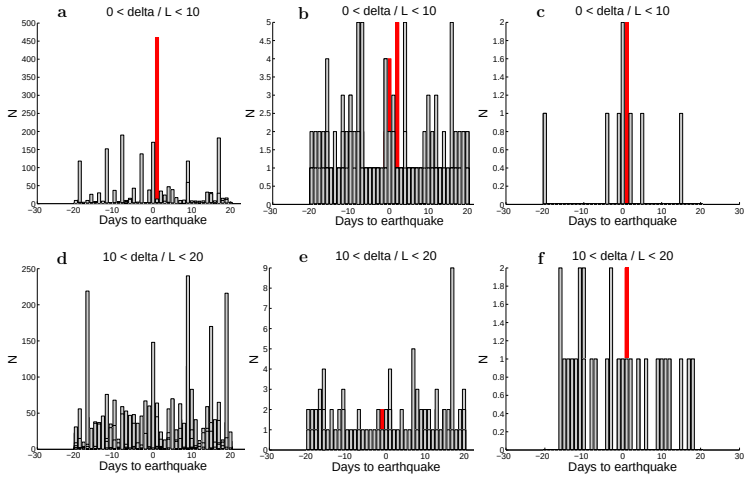

Figure 3.12: Stacked time series of landslides relative to earthquake occurrence times for New Zealand (a, d), Yosemite (b, e) and Australia (c, f) catalogues, for $0 < \Delta/L < 10$ (a, b and c) and $10 < \Delta/L < 20$ classes (d, e and f). Landslide stacks from the original landslide catalogue are displayed in red, whereas the landslide stacks from the 100 modified landslide catalogues are displayed in grey. Note for the d) plot, the landslide stacks from the 100 modified catalogues entirely overlap the landslide stacks from the original catalogue.

3.5.3 Climate - landslide interactions

To quantify the impact of climate on landslides, we compute the linear correlation coefficient r (e.g. Press et al., 1992) between the monthly landslide rates and the monthly weather variables, *i.e.* rainfall height, number of rain days, temperature. In the following, we focus on the binary catalogues, since the correlation coefficients are larger.

We found that the New Zealand, Val d'Arly, Australia and Wollongong landslide monthly rates correlate with both the monthly rainfall depth and the monthly number of rainy days (Table 3.8). The Grenoble landslides are anti-correlated with both the monthly minimum and maximum temperatures, whereas the New Zealand catalogue is only anti-correlated with the maximum temperatures (Table 3.8). It must be noted that the New Zealand monthly temperatures and New Zealand monthly rainfall are not correlated. This result therefore validates the correlations of New Zealand landslides with temperatures and with rainfall as two independent results.

On average, the correlation with rainfall depth is stronger than the one with the rainy

Table 3.8: *Monthly correlation between binary landslide rates and weather (rain, rain days, temperature). If the significance of correlation (given within brackets) is less than 0.05, the correlation is considered as significant, and the correlation coefficient value is in bold.*

catalogue	Rain	Number of rain days	Minimum temperature	Maximum temperature	Mean temperature
New Zealand	**0.35** (0.03)	**0.42** (< 0.01)	-0.29 (0.06)	**-0.35** (0.03)	no data
Wollongong	**0.62** (< 0.01)	**0.26** (< 0.01)	0.08 (0.33)	-0.02 (0.85)	no data
Australia	**0.32** (< 0.01)	no data	no data	no data	0.11 (0.20)
Yosemite	0.08 (0.16)	no data	0.08 (0.18)	0.07 (0.26)	no data
Val d'Arly	**0.15** (0.02)	**0.12** (0.05)	0.04 (0.49)	0 (0.95)	no data
Grenoble	0.11 (0.10)	0.06 (0.34)	**-0.14** (0.03)	**-0.16** (0.02)	no data

days. We observe that the correlation coefficients do not scale with the size of the rainfall forcing (Tables 3.4 and 3.8). Note than the correlation with temperature remains weak, if any. Only the catalogue whose landslide occurrences are closest to the uniform distribution, *i.e.* Grenoble area rockfalls catalogue, correlates with the slow recurrent temperature forcing.

3.6 Discussion and Conclusions

In this work, we aimed to identify and characterize landslide triggering patterns using six global landslide inventories. These landslide catalogues span different space and time scales, 15 to 4.10^3 km and 4 to 25 years, respectively and were gathered in different tectonic and climatic settings. The joint analysis of these landslide catalogues allows us to investigate possible scale effects on the landslide dynamics and on their relative forcings. Getting robust catalogues in time, space, size and independent of anthropogenic effects is a major issue when using landslide catalogues. Accordingly, we selected landslide catalogues over their period of constant binary rate, excluding landslides with either a time inaccuracy

larger than 2 days and/or no space location. These procedures result in catalogues which are self-consistent, producing robust results.

Nevertheless, as data on volume are poor for most catalogues, we cannot define a detection threshold above which catalogues are complete, therefore we could not correct the catalogues from their resolution (e.g. Dussauge et al., 2003). This is an issue when aiming to compare the different catalogues as it precludes the use of simple indexes such as landslide daily rates and densities. It is the reason why we propose other indexes/tools to characterize and compare landslide dynamics.

Figures 3.4 and 3.5 display clusters of landslides in time and space, evidencing triggering by rain and earthquakes. Daily patterns are shown to be variable in time, even at the relatively short time scales (4 to 25 years) we are looking at. These fluctuations also depend on the studied area. We do not resolve any linear relationships between landslide, rain and seismicity. The response of landslides to triggers is variable in space and time, most probably due to upper crust heterogeneities (geology, geomorphology) as well as heterogeneous daily/monthly external loadings (temperature, soil moisture, vegetation). Within such a context, we transfer to landslide analysis tools used to analyse other natural complex systems such as earthquakes and volcanic eruptions.

First, we compare the distribution of landslide inter-event times with a Poisson process. To go beyond the huge crises that may drive the clustering of time series, we further introduce binary catalogues, *i.e.* catalogues for which the landslide daily rate is set to either 0 (no landslide) or 1 (at least one landslide occurring on the studied day). Second, the landslide daily rate distributions confirm the robustness of temporal clustering. Then landslide inter-event distance distributions are analysed to constrain the driving processes, including the external forcings. The role of these processes is quantified using correlation between landslides and their candidate triggers as earthquakes, weather, landslide-landslide interactions.

The results, and their implications for landslide processes, are the following. First, landslides are strongly correlated in time, even when using binary catalogues to reduce the influence of crises. When focusing on the inter-event time distributions of binary catalogues, we show that the departure from a Poisson process emerges for inter-event times larger than a value t_r. t_r lies in the 30-250 days range for the different catalogues. For inter-event times larger than t_r, there are more large inter-event times than expected for uniformly distributed times. This deviation from a Poisson process for $t > t_r$ may be due to seasonal variations of climate, landslides being less frequent or absent during the dry season, hence leading to larger inter-event times than expected from a Poisson distribution.

For landslide rates, we find that a power-law distribution gives a good fit of daily rates between 1 and 1000 events per day, for the New Zealand, Yosemite, Australia and Wollongong catalogues. A possible deviation from a power law is found above 10 landslides per day for the New Zealand, Australia and Wollongong catalogues (Fig. 3.7 and section 3.4.4). The fact that landslide daily rate distributions accept a power law as a good description of the distribution implies that there is no characteristic scale for daily rate values. It possibly suggests that the same mechanism(s) are driving both the large landslide daily crises and the single events. When the largest daily rate values are known to be rainfall- or earthquake- triggered events, it suggests the smallest daily rates to be rainfall- or earthquake- triggered as well. As no obvious a-priori trigger is either reported or shown for each of these landslides, our results suggest that the delay between a landslide and a possible trigger may not be restricted to a few days, as is usually assumed for most landslide inventories. Delays between a landslide and its trigger, larger than a few days, are now increasingly suggested in several case-studies. As examples, Lin et al. (2008b) showed that the Chi-Chi earthquake raised the landsliding rates of the epicentral region above the pre-Chi-Chi rate, up to 5 years after the occurrence of the Chi-Chi mainshock. For rainfall triggering, Helmstetter and Garambois (submitted) showed that, for a large rockslide in the French Alps, rainfall can trigger small rockslides up to ten days after the maximum of rainfall intensity.

From a process point of view, the power-law distribution of landslide daily rates we resolve may be driven either by the direct response to triggers, since these latter are known to be power-law distributed in size (Gutenberg and Richter, 1956 for earthquakes and Peters et al., 2001; Peters and Christensen, 2002 for rainfall depth), or by the heterogeneous response of the brittle crust to external forcings.

We then constrain the spatial pattern of the landslide crises by focussing on landslides which occurred on the same day. For the Yosemite, Val d'Arly and Wollongong catalogues, the inter-event distances for dt=0 correspond to the spatial extent of the studied catalogue and only give a minimum triggering distance at dt=0. They are equal to 50, 10 and 30 km for the Yosemite, Val d'Arly and Wollongong catalogues, respectively. For the New Zealand, Australia and Grenoble catalogues, the inter-event distances for dt=0 are equal to 50 (up to 200), 30 and 3 km, respectively. These length scales are a measure of the combined effect of the trigger intensity and of the slope susceptibility.

We find no landslide-landslide interactions for any of the six catalogues. The absence of foreshock and aftershock is either real or due to the poor resolution of the landslide catalogues in volume (especially for the catalogues covering the largest areas) or in time (several events are recorded as the same event). In the last case, it still implies that there would be no foreshock or aftershock at time larger than the time accuracy of the catalogue (2 days).

We show that earthquakes trigger landslides for the New Zealand, Yosemite and Australia areas, which are also the areas with the largest seismicity rate. We find significant earthquake triggering for distances up to 10 times the earthquake fault size. The influence of $M < 4$ earthquakes on landsliding is found to be weak, if any, for all catalogues. Using the New Zealand and Yosemite earthquakes, we have no evidence of slope weakening induced by ground shaking up to 500 days after $M > 5$ earthquakes, *i.e.* we do not find any average increase of the landsliding rates after these earthquakes.

We found that the New Zealand, Val d'Arly, Australia and Wollongong landslide monthly rates correlate with both the monthly rainfall depth and the monthly number of rainy days (Table 3.8). The Grenoble landslides are anti-correlated with both the monthly minimum and maximum temperatures, whereas the New Zealand catalogue is only anti-correlated with the maximum temperatures (Table 3.8). Yosemite landslides are the only landslides which are not correlated to any weather variables. As the climatic conditions in Yosemite are not unusual, the absence of correlation might be due to the intrinsic characteristics of the Yosemite massif itself.

There are three candidates to reproduce the increase of landsliding rate after the 10 largest landslides we resolved for the New Zealand, Grenoble, Val d'Arly and Australia catalogues. First, a bias in landslide recording may follow a large event occurrence. The community in charge of landslide observation is expected to be more sensitive to landslides during the few days to weeks following a large landslide. Second, the combined analysis of landslide triggering behaviour after the 10 largest landslides along with the susceptibility to weather for each catalogue gives possible insights on a several weeks long effect of weather (Fig. 3.10)). When landslides correlated to rainfall (New Zealand, Val d'Arly, Australia), the average landslide rate after the largest landslides increases by ~ 1.5 relative to the rate before the large landslides. For the Grenoble catalogue, the only catalogue which is just correlated to temperature, the response is stronger than in the previous case with on average no event in the 20 days before the largest landslides and up to 6 events in the 20 days after. It supports the suggestion that temperature changes drive these averaged-rockfall sequences. The Yosemite catalogue, with correlation to neither rain nor temperature, is the only catalogue having the same number of landslides in the 20 days before and after the large landslide occurrences.

From the New Zealand, Val d'Arly, Australia and Grenoble landsliding behaviours after large landslide occurrences, it could be deduced that the largest events are the closest to instability, when landslide triggering is driven by rainfall or temperature.

All the results described above converge towards correlation between landslide occurrences in space and time. The six catalogues we worked with do not present the same intensity of time and space correlations. We propose these correlation values as indexes to estimate the landslide re-activity for a given area. We define the landslide re-activity as encompassing both slope susceptibility and forcing intensity, both of them driving the landslide dynamics (see also Vahrson, 1994 and Dilley et al., 2005). To synthesize our analyses and results towards the re-activity index values, we sort the catalogues from the most re-active one to the least re-active, *i.e.* New Zealand, Wollongong, Australia, Yosemite, Val d'Arly and Grenoble, respectively (Table 3.9).

While the New Zealand and Grenoble end members are well defined, it appears more difficult to classify the intermediate re-active areas. Comparing New Zealand to Grenoble French Alps events, we switch from high to low clustering (as quantified from the η values), power law versus random daily rates, time and space clusters to uniform distribution, 50 km triggering distance towards null and strong correlations to any external forcing except temperature minima, to correlation with temperature alone (Table 3.9). From the most re-active landslide area to the least re-active area, the global trends of the different parameters are: i) decreasing departure from randomness; ii) decreasing maximum daily rates and area over which the trigger operates; iii) decreasing landslide triggering for landslides occurring one day apart: iv) decreasing global interaction with earthquake, rainfall and temperature (Table 3.9).

Table 3.9: *Synthesis of landslides re-activity for the 6 studied areas, from the most re-active landsliding area (New Zealand) to the least re-active one (Grenoble).*

	New Zealand	Wollongong	Australia	Yosemite	Val d'Arly	Grenoble
η (binary)	2.3 (1.5)	3.4 (1.3)	1.8 (1.3)	2.1 (1.8)	1.5 (1.4)	1.2 (1.2)
Daily rate power-law exponent	2.04	1.93	3.01	3.04		
Inter-event distances, $dt = 0$ (km)	0-50 (up to 200)	0-30	0-20 (up to 200)	0-40	0-10	2-3
Triggered landslides, $dt = 1$	+	-	+	+	-	-
Correlation to earthquake	++	-	+	+	-	-
Correlation to rainfall	++	++	+	-	+	-
Correlation to temperature	+	-	-	-	-	+

Chapter 4

Unified picture for aftershocks and earthquake-triggered landslides

4.1 Introduction

The triggering of seismic aftershocks in space and time is not well understood and there is still some controversy in seismology about the relative importance of static stress changes versus dynamic stress changes. Static stress changes correspond to the coseismic stress step induced by an earthquake (see Stein, 1999 for a review) whereas the dynamic stress changes are associated with the passing of the seismic waves (e.g. Gomberg et al., 2003, Johnson and Jia, 2005). Recently, studies focused on the linear aftershock density distribution and here also interpretations diverge. Felzer and Brodsky (2006) showed that for short times after the mainshock (down to 5 minutes), the decay of aftershocks as a function of distance is well fitted by a single power-law over distances ranging between 0.2 and 50 km. They suggested that the consistency of the trend indicates that the same triggering mechanism is working over the entire range. As static stress changes at the more distant aftershocks are negligible, the authors suggest that dynamic stresses may be triggering all aftershocks. Gomberg and Felzer (2008) took up those results and developed a model of earthquake triggering probabilities which gave the result that either peak strain alone or strain rates

averaged over the duration of the rupture may be responsible for aftershock triggering. By contrast, Lippiello et al. (2009), with the same aftershock database as Felzer and Brodsky (2006), found that the aftershock linear density is non-monotonic and exhibits a maximum that depends on the mainshock magnitude, followed by a power-law decay. They find an exponent value controlling the asymptotic decay equal to two and interpret it as indicating static stress triggering, while an exponent value of one would have indicated dynamic triggering. They conclude, after implementing static stress diffusion within a stochastic model for aftershock occurrence, that static stress diffusion is responsible of the spatio-temporal patterns of triggered aftershocks.

To our knowledge, only the dynamic triggering has been explored for earthquake-triggered landslides. Several authors showed that the intensity of landsliding (number of landslides, area affected by landslides, total volume of landslides, maximum landslide - epicenter distance, etc.) scales with earthquake magnitude, as reviewed by Keefer (2002). Keefer (2000), from his analysis of landslides triggered by the $M_W = 6.9$ Loma Prieta earthquake, showed an exponential decrease of landslide concentration (number of landslides per unit area) with increasing distance from the epicenter as well as a power-law decrease of landslide concentration with increasing distance from the surface projection of the fault plane. More recently, Dadson et al. (2004) showed a linear relationship between the area affected by landsliding and the vertical component of the Peak Ground Acceleration for the $M_W = 7.6$ Chi-Chi earthquake, while Meunier et al. (2007) showed a linear relationship between the density of co-seismic landslides and both the vertical and horizontal components of Peak Ground Acceleration for the $M_W = 7.6$ Chi-Chi earthquake and the $M_W = 6.7$ Northridge earthquake. In the last two cases, the studied variables (area affected by landsliding and density of co-seismic landslides) are a combination of two variables: the number of landslides and their respective areas, which are not independent and present a power-law correlation (e.g. Stark and Hovius, 2001, Guzzetti et al., 2002, Malamud et al., 2004).

In this chapter, we study the frequency - distance distributions of five landslide and aftershock crises triggered by five $M_W > 5.5$ earthquakes. We compare i) the landslide distance distributions with their aftershock distance distribution counterparts and ii) the 5 landslide - aftershock pairs with each other. These two comparisons are performed for different measures of distance to check their influence on the distribution patterns (distance to hypocenter, to epicenter, to surface fault projection, to actual or inferred surface fault trace). We then compare the landslide and aftershock distance distributions to the Peak Ground Acceleration, Peak Ground Velocity and Peak Ground Distance distributions for the Northridge and Chi-Chi earthquakes. We then test the dynamic triggering model of Gomberg and Felzer (2008). Last, we discuss the possible mechanisms driving landslide triggering for the five earthquake sequences, *i.e.* static and dynamic stress changes.

4.2 Data and Methods

Landslide catalogues were retrieved from airborne inspection or satellite images, depending on the earthquake sequence. When landslides were given as a polygon of the landsliding area extent, we retrieved the barycenter of this polygon as the location of the landslide. Several biases and missing data affect these catalogues, in terms of landslide occurrence time, landslide area/volume and spatial extent of landslide recovery.

Landslide time accuracy corresponds to the time delay between the earthquake occurrence and the landslide reconnaissance, for airborne inspection, and varies from one to seven days (Table 4.2). For remote sensing landslide reconnaissance, it corresponds to the delay between the pre- and post- earthquake satellite images and varies from five to seven months (Table 4.2). All recent landslides spotted from the landslide reconnaissance are supposed to be triggered by the mainshock earthquake. As there is only one landslide reconnaissance performed after a given mainshock, the role of aftershocks in triggering landslides cannot be assessed and the catalogues integrate the global landslide response. Second, there are no volume nor area estimates for all landslides, hence it is not possible to correct all landslide catalogues from their detection threshold. Comparison between

landslide rates at a given distance can therefore only be relative. Last, the Kashmir landslide reconnaissance was limited to a single SPOT 5 image. As landslide reconnaissance is often limited to the area of intense landsliding, landslides occurring at large distances from earthquakes may be missing. There is no quantitative evaluation of such a bias.

For aftershock data, there are two levels of accuracy: the USGS online catalogue gives a complete catalogue of $M > 4.8$ earthquakes worldwide while local earthquake catalogues, when available, give a complete catalogue of at least $M > 2.8$ earthquakes (Table 4.1). Such local catalogues were retrieved for the well-instrumented Taiwan, New Zealand and California areas, whereas the USGS catalogue was used for the Kashmir area. Note that the mainshock and aftershocks localisations are different when using the USGS and the local catalogue, and different mainshock localisations lead to different landslide - mainshock and aftershock - mainshock distance distributions (see also Appendix B).

Three criteria, one in time, one in space and one in magnitude, are used for the selection of aftershocks. In time, aftershocks are selected up to three days after the mainshock, in order to limit aftershock cascading. This also corresponds to the time interval in which most earthquake-triggered landslides would fail and therefore allows comparison between landslides and aftershocks. In space, aftershocks are selected within 10 times the ruptured fault length L ($L = f(magnitude)$, Wells and Coppersmith, 1994) as this corresponds to the average maximum distances where mainshocks are found to trigger aftershocks (e.g. Felzer and Brodsky, 2006). In magnitude, aftershocks are selected if their magnitudes are greater than or equal to the magnitude of completude M_c of the aftershock sequence, calculated by the method of Ogata and Katsura (1993).

There are several ways to define the aftershock - mainshock and landslide - mainshock distances. We compare distance patterns using i) distance to hypocenter, ii) distance to epicenter, iii) distance to the surface projection of the seismogenic fault passing through epicenter and iv) distance to the surface fault trace (Chi-Chi, Pakistan) or to the inter-

section of the seismogenic fault with the surface, as deduced from the location of the hypocenter and the dip of the fault plane (Fiordland, Northridge, Rotoehu) (Table 4.1). For the distances to the surface projection of the fault plane or to the surface fault trace, we model the considered fault as a 2D plane (intersection of the fault plane with the surface plane) whose length is equal to the length of the theoretical ruptured fault length, as computed from the magnitude using the equation of Wells and Coppersmith (1994).

Note that to keep data treatment coherent for all five sequences, we kept the calculated ruptured fault lengths as the actual fault lengths, even though Chi-Chi and Kashmir actual surface fault trace lengths are smaller than the calculated ones.

Peak Ground Accelerations (PGA), Peak Ground Velocities (PGV) and Peak Ground Displacements (PGD) physically corresponding to strain rate, strain, and displacement, respectively (Gomberg and Felzer, 2008), were retrieved online at http://peer.berkeley.edu/smcat/ for the Chi-Chi and Northridge mainshocks. For the other earthquake sequences, the accelerograph networks are not as dense as the Chi-Chi and Northridge ones and no such good quality data are available. Still, it is to be noted that for the Chi-Chi and Northridge earthquakes, the ground motion recording stations are not in the landsliding area (Fig. 4.2). Indeed accelerographs are usually set up in plains while landslides occur in topographic relief areas. Therefore the comparison between the ground motion observations and landslides can only be made on an average qualitative basis.

4.3 Characteristics of the 5 sequences

We compare aftershock space distributions with landslide space distributions triggered by five earthquakes for which databases are available: Chi-Chi M_W7.6 earthquake (Taiwan), M_W7.6 Kashmir earthquake (Pakistan), M_W7.2 Fiordland earthquake (New Zealand), M_W6.6 Northridge earthquake (California) and M_W5.6 Rotoehu earthquake (New Zealand) (*cf.* Tables 4.1 and 4.2).

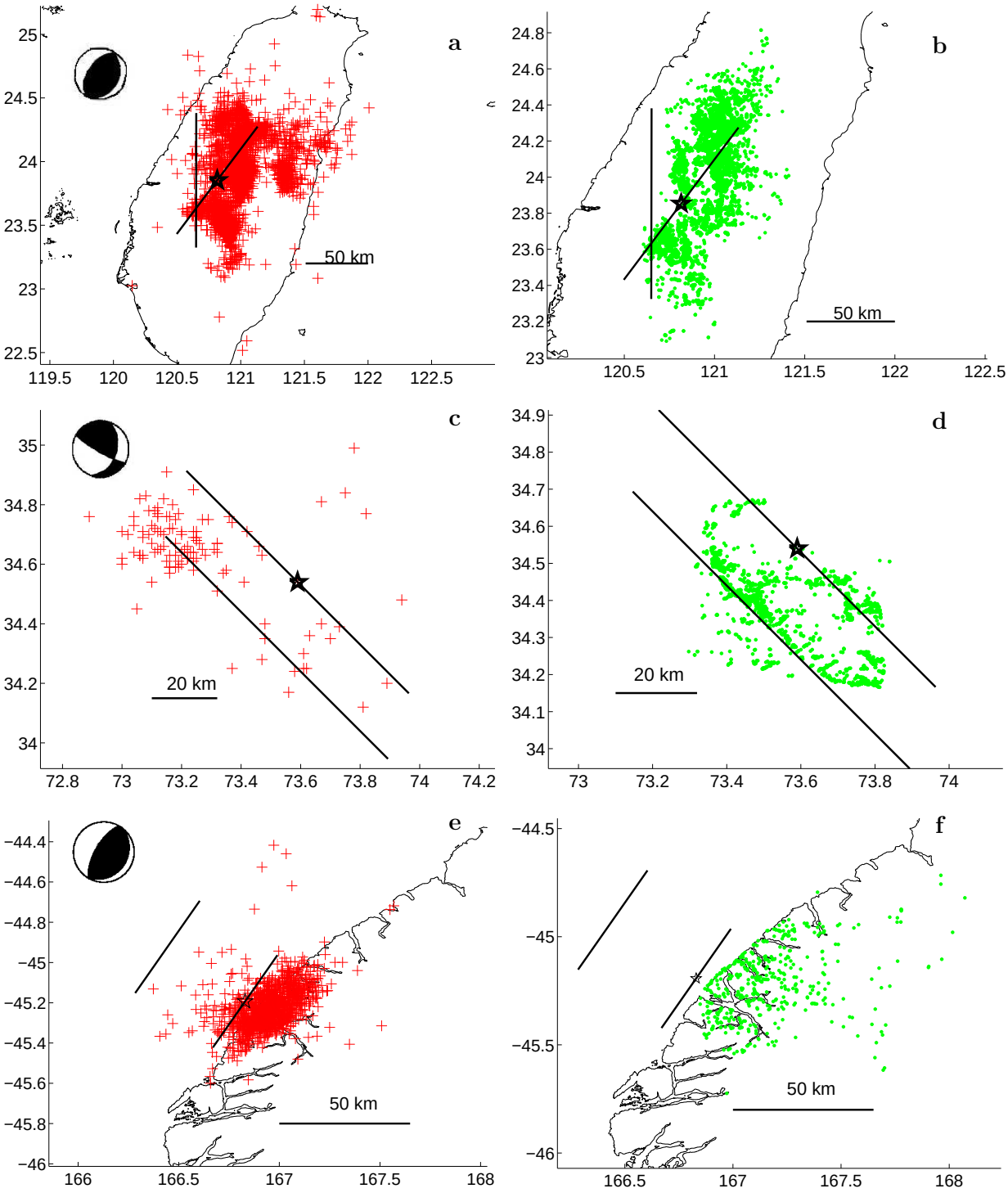
a
50 km
b
50 km
c
20 km
d
20 km
e
50 km
f
50 km

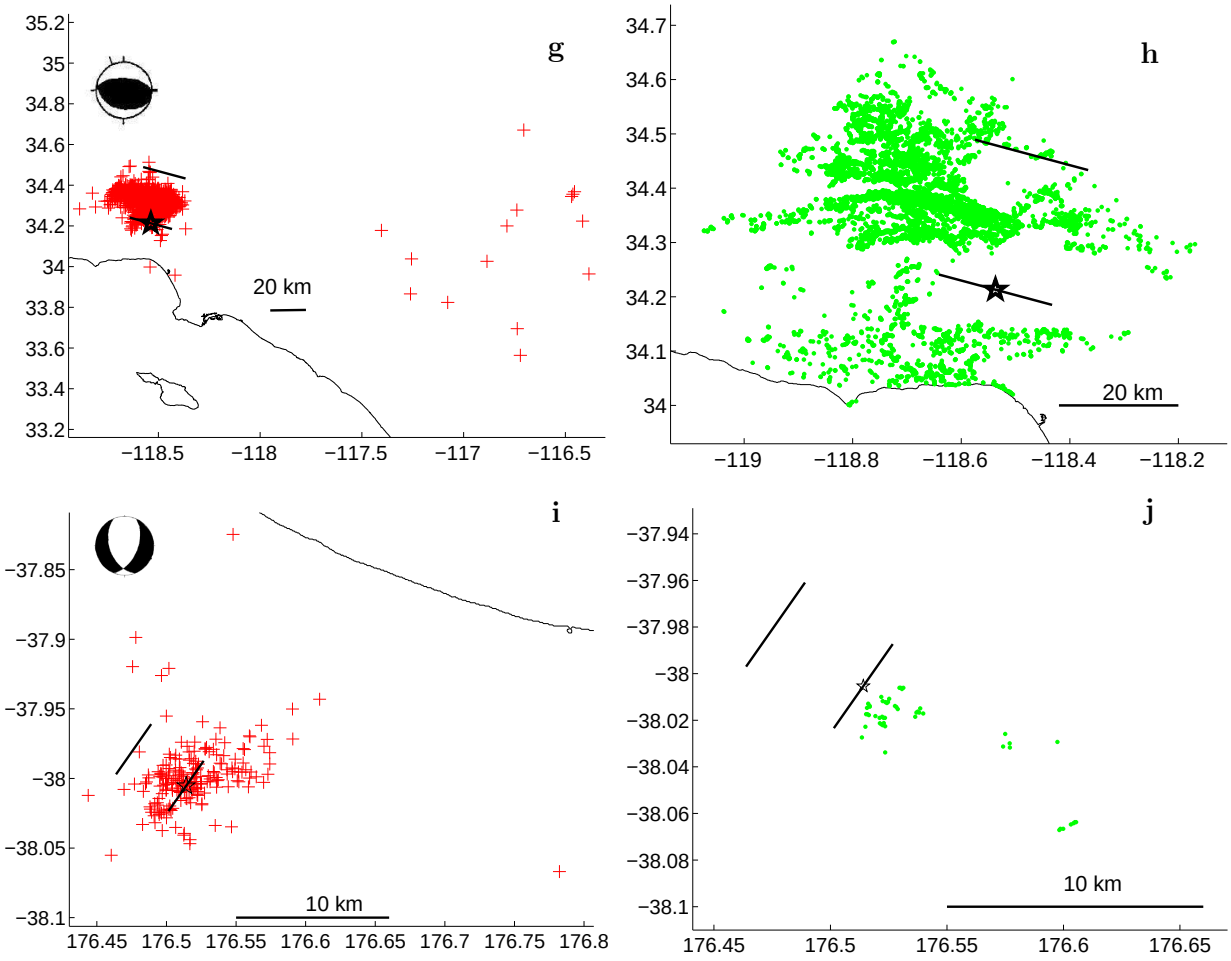

Figure 4.1: Aftershocks (red) and landslides (green) for the five earthquake sequences: M_W7.6 Chi-Chi earthquake aftershocks (a) and landslides (b); M_W7.6 Kashmir earthquake aftershocks (c) and landslides (d); M_W7.2 Fiordland earthquake aftershocks (e) and landslides (f); M_W6.6 Northridge earthquake aftershocks (g) and landslides (h) and M_W5.6 Rotoehu earthquake aftershocks (i) and landslides (j). Black star: epicenter, black line passing through epicenter: surface projection of the seismogenic fault, black line not passing through epicenter: actual or inferred surface fault trace.

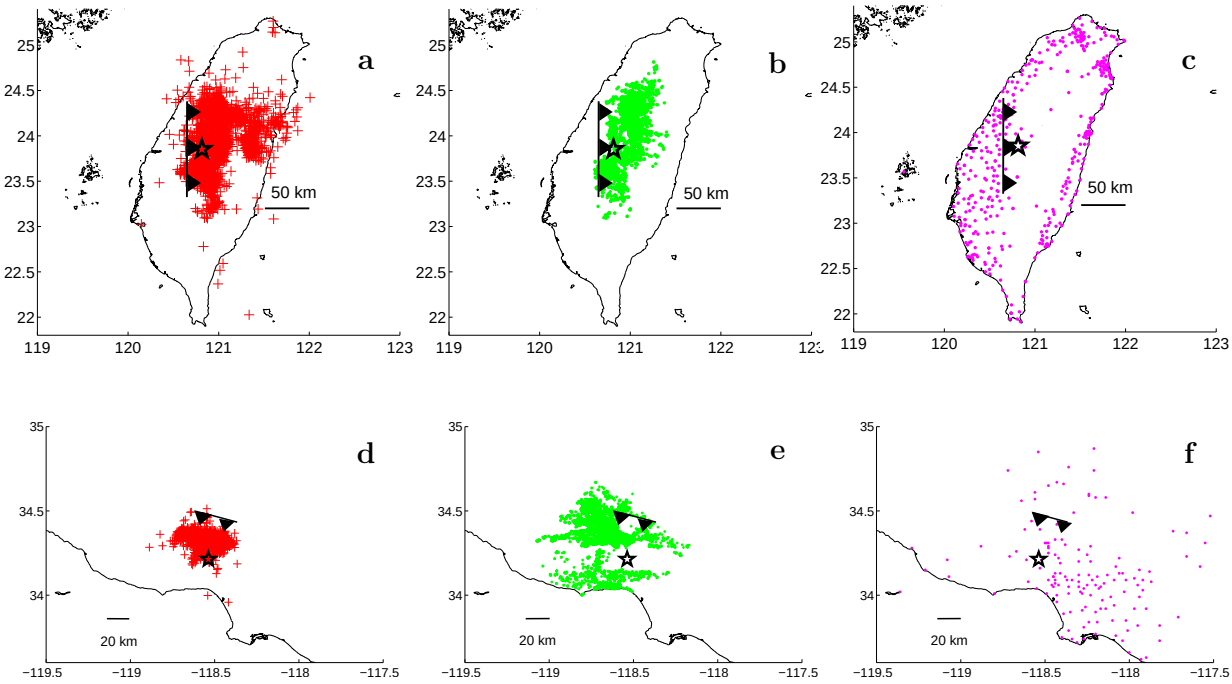

Figure 4.2: Location of aftershocks (red), landslides (green) and accelerographs (magenta). Chi-Chi earthquake (a-c) and Northridge earthquake (d-f). Black star: epicenter. Black line: surface fault trace (a-c) or inferred surface fault trace (d-f).

The M_w7.6 Chi-Chi earthquake occurred on 20 September 1999 in the western foothills of Taiwan. This inland thrust earthquake produced a surface break more than 80 km long along the Chelungpu fault (Zeng and Chen, 2001). The focal mechanism defines a mainshock with a depth of 8-10 km, a strike of N37° and a dip of 30° SE (Zeng and Chen, 2001). The associated 80 km long surface rupture strikes North-South, evidencing a strike-slip component. The Chi-Chi earthquake is characterised by low Peak Ground Acceleration and high Peak Ground Velocities (Tsai and Huang, 2000). More than 9000 landslides were mapped by the National Science and Technology Centre for Disaster Prevention using 20 m resolution SPOT satellite images taken one week after the mainshock occurrence. 90% of the landslides occurred on slopes steeper than 45° , preferentially oriented to the south, southeast and southwest (Liao and Lee, 2000).

The M_W7.6 Kashmir earthquake occurred on 8 October 2005 in the northwestern part of the Himalayas. It produced a surface break more than 75 km long along the Balakot-

Garhi fault. The mainshock hypocenter displays a thrust focal mechanism, with a fault striking N135°, a dip of 29° NE and a depth of 11 km (Avouac et al., 2006). This earthquake triggered more than 2000 landslides, mapped from a 2.5 m resolution SPOT 5 stereo images taken 12 and 19 days after the mainshock occurrence (Sato et al., 2007). Note that the landslide recording was limited to the extent of the stereo image. 70% of the landslides occurred on slopes inclined between 25 and 45°, preferentially oriented to the south and southwest (Sato et al., 2007). Rainfall conditions were drier than usual, with a particularly weak monsoon (Petley et al., 2005).

The M_W7.2 Fiordland earthquake occurred on 22 August 2003, ten kilometers offshore of the southwest of the South Island (New Zealand). It did not occur on the Alpine fault but involved thrusting along the shallow part of the underlying subduction interface between the Australian and Pacific plates. McGinty and Robinson (2007) proposed a fault model presenting two segments (a deeper one with a dip of 23° SE continued by a second one with a dip of 35° SE), striking N35°. This earthquake triggered more than 400 landslides, involving coarse crystalline rocks, on 35 - 60° slopes or greater, with 62% of slopes facing north-northeast to south-southwest and 20% of slopes facing north to northwest (Hancox et al., 2003). The airborne landslide reconnaissance was undertaken from 3 to 7 days after the earthquake (Hancox et al., 2003).

The M_W6.6 Northridge earthquake occurred on 17 January 1994 on a blind thrust fault below the San Fernando valley, southern California. The mainshock hypocenter was 19 km deep, with a 35° SSW dip and N105° strike (Hauksson et al., 1995). This earthquake, situated more than 10 km from any topographic relief, triggered more than 11,000 landslides. The landslide reconnaissance was carried out on the day of the earthquake thanks to high-altitude aerial photography. 69% of the recorded landslides occurred on slopes between 20 to 40° and involved weakly cemented clastic sediments (Harp and Jibson, 1996). Rainfall in the Northridge area was lower than usual before the earthquake (Harp, personal communication, September 2009).

The M_W5.6 8.5 km depth Rotoehu earthquake occurred on 18 July 2004 in the Taupo Volcanic Zone (New Zealand). The normal focal mechanism dips 61° SE and has stress pat-

Table 4.1: *Aftershock databases.*

	Chi-Chi[a]	Kashmir[b]	Fiordland[c]	Northridge[d]	Rotoehu[e]
Date	20 Sep 1999	8 Oct 2005	22 Aug 2003	17 Jan 1994	18 Jul 2004
Catalogue	Local	USGS	Local	Local	Local
M_c [f]	2.72 ± 0.04	4.84 ± 1.46	2.77 ± 0.07	1.90 ± 0.06	2.48 ± 0.15
M_W	7.6	7.6	7.2	6.6	5.6
Depth (km)	8-10	11	24	17.5	5
Focal mechanism	thrust	thrust	thrust	thrust	normal
Strike surface fault	N-S	N135			
Strike focal mechanism	N37	N135	N35	N105	3N5
Dip [g]	29-30SE	29NE	23-35SE	35SSW	61SE
Surface rupture (km)	80	75	No	No	No
Specificity of mainshock	Low PGA High PGV		offshore	10 km from topography	

[a]Characteristics of earthquake data from Tsai and Huang (2000); Zeng and Chen (2001)

[b]USGS earthquake database online at http://neic.usgs.gov/, characteristics of earthquake data from Avouac et al. (2006)

[c]Local earthquake database online at http://magma.geonet.org.nz/, characteristics of earthquake data from Reyners et al. (2003), McGinty and Robinson (2007)

[d]Local earthquake database online at http://neic.usgs.gov/, characteristics of earthquake data from Hauksson et al. (1995) and Wald et al. (1996)

[e]Local earthquake database online at http://magma.geonet.org.nz/, characteristics of earthquake data from Hurst et al. (2008)

[f]calculated thanks to the method of Ogata and Katsura (1993)

[g]from seismic/geodetic inversion

terns consistent with the extension of the Taupo Volcanic Zone in a northwest-southwest direction (Hurst et al., 2008). The earthquake triggered more than 40 landslides in unconsolidated pyroclastics and tephra deposits, preferentially affecting 45 to 75° slopes facing south and east. The airborne landslide reconnaissance took place from 1 to 6 days after the earthquake (Hancox et al., 2004). Conditions were particularly wet at the time of the earthquake occurrence, as it rained more than 220 mm in the three preceding days (Hancox et al., 2004).

Table 4.2: *Landslide databases.* Δt *relates to the time delay between the mainshock and the landslide recovery.*

	Chi-Chi[a]	Kashmir[b]	Fiordland[c]	Northridge[d]	Rotoehu[e]
Measurement	20 m SPOT images	2.5 m SPOT images	Airborne inspection	High-altitude aerial photography (1:60,000)	Airborne inspection
Δt (days) after mainshock	6-7	12, 19	3-7	0	1-6
Δt (days) before mainshock	5 months	7 months			
N landslides	9272	2424	459	11,111	45
V_{max} (m^3)	125 10^6	80 10^6	7 10^5	8 10^6	3-5 10^3
Geology	Heterogeneous	Heterogeneous	coarse crystalline rocks	weakly cemented clastic sediments	Unconsolidated pyroclastics and tephra deposits
Rainfall before earthquake	Average	Below average	Average	Below average	Above average (223-312 mm 3 days before)
Slopes (°)	90% >45	70% 25-45	35-85	69% 20-40	45-75
Preferred orientation	S, SE, SW	S, SW	N, NW	no data	S, E

[a]Characteristics of landslide data from Liao and Lee (2000), Lin et al. (2003), Khazai and Sitar (2004) and Chen and Wan (2004)

[b]Characteristics landslide data from Sato et al. (2007), Harp and Crone (2006) and Petley et al. (2005)

[c]Characteristics of landslide data from Hancox et al. (2003)

[d]Characteristics of landslide data from Harp and Jibson (1996)

[e]Characteristics of landslide data from Hancox et al. (2004)

4.4 Results

4.4.1 Landslide and aftershock distance distributions

Most, if not all, of the landslides and aftershocks for the five sequences occurred on the hanging wall. The actual or inferred surface fault is a good boundary delimitating landslide and aftershock occurrences (Figure 4.1). There is a good overlap of the landslide distance distributions and their aftershock distance distribution counterparts, for all five sequences (Fig. 4.3). This result is robust whatever the type of distance distribution is used (to hypocenter, to epicenter, to fault surface projection, to actual or inferred surface fault trace). The differences in geologic setting and mainshock characteristics do not influence the overlap between each landslide and aftershock distance distribution pairs. However, there are second order differences between those five pairs. In the near-field, *i.e.* for distances less than the ruptured fault length, we find large differences between the landslide and aftershock distributions for the Fiordland and Northridge sequences (Figures 4.3 to 4.6). These differences primarily arise from the mainshock locations: offshore for the Fiordland sequence, in the plains for the Northridge sequence, where no landslides can occur. In addition, we find aftershocks to be triggered further away than landslides for the Chi-Chi and Kashmir events. For the 3 other sequences, we find that, in average, landslides are triggered further away than aftershocks. The extreme distances are still found for aftershocks, however.

Each landslide-aftershock pair appears as specific to a given mainshock (Figs 4.3, 4.4). When comparing landslide and aftershock distances to surface fault distributions between the five sequences, we find 3 different patterns: i) increase then decrease of events with distance (Fiordland, Northridge, Rotoehu); ii) plateau followed by a decrease of events (Chi-Chi) or iii) decrease of the number of events with distance (Kashmir). The exponent values controlling the asymptotic decay vary from one (Kashmir events) to three or larger than three for most events (refer to Appendix C) for landslide and aftershock discrete

distance distributions and for the estimation of exponent values.

In order to remove the local effects which possibly drive the differences between the five landslide - aftershock pairs, we restrict our analysis to events occurring on the hanging wall, bounded by a width equal to the ruptured fault length (Fig. 4.4, middle and right). There are no major differences in the distance distributions when using all events or the events restricted to the hanging wall and therefore the specificities for each landslide - aftershock pairs are kept.

We then check the influence of the mainshock magnitude by normalising the distances by the earthquake dimension, *i.e.* the ruptured fault length L (with L=f(M), Wells and Coppersmith, 1994) (Figs 4.7b and 4.8b). For both aftershock and landslide distance distributions, $M_w < 7.5$ peak values of aftershock and landslide rates collapse close to one fault length. The two M_w 7.6 mainshocks triggered landslides and aftershocks at much shorter distances than expected from their magnitude and the landslide and aftershock distributions do not collapse with the $M_w < 7.5$ landslide and aftershock distance distributions. We perform the same scaling on the distance distributions of events situated on the hanging wall, within the width of the ruptured fault length, and find the same results (Figs 4.9b and 4.10b).

4.4.2 Ground motions and triggered landslide and aftershock space distributions

We compare landslide and aftershock distributions to ground motion observations (Peak Ground Acceleration, PGA; Peak Ground Velocity, PGV; Peak Ground Displacement, PGD) for the Chi-Chi and the Northridge sequences.

For distances smaller than 0.5 (Chi-Chi sequence) and 1 (Northridge sequence) times the fault length, we find a monotic decrease for the Chi-Chi PGA and the Northridge PGA, PGV and PGD, a plateau for the Chi-Chi PGD and an increase for the Chi-Chi PGD. For these distances, the number of landslides and aftershocks increase with distance for both the Chi-Chi and Northridge sequences (Figs 4.11 and 4.12).

For distances larger than 0.5 (Chi-Chi sequence) and 1 (Northridge sequence) times the fault length, we find a monotic decrease of the Chi-Chi and Northridge PGA, PGV and PGD as well as a monotic decrease of the landslide and aftershock distance distributions. The exponent values controlling the asymptotic decay are different for ground motion observations and landslide and aftershock distance distributions, except for the Chi-Chi PGD and the Chi-Chi landslide and aftershock distributions (Figs 4.11 and 4.12). Hence the Chi-Chi PGD is the parameter presenting the best qualitative fit to both the Chi-Chi landslide and aftershock distance distributions.

We further test the scalings proposed by Gomberg and Felzer (2008), empirically found from the PGA, PGV and PGD values of 22 Japanese earthquakes with $3.0 < M < 6.0$. The authors propose a scaling with hypocentral distance r and mainshock rupture dimension D being $r^2 \times D^{-1.4}$ for PGA, $r^{1.8} \times D^{-1.6}$ for PGV and $r^{1.5} \times D^{-1.8}$ for PGD. If aftershocks or landslides are triggered by PGA, PGV or PGD, we expect these scalings to remove dependence on r and D of the aftershock and landslide distance distributions. This method has the advantage of testing the PGA, PGV and PGD influences on triggering, without the actual PGA, PGV and PGD values. Note that these scalings were performed on hypocentral distances by Gomberg and Felzer (2008), and this is the reason why we use such distances for testing the scalings.

We resolve a mixed response to the proposed scalings on the Chi-Chi and Northridge PGA, PGV and PGD values, with a tendency to over-correct the values for the two sequences (Fig. 4.13). Nevertheless, on average, scaled PGA, PGV and PGD values cover a smaller order of magnitude than non-scaled values. We find a mixed response to the proposed scalings on the five landslide and aftershock distance distributions as well (Fig. 4.14). Here also, the dependence on r and D is not completely removed for the distance distributions.

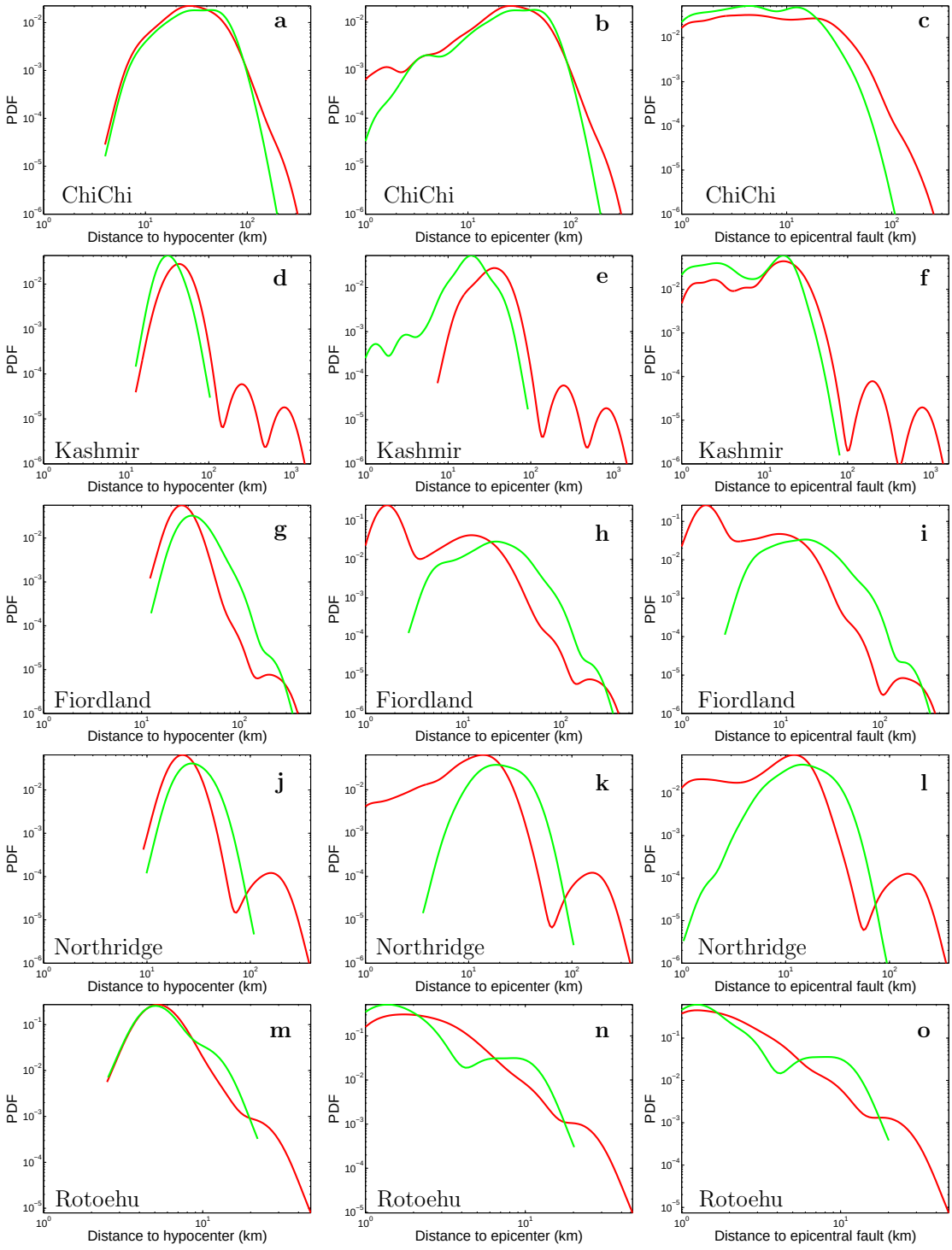

Figure 4.3: Aftershock-mainshock (red curves) and landslide-mainshock (green curves) distance Probability Density Functions (PDF). Left: Distance to hypocenter, Middle: Distance to epicenter, Right: Distance to seismogenic fault through epicenter for the five events. The PDF were computed using a log binning and then convolved with a gaussian kernel, e.g. Izenman (1991).

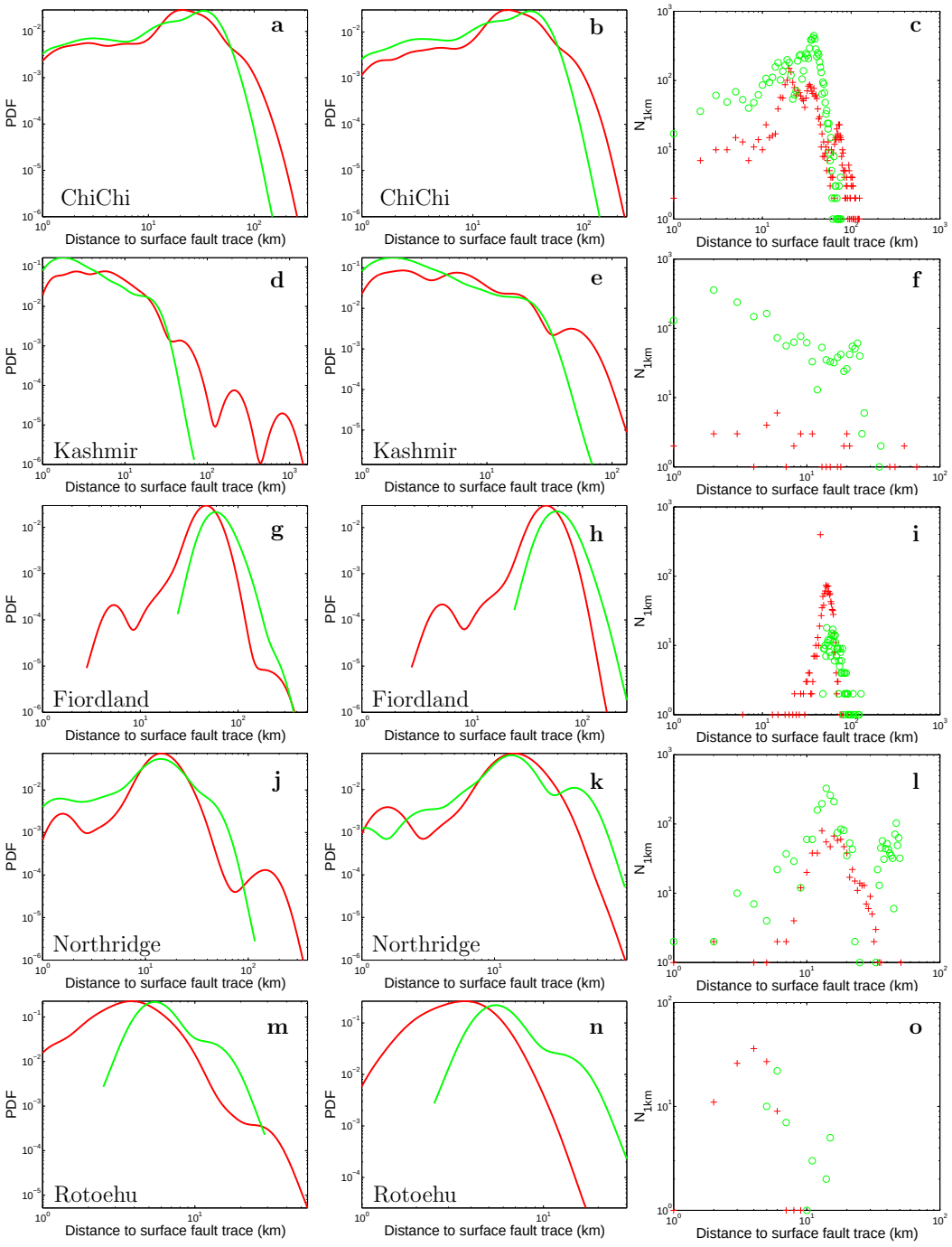

Figure 4.4: Aftershock-mainshock (red curves) and landslide-mainshock (green curves) distance Probability Density Functions (PDF) and discrete distribution. Left: Distance to actual (Chi-Chi and Kashmir) or inferred (Fiordland, Northridge, Rotoehu) surface fault trace. Middle: Distance to actual or inferred surface fault trace, for the events on the hanging wall, bounded to the width of the ruptured fault length. Right: same than middle graphs, discrete distribution. The PDF were computed using a log binning and then convolved with a gaussian kernel, e.g. Izenman (1991).

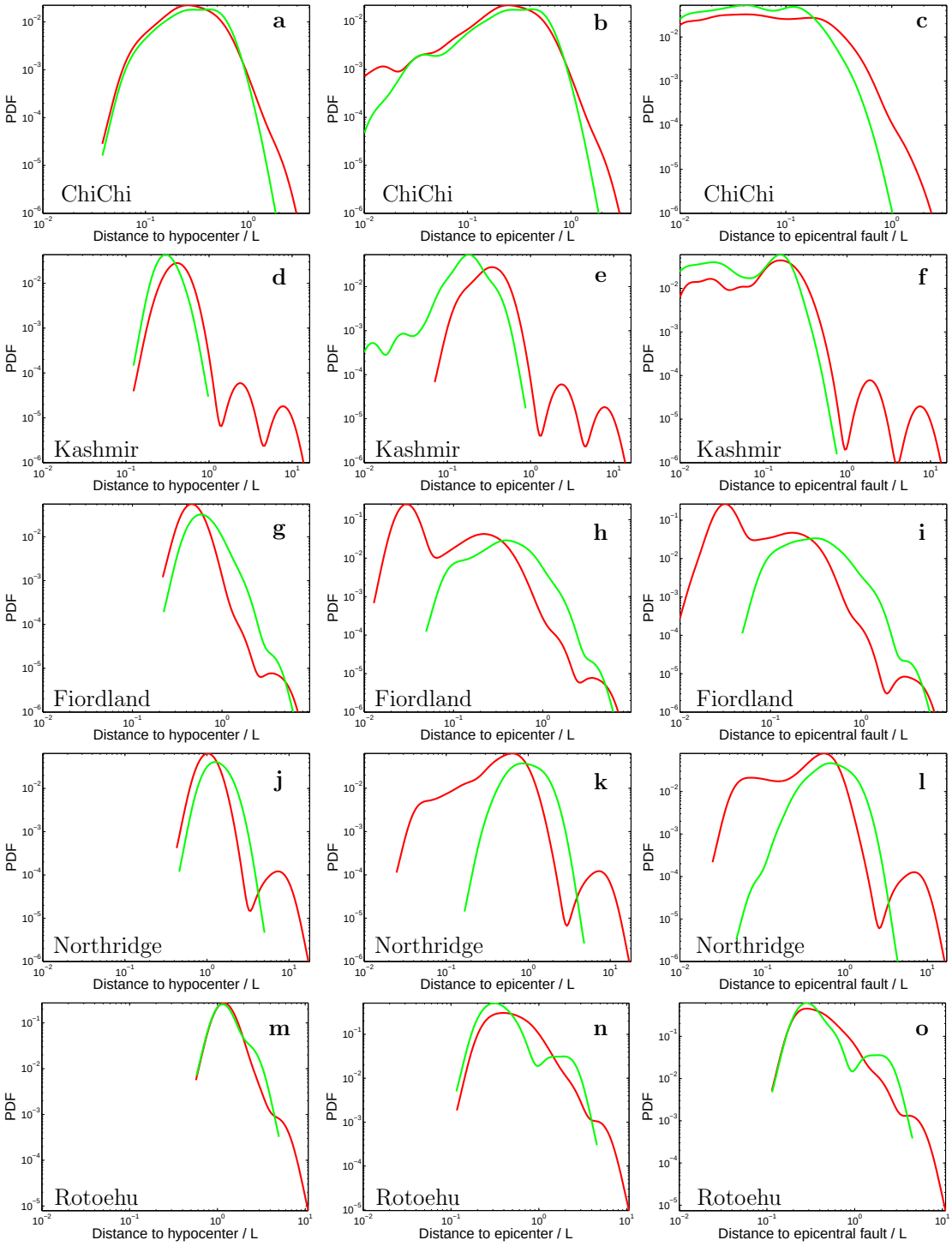

Figure 4.5: Same as Figure 4.3, for distances normalised by the earthquake dimension, *i.e.* the ruptured fault length.

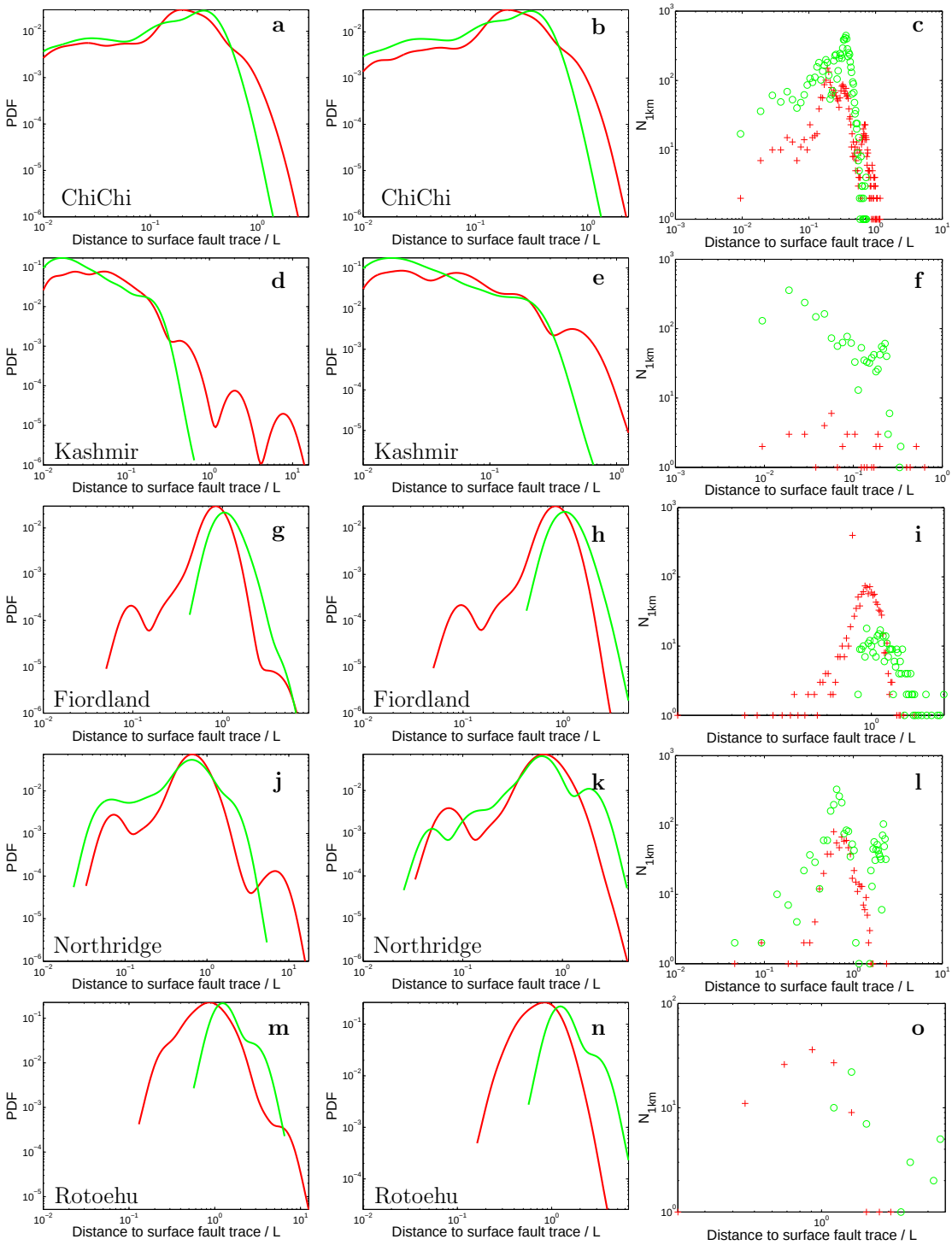

Figure 4.6: Same as Figure 4.4, for distances normalised by the earthquake dimension, *i.e.* the ruptured fault length.

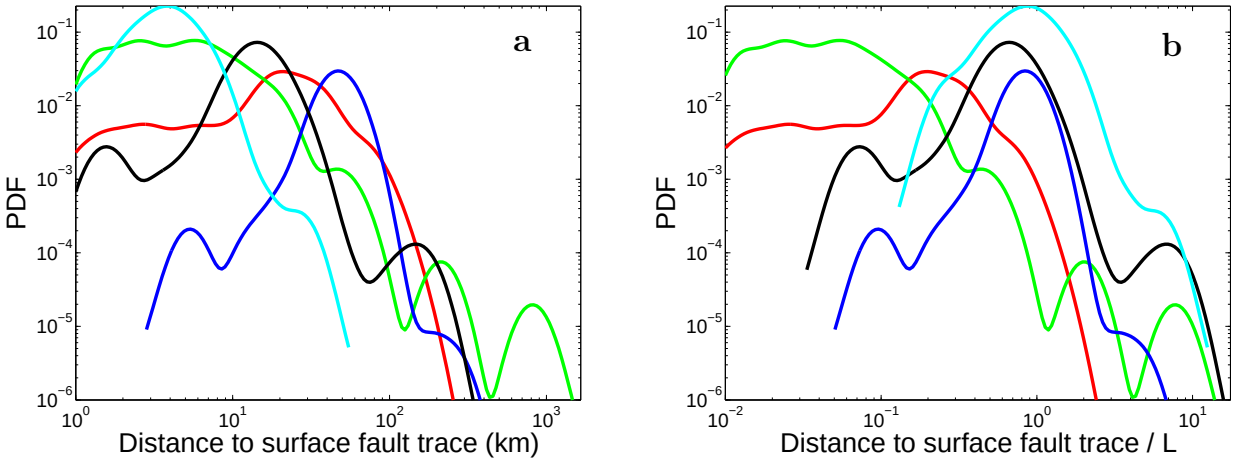

Figure 4.7: Distribution of aftershock distances. a) Distance to surface fault trace; b) Distance to surface fault trace normalised by the dimension of the earthquake, *i.e.* the ruptured fault length. Red curve: Chi-Chi earthquake, green curve: Kashmir earthquake, blue curve: Fiordland earthquake, black curve: Northridge earthquake, cyan curve: Rotoehu earthquake.

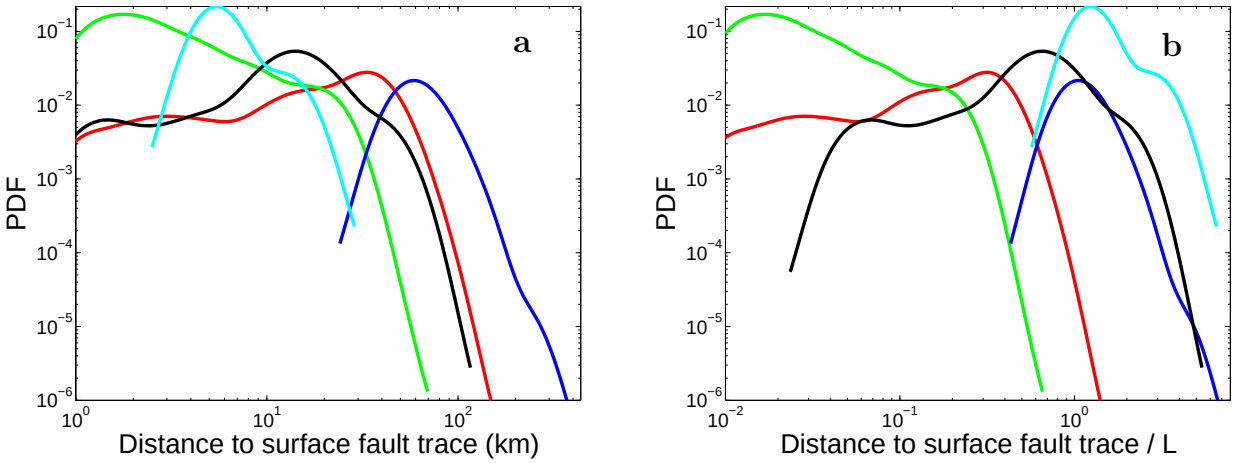

Figure 4.8: Distribution of landslide distances. a) Distance to surface fault trace; b) Distance to surface fault trace normalised by the dimension of the earthquake, *i.e.* the ruptured fault length. Red curve: Chi-Chi earthquake, green curve: Kashmir earthquake, blue curve: Fiordland earthquake, black curve: Northridge earthquake, cyan curve: Rotoehu earthquake.

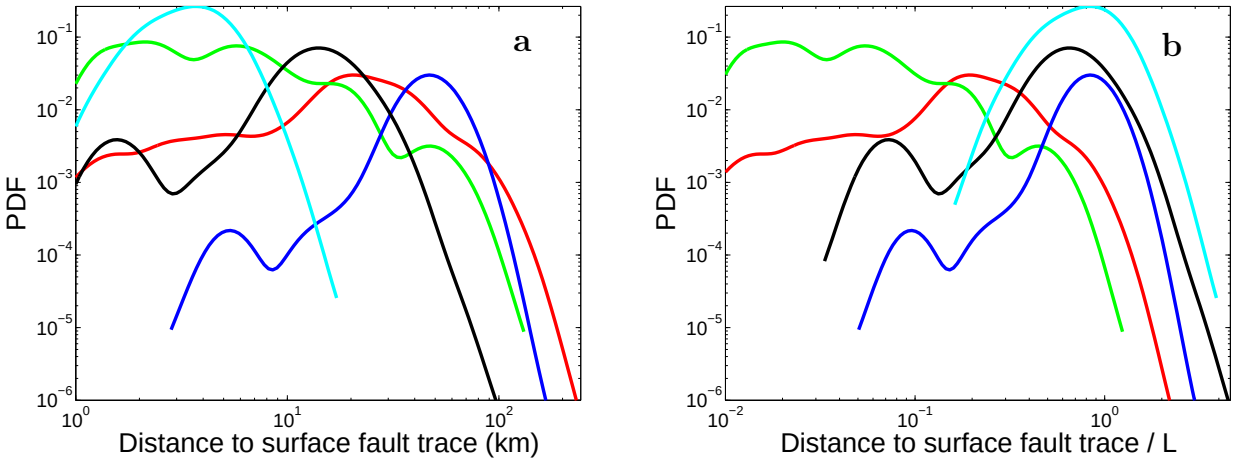

Figure 4.9: Same as Figure 4.7, for the aftershocks which occurred on the hanging wall, within the width of the ruptured fault length.

4.5 Discussion

Landslide distance distributions display similar patterns to their aftershock distance distribution counterparts, for the five sequences we studied. This result is robust whatever the type of distribution chosen: to hypocenter, to epicenter, to surface projection of the fault, to actual or inferred surface fault trace and for both all events and events on the hanging wall, bounded to the width of the ruptured fault length. We suggest that landslide and aftershock triggering is driven by the same mechanisms *i.e.* dynamic and static stress changes. For most landslide and aftershock distance distributions, we found asymptotic decays with an exponent larger than 3. The exponent values do not favor either dynamic triggering (theoretical exponent equal to 1) or static triggering (theoretical exponent equal to 2).

As dynamic triggering is the mechanism responsible for large distance aftershock triggering (e.g. Felzer and Brodsky, 2006) and aftershocks were triggered further away than landslides for the five sequences, we can deduce that dynamic triggering is more efficient in triggering aftershocks than landslides. Note that we checked that topography was available for triggering landslides in the areas where the larger distance aftershocks were triggered. However, landslides which occurred far away from the epicenter could have been missed

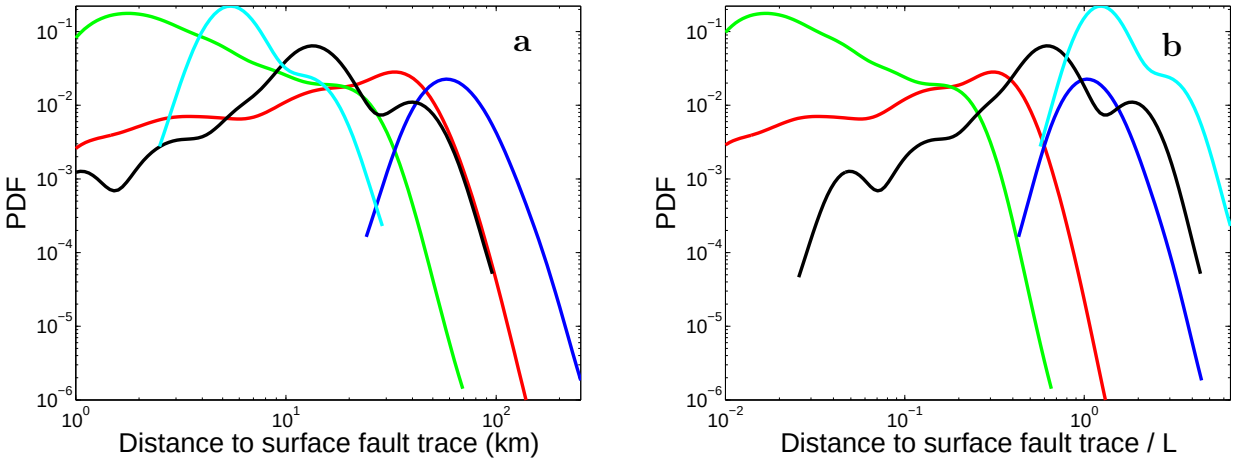

Figure 4.10: Same as Figure 4.8, for the landslides which occurred on the hanging wall, within the width of the ruptured fault length.

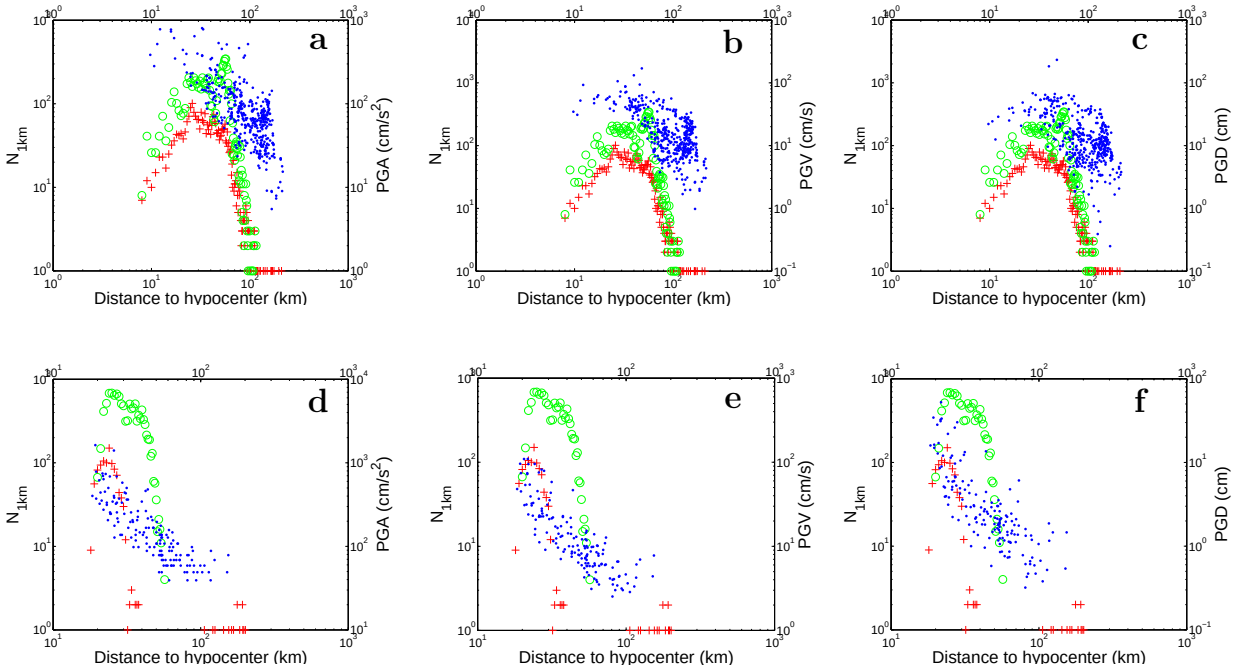

Figure 4.11: Aftershock (red), landslide (green) and ground motion (blue) hypocentral distance distributions (one kilometer bins) for Chi-Chi (a-c) and Northridge (d-f) earthquakes. Left: PGA, Middle: PGV, Right: PGD.

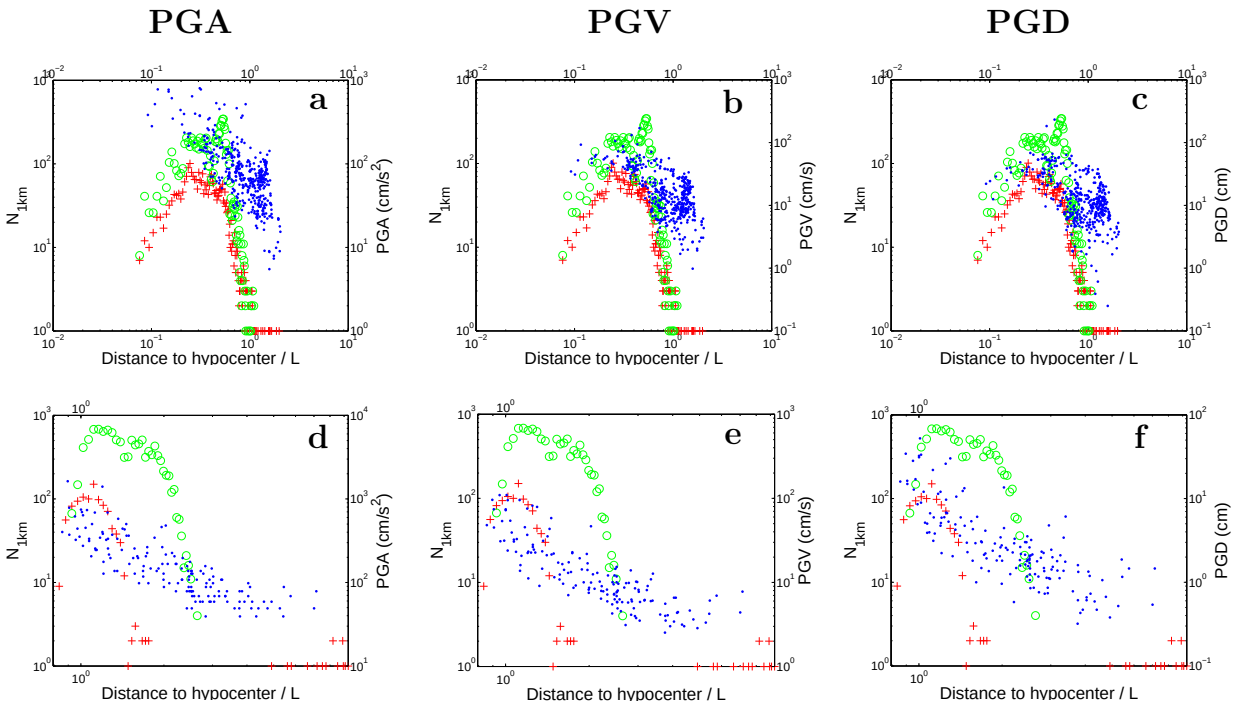

Figure 4.12: Same as Figure 4.11, for distances normalised by the earthquake dimension, *i.e.* the ruptured fault length.

during the landslide reconnaissances and future reconnaissances after large earthquakes should encompass distances at least as far as ten times the ruptured fault length from the fault (the distance up to which aftershocks are known to be triggered, Felzer and Brodsky, 2006). The near-field behaviour between aftershock and landslide distance distributions is either roughly similar or strongly influenced by the available topography. Therefore we cannot deduce from near-field specifics any difference in landslide and aftershock triggering.

Each landslide - aftershock pair appears as specific to a given mainshock. These heterogeneities can be due to the triggering mainshock characteristics and/or to the local geological and weather conditions. From the analysis of the five sequences, we find that the two surface-rupturing earthquakes display different distance distribution patterns to the three buried earthquakes.

For distances less than 0.5 times the fault length, the two surface-rupturing earthquakes triggered relatively more aftershocks and landslides than the non-surface-rupturing earth-

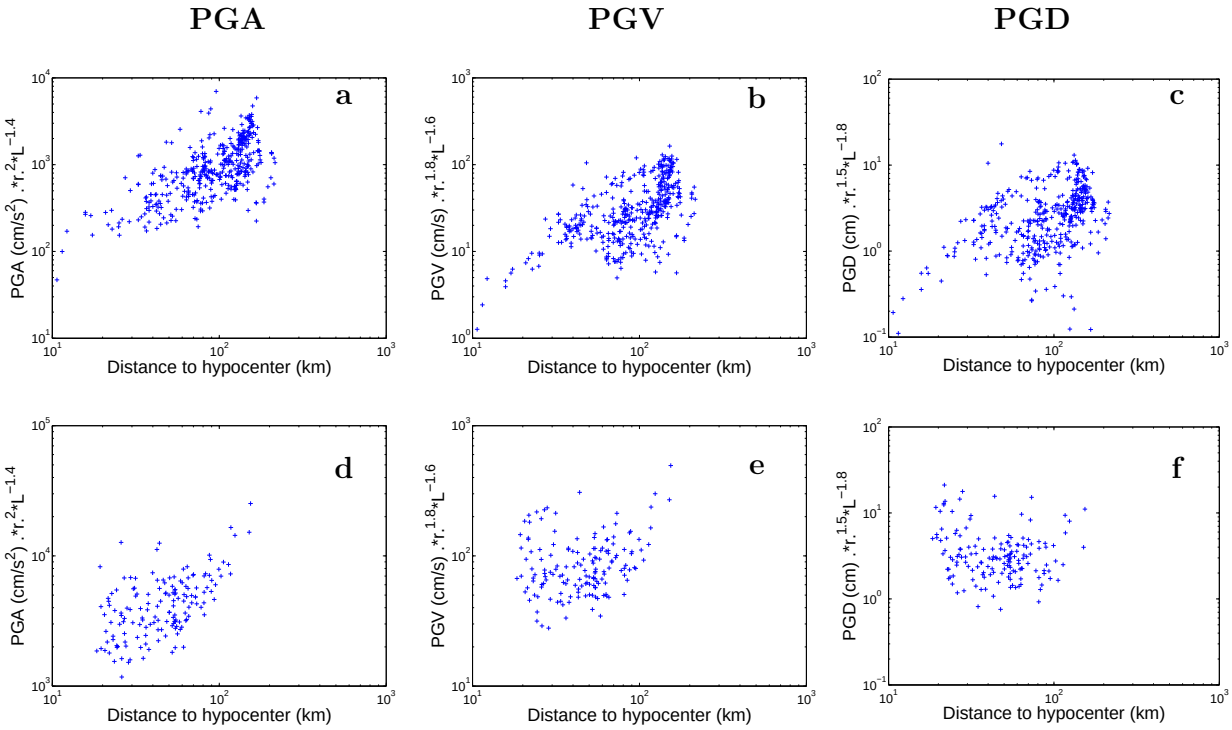

Figure 4.13: Scaled PGA (left), PGV (middle) and PGD (right) values from Gomberg and Felzer (2008) model for the Chi-Chi earthquake (a-c) and the Northridge earthquake (d-f).

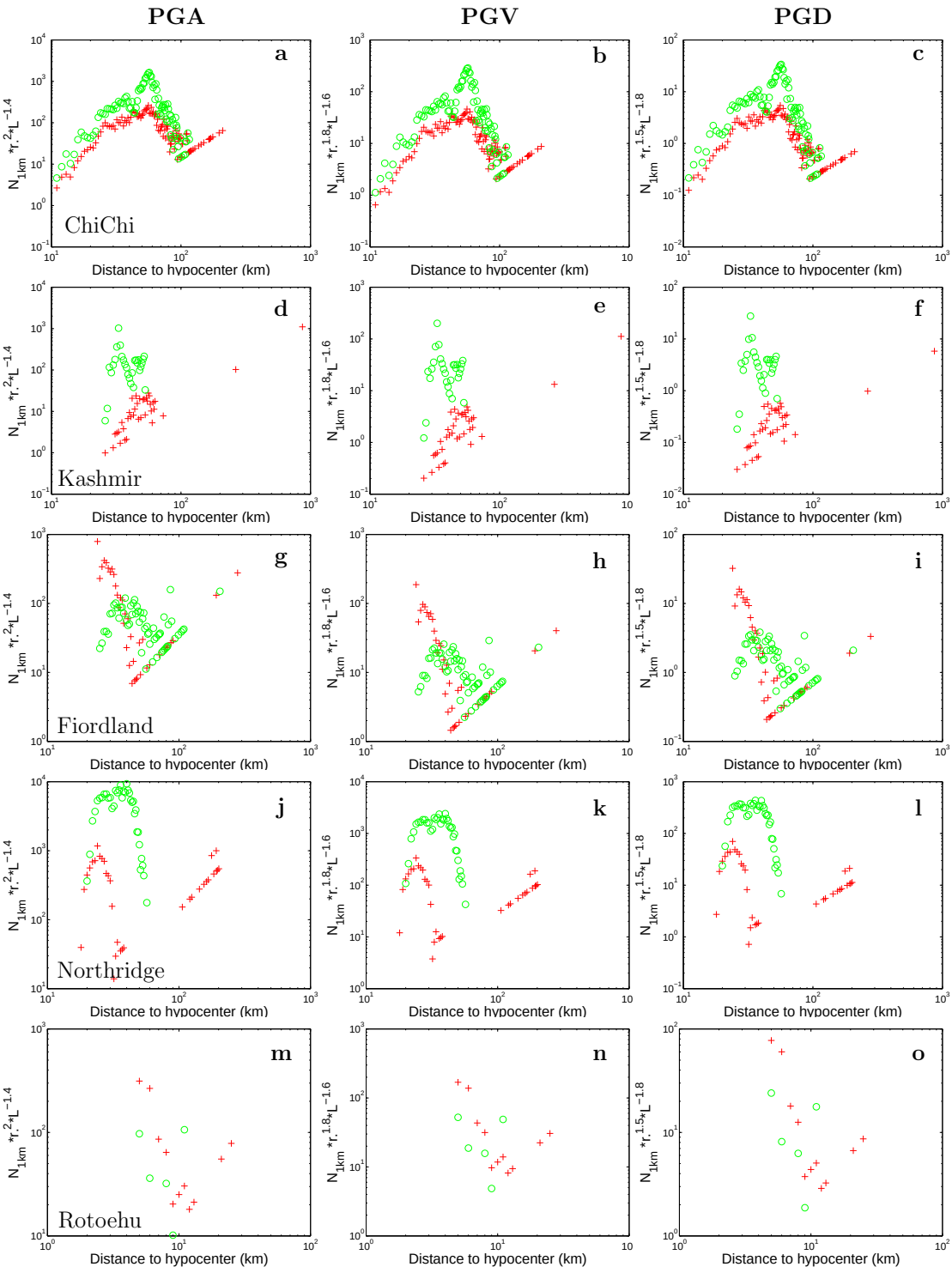

Figure 4.14: Aftershock-mainshock (red crosses) and landslide-mainshock (green circles) distances from the actual or inferred surface fault trace, for 1 km bins. Left: scaling with PGA, Middle: scaling with PGV, Right: scaling with PGD.

quakes. In addition, for distances less than 0.1-0.2 times the fault length, we find a plateau of the number of aftershocks for distances calculated to the surface fault trace for the two surface-rupturing earthquakes (Figs 4.6 and 4.7b). For the three buried earthquakes, still for distances calculated to the inferred surface fault trace, we find an increase followed by a decrease of the number of aftershocks, with the maximum of aftershocks being at a distance of one fault length (Fig. 4.7b). The fact that we do not find the same aftershock distance patterns for distances to surface fault trace for the surface-rupturing earthquakes and the non-surface-rupturing earthquakes suggests a difference in the mechanisms driving aftershock triggering in the two cases. It is important to note that we find the same patterns for landslide distance distributions but these results cannot be interpreted in terms of landslide triggering mechanisms as the lack of landslides in the near-field is primarily associated to the absence of topography for both the Fiordland and Northridge areas.

For distances more than 0.5 times the fault length, the two surface-rupturing earthquakes triggered landslides and aftershocks at shorter distance than expected from their magnitudes (Figs 4.7b and 4.8b). If we consider ground motion to drive aftershock and landslide triggering, then this result is not in agreement with Pitarka et al. (2009) who showed that surface-rupturing earthquakes generated weaker near-fault ground motion than buried earthquakes, while at larger distances the tendency was reversed.

The local conditions appear to influence the landslide and the aftershock distance distributions. Indeed, the two end-members of the distance distributions, Kashmir and Rotoehu landslides and aftershocks, are associated with drier than usual and wetter than usual conditions, respectively (Figs 4.7, 4.8 and Table 4.2). The influence of rainfall in triggering both landslides and aftershocks has previously been demonstrated (see De Vita et al., 1998 for a reference list on landslide triggering by rainfall and Muço, 1999; Ogasawara et al., 2002 and Hainzl et al., 2006 for the influence of rainfall on earthquake triggering).

We find no linear scaling of the number of landslides with PGA for the Chi-Chi and Northridge sequences, unlike the linear scaling demonstrated between landslide density and PGA by Dadson et al. (2004) and Meunier et al. (2007). The PGA, PGV and PGD

empirical scalings of Gomberg and Felzer (2008) tested on the five landslide and aftershock distance distribution pairs only partially collapse the distributions (Fig. 4.14). These three scalings do not favor any of the three ground motion variables as driving the landslide and aftershock distance distributions. We find that the Chi-Chi Peak Ground Displacement is the ground motion which gives the best qualitative fit with Chi-Chi landslide and aftershock distance distributions (Fig. 4.11). In addition, the role of static stress changes is enhanced by the occurrence of most landslides and aftershocks on the hanging wall (Fig. 4.1). Indeed, Ma et al. (2005) showed that the maximum Coulomb stress changes (up to 2 bars) occurred on the hanging wall, for an idealized case of thrust for the Chi-Chi earthquake (Fig. 4.15). Nevertheless, all Chi-Chi landslides and aftershocks are not located within the zone of positive Coulomb stress changes. In the same way, we can extrapolate the Chi-Chi idealized thrust model to the three other thrust sequences. Here also, not all landslides and aftershocks are situated within the zone of positive Coulomb stress changes. Other mechanisms are known to influence landslides and aftershocks triggering. We already mentioned dynamic triggering, especially for the landslides occurring more than the ruptured fault length from the fault. Another phenomenon known to enhance landslide failure is site amplification. For instance, Sepúlveda et al. (2005) showed that the observed extensive rock sliding and falling at Pacoima Canyon, triggered by the M_W=6.6 Northridge mainshock, would not have been possible under unamplified seismic conditions.

To further constrain the static stress changes for landslide triggering, we investigate the orientation and angle of the slopes where landslides were preferentially triggered. Indeed, it is known that the static stress changes are maximal for optimally oriented faults, *i.e.* faults roughly parallel to the seismogenic fault and its conjugate (King et al., 1994; Stein, 1999; Xu et al., in press). We find that Kashmir, Northridge and Rotoehu landslides were indeed predominantly triggered on slopes whose angles were close to the seismogenic fault dip (see Tables 4.1 and 4.2). For the Chi-Chi and Fiordland earthquakes, we find that their seismogenic fault dips ($\sim 30^\circ$) are less steep than the slope angles where landslides were predominantly triggered (larger than 45° for both sequences). However, the slopes in the vicinity of the Fiordland earthquake (Hancox et al., 2003) and of the Chi-Chi earthquake

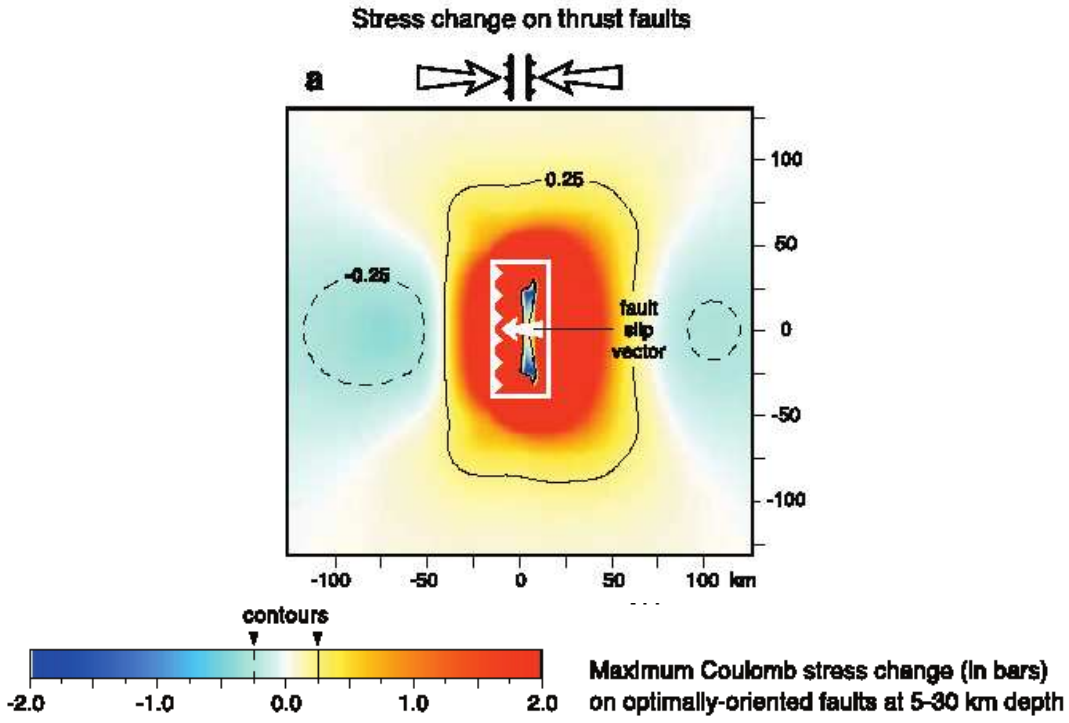

Figure 4.15: Maximum Coulomb failure stress change within the seismogenic crust for idealized Chi-Chi ruptures. The source is 78 km long and dips 29° E. Stress resolved on optimally oriented thrust faults with an E-W regional compression and a source rake of 90°. From Ma et al. (2005).

(Chen and Wan, 2004) are very steep, hence we cannot interpret these results.

In terms of slope orientations, we find that landslides were predominantly triggered on slopes whose orientations are similar to the fault dip direction for the Kashmir, Fiordland and Rotoehu sequences. However, we find no particular increase of landslide activity on slopes whose orientations are parallel to the conjugate of the seismogenic fault and the Chi-Chi sequence does not display similar landslide-prone slope orientations and fault dip direction. It is important to note that information on slope orientations is poor and it is difficult to further investigate this parameter.

Based on these results, we propose a simple model of landslide triggering by earthquakes. As landslides triggering seems to be mostly influenced by the static stress changes, earthquake-triggered landslides should mostly occur on optimally oriented planes. In compressive tectonic regime, earthquake-triggered landslides should occur preferentially on 30° slopes, whereas in extensional tectonic regime our model predicts earthquake-triggered landslides to occur on 60° slopes. Some complexity is added to this simple model when the actual topographic relief does not present the preferentially oriented slopes. Then the patterns predicted by our model must be connected to available slope angles. Last, this model needs to be tested on other earthquake-triggered landslide databases, especially with earthquakes presenting normal focal mechanisms, in order to validate it.

Conclusions and perspectives

First we review the main issues encountered while working with available landslide databases, as well as the strategies we developed to select coherent catalogues from these databases and to assess our results as robust. We then summarize possibilities offered by instrumentally recorded landslide catalogues and the limitations of these catalogues. Next, we synthesize the main results obtained from this study and their implications. Finally, we focus on some results needing further investigation: evapotranspiration as a plausible candidate to the anti-correlation of New Zealand landslides to temperatures, the differences in landsliding activity for Grenoble, Val d'Arly and Yosemite areas, and static stress changes triggering of earthquake-triggered landslides.

Landslide databases

The landslide databases we used are unique as there are very few available rockfall and landslide databases with a two days temporal accuracy and covering periods of time longer than 1 year. These databases suffer from several biases as they were gathered from human observations (see also Appendix D for our recommendations on the needed information from a landslide database). In time, the accuracy is driven by the frequency of the visits to the studied site by a landslide-aware community (Dussauge et al., 2003). In space, accuracy is dependent on the population distribution and extent of urbanized areas (Glade, 1998). Landslides occurring in remote uninhabited areas, or occurring in areas where no particular attention is paid (unlike aerial reconnaissance after $M > M6$ earthquake or

high rainfall for example), will be missing from the databases. Last, volumes are either not recorded or only roughly estimated, as quantifying tools were not used (Dussauge et al., 2003). Therefore, as pointed out in chapter 3, there can be no correction of the landslide databases from their detection threshold and we could not define complete catalogues with all landslide volumes above the completude volume. In addition to landslide recording biases, it is important to note that landslide databases encompass two signals, a natural one and an anthropogenic one, which are difficult to distinguish without relevant information. For instance, deforestation may enhance landslide frequency and decrease landslide sizes (Glade, 1998) or remediation works may decrease the landslide frequency (Dussauge et al., 2002).

In order to deal with these issues, we adopted two different strategies. The first strategy, used in Chapter 2, consisted of performing tests on the New Zealand catalogue and assessing the robustness of our results by performing the same tests on catalogues subsampled in space, time and rate. As a second strategy, used in Chapter 3, we restricted the landslide catalogues to the period of time where the most roughly constant binary landslide rates were observed. The main disadvantages of this technique are to dismiss a large quantity of data and to preclude the analysis of the long-term landsliding rates. Nevertheless, this procedure provides catalogues which are self-consistent, producing robust results for the analysis of short-term landsliding rates. Still, we may miss some events at a shorter time scale. For example, the studied catalogues presented neither precursory slides nor afterslides (chapter 3, fig. 3.11) before or after the occurrences of the ten largest landslides. We can then wonder if the absence of such events is a catalogue bias or a reality. Indeed, while Amitrano et al. (2005) report no precursory slides before the collapse of a 1-2.10^3 m^3 chalk cliff, McSaveney (2002) and Rosser et al. (2007) report an increase in rockfalls in the days to months preceding large rockfalls in New Zealand and in England, respectively, and Wieczorek et al. (1995) report an inverse power-law decay of the number of rockfalls with time in the subsequent months after the Middle Brother (Yosemite, California) 600,000 m^3 rockfall.

In order to gather better databases, for which the sampling in time, space and size is

coherent, there is a need for landslide observatories aiming at setting up such databases. Instrumental recording of landslides would also give better databases. There are a few examples of instrumentally-recorded landslide catalogue. For instance, Rousseau (1999), on two cliffs of La Réunion, and Zimmer et al. (2008), on one cliff of the Yosemite Park, showed that continuous seismic monitoring of cliffs allowed rockfall events to be detected and catalogued. The major advantage of a seismically-gathered database is the precise time accuracy (up to the second) of the events. Besides, such a technique is promising since it is possible to monitor seismically several-kilometer-long cliffs to mountainous areas of several square kilometers, even though this has not been done yet.

In addition, since $V > 10^3\ m^3$ rockfall events produce a seismic signature that can be separated from earthquake signature (e.g. McSaveney and Downes, 2002; Deparis et al., 2008), this opens a possibility for the establishment of large rockfall databases from the analysis of local network seismograms. One of the main advantages of the development of such databases is the already large available period of time on which there would be data. The main drawbacks are the high volume detection threshold, e.g. $V > 10^3\ m^3$ with a local seismic network aiming at recovering $M > 1$ earthquakes (Deparis et al., 2008) and the fluctuation of this detection threshold with noise fluctuation, e.g. increase of noise with heavy rainfall. Thanks to terrestrial 3D laser scanners, Rosser et al. (2007) studied the rockfall activity of six coastal cliffs, corresponding to a surface of $\sim$100,000 m^2. They surveyed their field sites monthly for a period of 32 months. This method presents the advantage of locating very precisely the rockfall departure areas and the rockfall volumes, whereas the drawbacks are the absence of quantification of the number of rockfalls and a time accuracy equal to the survey frequency. Tralli et al. (2005) presented remote sensing techniques such as InSAR, GPS, visible and near infrared/thermal infrared (VNIR/TIR) imaging, multi parameters SAR, laser altimetry and microwave imaging as suitable for landslide systematic monitoring and gathering. The main advantage of such techniques is the large study area that can be dealt with. The main disadvantages are a time accuracy equal to the survey frequency and a size limitation to landslide detection.

The coseismic landslide databases used in chapter 4 were recovered from satellite images (SPOT), airborne inspection and high-altitude aerial photography. These techniques offer different resolutions and area coverage (e.g. area limited to one SPOT image for the Kashmir earthquake triggered landslides) and were all conducted only once after the mainshock occurrence. This latter point is critical to study the effect of aftershocks on landslide triggering. There is, to our knowledge, no example of more than one landslide reconnaissance after a landslide triggering earthquake although it would be interesting to have daily landslide reconnaissance in the following days (the shorter the frequency, the better).

Main results and implications

Chapters 2 and 3 highlighted several landsliding patterns, retrieved for most if not all catalogues. Landslide daily rates for New Zealand, Wollongong, Australia and Yosemite landslides attest for large volatility of landslide occurrences, appearing larger than those estimated for earthquake and rainfall rates, respectively. Grenoble and Val d'Arly landslide rates appear as more regular than the landslide rate of the four other catalogues. Still, no entire and binary landslide time occurrences are uniform and landslide waiting times do not follow a Poisson process. For the New Zealand landslides, we find a power-law to be a good fit of the waiting time distribution, for waiting times longer than 9 days. This result is robust when tested on subcatalogues selected over area extent and time. For these catalogues, we also find a power-law as a good fit of the waiting time distributions, but only for waiting times longer than 10 to 38 days. Power-law distributions are not found for the waiting time distributions of the five other catalogues, as there are not enough data to validate the power laws. We evidence a clear departure from a Poisson process for landslide waiting times larger than 30 to 250 days, depending on the catalogues.

For the New Zealand landslides, we suggested that landslides are correlated to each other and that the correlation between landslides which occurred more than nine days apart emerged from i) cyclonic weather system transit times across New Zealand, as New

Zealand rainfall and landslides display significant correlation, ii) triggering delay between rainfall and landsliding and iii) seasonal conditions favoring landslide triggering (low temperatures and higher rainfall in winter). We also suggested that the randomness observed for landslides which occurred less than nine days apart was caused either by the poor time accuracies of the landslide catalogue or by overlaps in time of sequences of triggered events independent in space. These last hypotheses cannot be extrapolated to the other landslide catalogues, as the retrieved waiting times for which we observe a departure from randomness are too large (up to 250 days). For these events, we suggest the deviation from a Poisson process to be due to seasonal variations of climate, landslides being less frequent or absent during the dry season, hence leading to larger inter-event times than expected from a Poisson distribution.

We retrieve a power-law as a good fit of the landslide daily rate distributions, for daily rates larger than one event per day, for the New Zealand, Yosemite, Australia and Wollongong catalogues. The power law gives a good fit for daily rates between 1 and 1000 landslides per day. A possible deviation from a power law is found above 10 landslides per day for the New Zealand, Australia and Wollongong catalogues. The fact that landslide daily rate distributions display a power-law behaviour implies that there is no characteristic scale for daily rate values and suggests that the same mechanism(s) are driving both the large landslide daily crises and the smaller daily rate crises. The power-law distribution of landslide daily rates may be driven either by the direct response to triggers, which are known to be power-law distributed in size, or by a generic response of the heterogeneous brittle crust to external forcings.

For all catalogues, no landslide-landslide interaction is evidenced. A better resolution in time is needed to further investigate such interaction, as well as catalogues presenting a better detection threshold in size. We show that earthquakes trigger landslides for the New Zealand, Yosemite and Australia areas to distances up to ten times the ruptured fault length. The influence of $M < 4$ earthquakes on landsliding is found to be weak, if any, for all catalogues. The effect of aftershocks could not be assessed with the available catalogues, as the resolution in time is too weak. The effect of $M < 4$ earthquakes on landsliding for

all areas is negligible, if any. Landslide-climate interactions were demonstrated for all catalogues but the Yosemite one. New Zealand, Wollongong, Australia and Val d'Arly monthly landslide rates display correlation with both the monthly rainfall height and the number of rain days per month. New Zealand and Grenoble landslides display anti-correlation to temperatures.

We propose indexes to estimate the landslide re-activity for a given area. We define the landslide re-activity as encompassing both the slope susceptibility and the forcing intensity, both of them driving the landslide dynamics. From the most re-active landslide area to the least re-active area, the different indexes, and their global trends, are: i) decreasing departure from randomness; ii) decreasing maximum daily rates and area over which the trigger operates; iii) decreasing landslide triggering for landslides occurring one day apart; iv) decreasing global interaction to earthquake, rainfall and temperature (Table 3.9).

From our analysis of landslide and aftershock distance distributions found after five $M_W > 5.5$ mainshocks, we find similar distance patterns when comparing the landslide distance distributions to their aftershock distance distribution counterparts. The result suggests that the same mechanisms are driving both landslide and aftershock triggering and shed light on the possible role of static stress changes in triggering landslides. When comparing the five landslide - aftershock distribution pairs from a given mainshock, we do not find a clear common pattern. Differences in mainshock characteristics, e.g. surface-rupturing earthquake versus buried earthquake, as well as local conditions, e.g. antecedent rainfall, appear to play a significant role in landslide and aftershock triggering. Neither Peak Ground Acceleration nor Peak Ground Displacement appears to have a linear influence on landslide and aftershock triggering. Peak Ground Displacement and associated static stress changes are found to be the most likely process driving landslide and aftershock triggering.

Perspectives

We first showed in Chapter 2 that New Zealand landslides are significantly anti-correlated to temperature and suggested that evapotranspiration (ET) was the cause of this anti-correlation. ET is the discharge of water from the earth's surface to the atmosphere by evaporation from lakes, streams, and soil surfaces and by transpiration from plants. ET is maximal in spring and summer, when temperatures and daylight hours are highest and when grasses and other annual plants reach their peak growth period (Glade et al., 2005). Our assumption is that New Zealand landslides' anti-correlation to temperature is due to ET, as ET partially drives soil moisture, which drives landslide triggering. Indeed, Glade et al. (2005) showed that soil moisture was driven by both rainfall and ET (Fig. 4.16) and that the time interval in which positive pore pressure may be formed corresponded to the period of year with the largest landsliding activity in the Santa Cruz Mountains (California, USA). The importance of soil moisture in landslide triggering was also demonstrated by Sidle and Ochiai (2006), Crozier (1999) and Glade (2000) who showed that landslide prediction was more accurate when taking into account antecedent soil moisture. In addition, ET could also be a cause of the non-linearity between rainfall and landsliding (see chapter 3; Hufschmidt and Crozier (2008)) as well as a cause of the non-linearity between soil moisture and rainfall (Ray and Jacobs, 2007). It would then be interesting to quantitatively assess ET for given areas and check if its variations (seasonal to daily) can explain variable landslide triggering. Such studies should be restricted to regional studies, as ET values depend on climate (Monteith, 1981; Glade et al., 2005) and vegetation. For studies encompassing several square kilometers, satellite images can give soil moisture (Ray and Jacobs, 2007) which could be used as a proxy of ET, once decorrelated from the rainfall signal. For slow-moving monitored landslides, we suggest that wind and soil moisture as well as rainfall and temperature should be recorded in order to assess ET.

The difference of behaviour between the Val d'Arly landslides and the Grenoble landslides deserves to be further investigated. The two locations are only 100 km apart but

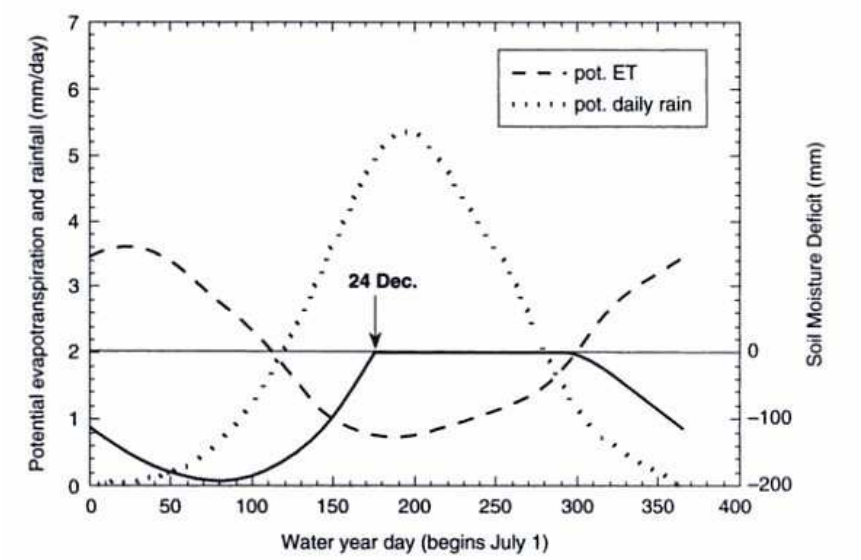

Figure 4.16: Variations in rainfall, evapotranspiration and soil moisture content in a typical year on a hillslope in the Santa Cruz Mountains (California, USA). The time period late December - late March corresponds to the maximum of landslide occurrences. From Glade et al. (2005).

Val d'Arly landslides show correlation with rainfall whereas Grenoble landslides show anti-correlation with temperature. The two main differences between those areas are the rock types and the rainfall pattern, and it is likely that one of these variables is driving the response to weather. In order to assess the influence of rock type, laboratory tests could be performed on Val d'Arly's micashist and Grenoble's limestone samples, the parameters to test being the influence of temperature and rainfall on these two samples. These laboratory tests should also be performed on Yosemite granite samples, as the absence of correlation between landslides and monthly weather variables is also intriguing. The influence of the rainfall pattern on slope stabilities could be tested using laboratory experiments as well. The question is whether cyclic rainfall is more efficient in triggering landslides than continuous rainfall (see Fig. 4.17 for the Val d'Arly and Grenoble monthly rainfall characteristics). This question was also raised in Chapter 2 where we showed higher landslide activity for the North Island of New Zealand, exposed to cyclic annual rainfall, than in the West Coast of the South Island, exposed to continuous high rainfall rates. Analogous

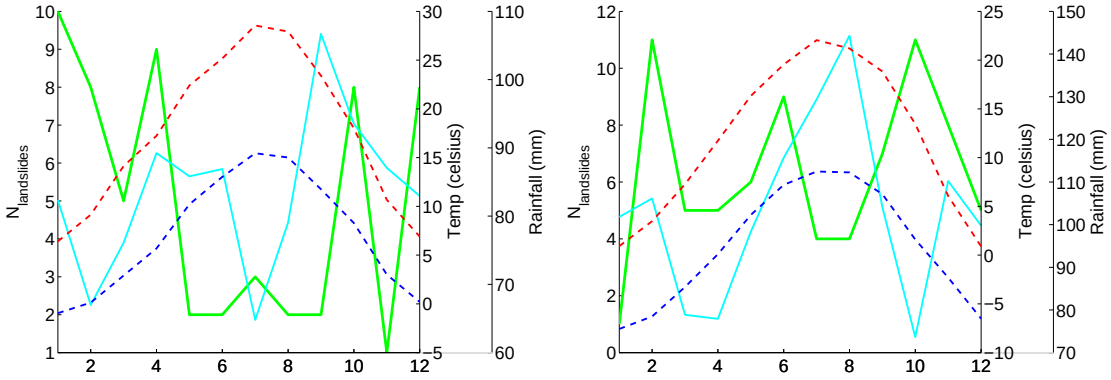

Figure 4.17: Monthly binary landslide rate (bold green line) and monthly averaged weather variables (blue dashed line: minimum temperatures, red dashed line: maximum temperatures, cyan line: rainfall height) for Grenoble (left) and Val d'Arly (right).

experiments could be conducted by modelling the slopes as simple tilted planes involving either one material or several materials (overlapped so as to model layers), exposed to either continuous rainfall or cyclic rainfall.

Finally, the perspectives opened by Chapter 4 are numerous. First, our model of landslide triggering by static stress changes needs to be tested on other earthquake-triggered landslide databases. As we had only one sequence of landslides and aftershocks triggered by a normal mainshock, priority should be given on other sequences triggered by normal mainshocks. Then, the landslide spatial occurrences should be plotted along the Coulomb static stress maps, for all sequences, in order to compare landslide occurrences and the Coulomb stress values associated. This model is very promising as it could predict where the landslides would occur after large earthquakes.

Appendices

Appendix A

Frequency-volume distributions

The frequency-volume distribution of landslide catalogues follows a power-law for volumes larger than V_0 (e.g. Dussauge et al., 2003). For volumes smaller than V_0, the catalogues are not complete, accounting for a lack of landslide recording. Although the number of landslides associated with a volume estimate is low, we check the frequency-volume distributions for a power law for the New Zealand (NZ), Yosemite, Grenoble, Val d'Arly and Australia catalogues (Table 3.2), via the method of Clauset et al. (2009), as presented in section 2.3.2.

Figure A.1 gives the frequency-volume distribution of the five catalogues and Table A.1 summarizes the parameters of the best power-law fit along with the goodness-of-fit values. Note that the values given for NZ are the same than in chapter 2 and are given here for comparison. We find that Yosemite and Grenoble volume distributions are power-law, as shown by Dussauge et al. (2002) via a χ^2_r test, but on different period of time. We find that the Val d'Arly volume distribution rejects the power-law as a good fit for the data. When we select the 2.2 km portion of the road accounting for a single cliff, as carried out by Dussauge et al. (2002), then we find that the volume distribution is fitted by a power-law. In the same way, we showed that the NZ landslide volume distribution rejects the power-law when considering the entire catalogue whereas the July 2001 - 2004 (where the sampling method is homogeneous) NZ landslide volume distribution is fitted

by a power-law (chapter 2). These results emphasise the importance of coherent sampling over time and space in order to have a power-law behavior of the volume distribution, and therefore a known coherent landslide dataset. We find that the Australia landslide volume distribution rejects the power-law as a good fit for the data. This result may reflect either that the sampling in space and time is not coherent and/or the volume estimates are biased. Another possibility is that the Australia landslide volume distribution does not accept a power-law as an intrinsic characteristic of Australia landsliding.

The exponent values of the best power-law are within error bars of one another for all catalogues. The value of the exponent is $b \approx 1.40$, which therefore is independent of the landslide type, geology and climate settings, extension and duration of the catalogue, as stated by Dussauge et al. (2002). The volumes of completude greatly vary from one catalogue to another, and reflect the resolution of the catalogues. The standard deviation of V_0 varies from 100 to more than 2000 m^3. The large values may reflect the small number of volume estimates on which the calculations are performed. Note the small number of landslides above the completude volume (N_{Vo} in Table A.1), precluding any analysis on catalogues corrected from their resolution, *i.e.* with volumes larger than V_0.

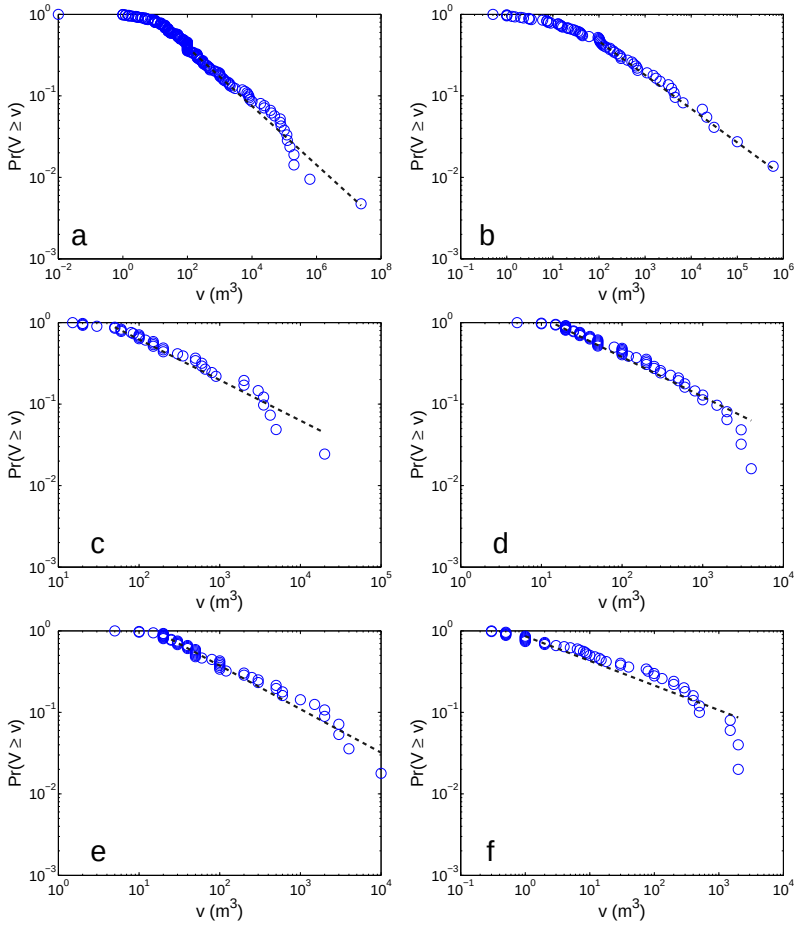

Figure A.1: Cumulative distribution of landslide volumes (blue circles) and their best Kolmogorov-Smirnoff power-law fit (black dashed line). a) New Zealand landslides; b) Yosemite landslides; c) Grenoble cliffs landslides; d) Val d'Arly cliffs landslides; e) Val d'Arly cliff landslides, on the 2.2 km portion of the road corresponding to a single cliff; f) Australia landslides. Values of exponents b and volumes of completude V_0 are given in table A.1. Note that the exponent of the cumulative distribution (CDF) function is equal to $b-1$ (e.g. Bonnet et al., 2001)

Table A.1: Frequency-volume distribution of landslides: number N of landslides associated with a volume, power-law exponent b, volume of completude V_0 and associated probability p that the distribution follows the best power-law fit. $p > 0.1$ - in bold in the table - accepts power-law as a possible description of the data. N_{Vo} gives the number of landslides with a volume larger than the volume of completude.

Catalogue	N	Exponent b	V_0	p-value	N_{Vo}
NZ July 2001-2004	210	1.36 ± 0.04	150 ± 2300	**0.26**	72
Yosemite 1980-2004	73	1.41 ± 0.14	108 ± 440	**0.81**	33
Grenoble 1982-2005	41	1.50 ± 0.32	50 ± 560	**0.15**	36
7 km Val d'Arly road, 1954-1976	62			0.01	0
2.2 km Val d'Arly road, 1954-1976	52	1.53 ± 0.11	25 ± 110	**0.45**	42
Australia 1996-2007	53			0	0

Appendix B

Local versus USGS earthquake catalogues

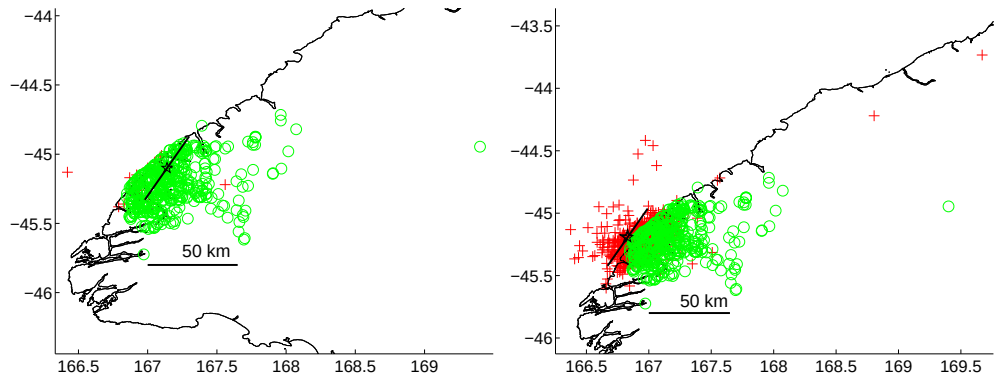

Figure B.1: Fiordland M_W7.2 earthquake (black pentagram), sequence of aftershocks (red markers) and triggered landslides (green markers). Left: as retrieved from USGS seismicity catalogue, Right: as retrieved from local seismicity catalogue. Note that the mainshock epicenter was relocated onshore for the USGS catalogue and that the number of aftershocks is smaller for the USGS catalogue.

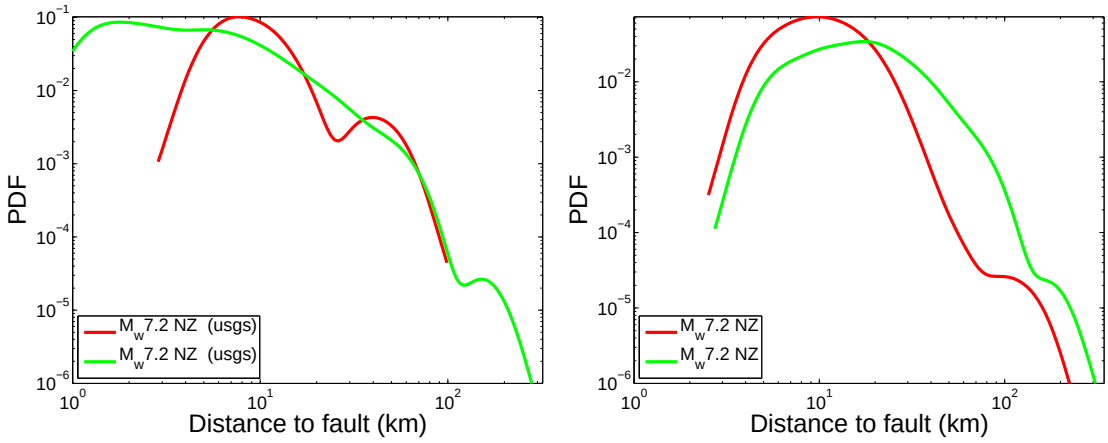

Figure B.2: Landslide (green) and aftershock (red) distance distributions. Left: distance distributions as retrieved from the USGS seismicity catalogue; right: distance distributions as retrieved from local seismicity catalogue. The onshore relocation of the mainshock from the USGS catalogue leads to different distance distributions. This study emphasises the importance of retrieving accurate relocation of earthquakes (see also Parsons, 2002 for biases induced by non accurate earthquake relocations).

Appendix C

Aftershock and landslide discrete distance distributions

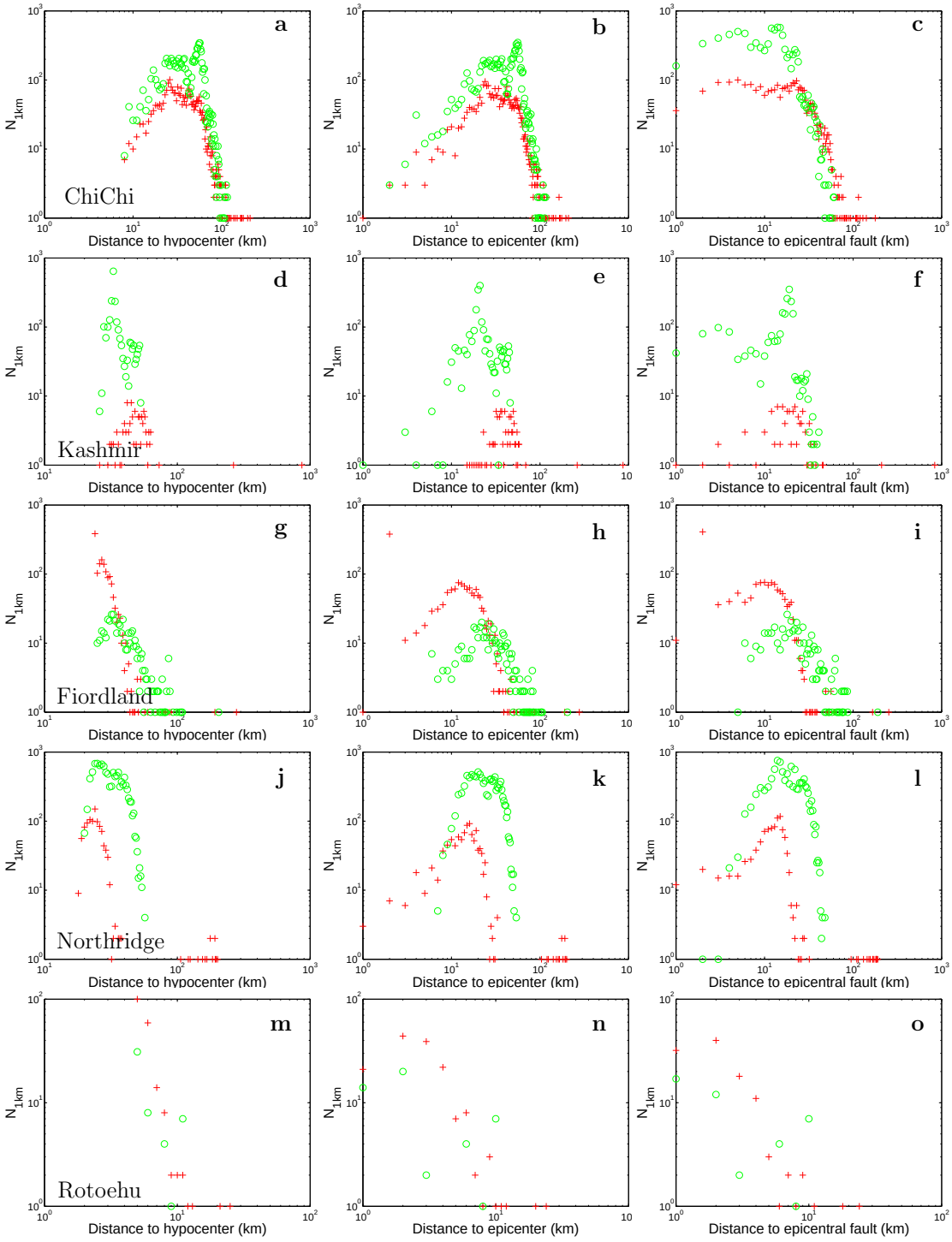

Figure C.1: Aftershock-mainshock (red crosses) and landslide-mainshock (green circles) number of events per 1 km bins. Left: Distance to hypocenter, Middle: Distance to epicenter, Right: Distance to seismogenic fault through epicenter for the five events.

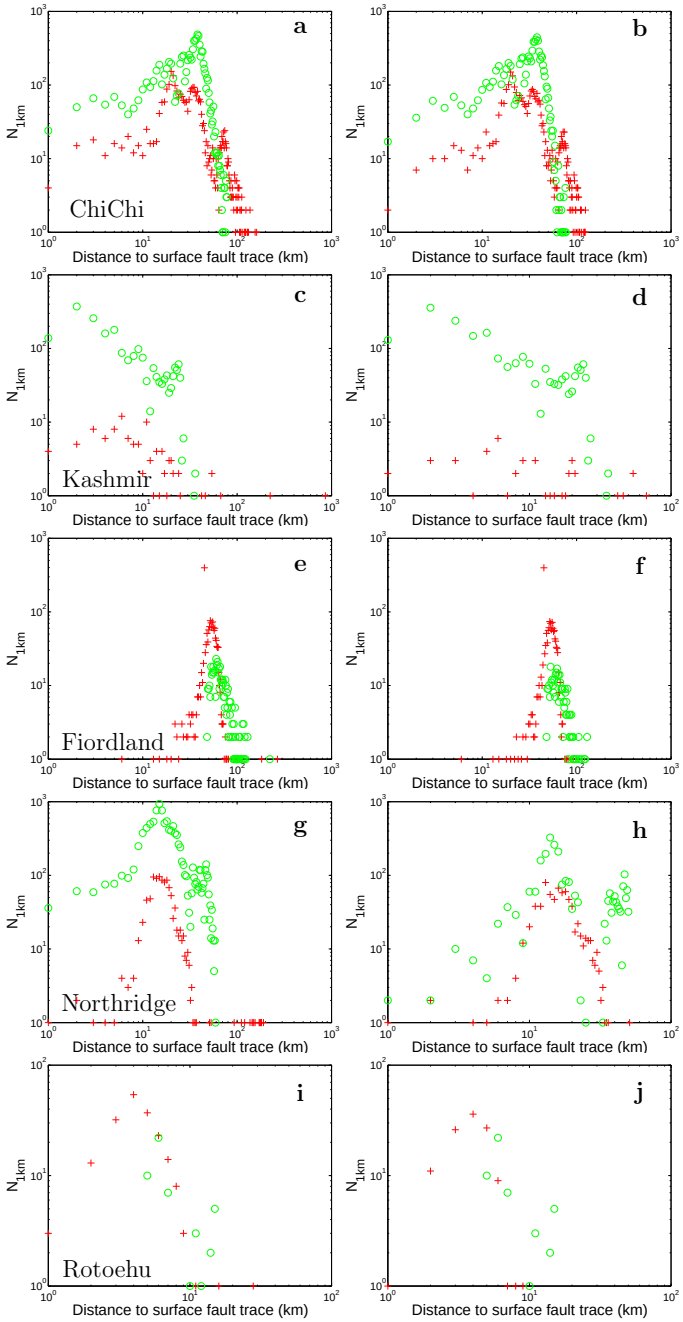

Figure C.2: Aftershock-mainshock (red crosses) and landslide-mainshock (green circles) number of events per 1 km bins. Left: Distance to actual (Chi-Chi and Kashmir) or inferred (Fiordland, Northridge, Rotoehu) surface fault trace. Right: Distance to actual or inferred surface fault trace, for the events on the hanging wall, bounded to the width of the ruptured fault length.

Appendix D

Construction of a landslide database

On the construction or updating of landslide and rockfall databases, our recommendations are the following. Files should be in text format, with each field/column separated by a "tabulation" (unlikely to be found in the actual information content of the database, contrary to "space", "comma", "semi-column" and other field separators). Excel (and other) spreadsheets should be avoided since from one spreadsheet software to another, automatic recognition of some formats (e.g. dates) are different and the actual data may be changed. Each field should display either a numerical value or specific key words, allowing for automated processing of the database. If pieces of information are missing for some landslides, we suggest to insert "NaN" (Not a Number) if the expected data is a number or "none" if the expected data is text. "Comments" field should not contain any important information but only give some context and precisions when available. Uncertainties on day accuracy, location, volume and any other numerical values should always be given. If the value is 100% certain then the uncertainty should be set to 0.

On the landslide information provided by a database, we suggest the following fields to be completed for each landslide.

- Fields 1 - 6: year, month, day, hour, minute, seconds (one field per data to avoid possible mix between the dd/mm/yyyy and the mm/dd/yyyy formats)

- Field 7: time accuracy (e.g. in case of earthquake triggered landslides, the date should be the one of the mainshock and the time accuracy the number of days after which the reconnaissance survey was performed)

- Fields 8 - 15: WGS84 latitude, WGS84 latitude uncertainty , WGS84 longitude, WGS84 longitude uncertainty, x local coordinates, x local coordinates uncertainty, y local coordinates, y local coordinates uncertainty,

- Field 16: elevation of landslides

- Fields 17 - 19: volume of landslide, volume uncertainty, volume class (1: $V < 10\ m^3$, 2:$10 < V < 10^2\ m^3$, 3:$10^2 < V < 10^3\ m^3$, 3:$10^3 < V < 10^4\ m^3$, 4:$10^4 < V < 10^5\ m^3$, 5:$10^5 < V < 10^6\ m$ 3, 6:$V > 10^6\ m^3$)

- Fields 20 - 21: area of landslide, area uncertainty

- Fields 22 - 23: type of material (rock, fine soils, coarse soils), type of movement (fall, topple, translational slide, rotational slide, spread, flow)

- Field 24: anthropogenic factor (1:yes, 0:no)

- Field 25: comment

- Field 26: data source

It is questionable whether the landslide database should propose a trigger mechanism or not since the association of a landslide with a trigger should not be made without rigorous timing of events, possibly numerical modelling to check if the trigger mechanism proposed is strong enough to trigger the landslide. On the contrary, daily or best hourly rainfall, temperatures, evapotranspiration and wind data close to the landslide on the 10 (or more) antecedent days would be most useful as it can be difficult to retrieve them directly for each landslide, especially when the database covers a wide area.

Finally, a covering sheet should come with the database, with persons to contact for details on the database and a list of the publications associated with the database. The sheet should review every field and detail how they were completed. Also, the sheet should detail any change in landslide recording, any major change in the slope susceptibility linked to anthropogenic activity (deforestation, road cuts, remediation works...) and any phenomena which could have affected landslide activity or recording.

Bibliography

N.S. Ai and T.D. Miao. A model of progressive slope failure under the effect of the neotectonic stress field. *Catena Supplement*, 10:21–29, 1987.

K. Aki. Maximum likelihood estimate of b in the formula log N= a-bM and its confidence limits. *Bulletin of Earthquake Research Institute, Tokyo University*, 43:237–239, 1965.

M. Alava, D. Amitrano, F. Dalton, V. De Rubeis, J.R. Grasso, A. Helmstetter, A. Petri, P. Sbarra, J. Schweizer, L. Tatard, P. Tosi, A. van Herwijnen, S. Vinciguerra, M. Zaiser, and S. Zapperi. Triggering of instabilities in materials and geosystems. TRIGS report: White Paper, 2008. Available at www.trigs.eu/wp-content/whitepaper.pdf.

D. Amitrano, J.R. Grasso, and G. Senfaute. Seismic precursory patterns before a cliff collapse and critical point phenomena. *Geophysical Research Letters*, 32(8):8314–8314, 2005.

J.P. Avouac, F. Ayoub, S. Leprince, O. Konca, and D.V. Helmberger. The 2005, Mw 7.6 Kashmir earthquake: Sub-pixel correlation of ASTER images and seismic waveforms analysis. *Earth and Planetary Science Letters*, 249(3-4):514–528, 2006.

A. Basile, G. Mele, and F. Terribile. Soil hydraulic behaviour of a selected benchmark soil involved in the landslide of Sarno 1998. *Geoderma*, 117(3-4):331–346, 2003.

E. Bonnet, O. Bour, N.E. Odling, P. Davy, I. Main, P. Cowie, and B. Berkowitz. Scaling of fracture systems in geological media. *Review of Geophysics*, 39:347–383, 2001. 10.1029/1999RG000074.

S.M. Brooks, M.J. Crozier, N.J. Preston, and M.G. Anderson. Regolith stripping and the control of shallow translational hillslope failure: application of a two-dimensional coupled soil hydrology-slope stability model, Hawke's Bay, New Zealand. *Geomorphology*, 45(3-4):165–179, 2002.

S.M. Brooks, M.J. Crozier, T.W. Glade, and M.G. Anderson. Towards Establishing Climatic Thresholds for Slope Instability: Use of a Physically-based Combined Soil Hydrology-slope Stability Model. *Pure and Applied Geophysics*, 161(4):881–905, 2004.

Bureau of Meteorology. http://www.bom.gov.au/lam/climate/levelthree/ausclim/ausclim.htm, September 2009.

N. Caine. The rainfall intensity-duration control of shallow landslides and debris flows. *Geografiska Annaler*, 62(1-2):23–27, 1980.

H. Chen and J.P. Wan. The effect of orientation and shape distribution of gravel on slope angles in central Taiwan. *Engineering geology*, 72(1-2):19–31, 2004.

M. Chigira and O. Yokoyama. Weathering profile of non-welded ignimbrite and the water infiltration behavior within it in relation to the generation of shallow landslides. *Engineering geology*, 78(3-4):187–207, 2005.

G. Chiodini, C. Cardellini, A. Amato, E. Boschi, S. Caliro, F. Frondini, and G. Ventura. Carbon dioxide Earth degassing and seismogenesis in central and southern Italy. *Geophysical Research Letters*, 31(7):L07615, 2004.

A. Clauset, C.R. Shalizi, and M.E.J. Newman. Power-law distributions in empirical data. *Society for Industrial and Applied Mathematics Review*, 2009.

S.C. Cox and S.K. Allen. Vampire rock avalanches of January 2008 and 2003, Southern Alps, New Zealand. *Landslides*, 6(2):161–166, 2009.

G. Crosta. Regionalization of rainfall thresholds: an aid to landslide hazard evaluation. *Environmental Geology*, 35(2):131–145, 1998.

M.J. Crozier. Multiple-occurrence regional landslide events in New Zealand: Hazard management issues. *Landslides*, 2(4):247–256, 2005.

M.J. Crozier. The climate-landslide couple: a Southern Hemisphere perspective. *Paleoclimate Research*, 19:329–350, 1996.

M.J. Crozier. Prediction of rainfall-triggered landslides: A test of the antecedent water status model. *Earth Surface Processes and Landforms*, 24(9):825–833, 1999.

S.J. Dadson, N. Hovius, H. Chen, W.B. Dade, J.C. Lin, M.L. Hsu, C.W. Lin, M.J. Horng, T.C. Chen, J. Milliman, et al. Earthquake-triggered increase in sediment delivery from an active mountain belt. *Geology*, 32(8):733, 2004.

P. De Vita, P. Reichenbach, J.C. Bathurst, M. Borga, G. Crosta, M. Crozier, T. Glade, F. Guzzetti, A. Hansen, and J. Wasowski. Rainfall-triggered landslides: a reference list. *Environmental Geology*, 35(2):219–233, 1998.

V. Del Gaudio, R. Trizzino, G. Calcagnile, A. Calvaruso, and P. Pierri. Landsliding in seismic areas: the case of the Acquara-Vadoncello landslide (southern Italy). *Bulletin of Engineering Geology and the Environment*, 59(1):23–37, 2000.

G. D. Dellow and G. T. Hancox. The influence of rainfall on earthquake-induced landslides in new zealand. In *Proceedings of technical groups*, volume 31, pages 355–368. Institution of Professional Engineers New Zealand, 2006.

J. Deparis, D. Jongmans, F. Cotton, L. Baillet, F. Thouvenot, and D. Hantz. Analysis of rock-fall and rock-fall avalanche seismograms in the French Alps. *Bulletin of the Seismological Society of America*, 98(4):1781, 2008.

A.S. Dhakal and R.C. Sidle. Distributed simulations of landslides for different rainfall conditions. *Hydrological Processes*, 18(4):757–776, 2004.

J. Dieterich. A constitutive law for rate of earthquake production and its application to earthquake clustering. *Journal of Geophysical Research - Solid Earth*, 99(B2):2601–2618, 1994.

J. Dieterich, V. Cayol, and P. Okubo. The use of earthquake rate changes as a stress meter at Kilauea volcano. *Nature*, 408(6811):457–460, 2000.

M. Dilley, R.S. Chen, and U. Deichmann. *Natural disaster hotspots: a global risk analysis*. World Bank Publications, 2005.

T.H. Dixon, M. Miller, F. Farina, H. Wang, and D. Johnson. Present-day motion of the Sierra Nevada block and some tectonic implications for the Basin and Range province, North American Cordillera. *Tectonics*, 19(1):1–24, 2000.

C. Dussauge, A. Helmstetter, J.R. Grasso, D. Hantz, P. Desvarreux, M. Jeannin, and A. Giraud. Probabilistic approach to rock fall hazard assessment: potential of historical data analysis. *Natural Hazards and Earth System Sciences*, 2:15–26, 2002.

C. Dussauge, J.R. Grasso, and A. Helmstetter. Statistical analysis of rockfall volume distributions: implication for rockfall dynamics. *Journal of Geophysical Research - Earth Surface*, 108(B6), 2003.

K.R. Felzer and E.E. Brodsky. Decay of aftershock density with distance indicates triggering by dynamic stress. *Nature*, 441(7094):735–738, 2006.

S.J. Fitzsimons and H. Veit. Geology and geomorphology of the European Alps and the Southern Alps of New Zealand. *Mountain Research and Development*, 21(4):340–349, 2001.

J.C. Flageollet, O. Maquaire, B. Martin, and D. Weber. Landslides and climatic conditions in the Barcelonnette and Vars basins (Southern French Alps, France). *Geomorphology*, 30(1-2):65–78, 1999.

P. Flentje and R.N. Chowdhury. Managing landslide hazards on the Illawarra escarpment. *Faculty of Engineering-Papers*, 2005.

P. Flentje, D. Stirling, and R.N. Chowdhury. Landslide Susceptibility and Hazard derived from a Landslide Inventory using Data Mining–An Australian Case Study. *Faculty of Engineering-Papers*, page 368, 2007.

M. Frayssines and D. Hantz. Failure mechanisms and triggering factors in calcareous cliffs of the Subalpine Ranges (French Alps). *Engineering Geology*, 86(4):256–270, 2006.

D. Fuchu, C.F. Lee, and W. Sijing. Analysis of rainstorm-induced slide-debris flows on natural terrain of Lantau Island, Hong Kong. *Engineering Geology*, 51(4):279–290, 1999.

T. Glade. Applying Probability Determination to Refine Landslide-triggering Rainfall Thresholds Using an Empirical Antecedent Daily Rainfall Model. *Pure and Applied Geophysics*, 157(6):1059–1079, 2000.

T. Glade. Establishing the frequency and magnitude of landslide-triggering rainstorm events in New Zealand. *Environmental Geology*, 35(2):160–174, 1998.

T. Glade, M. Anderson, and M.J. Crozier. *Landslide hazard and risk*. Wiley, 2005.

J. Gomberg and K. Felzer. A model of earthquake triggering probabilities and application to dynamic deformations constrained by ground motion observations. *Journal of Geophysical Research - Solid Earth*, 113(B10):B10317, 2008.

J. Gomberg, P. Bodin, and P.A. Reasenberg. Observing earthquakes triggered in the near field by dynamic deformations. *Bulletin of the Seismological Society of America*, 93(1): 118–138, 2003.

U. Gruner. Climatic and meteorological influences on rockfall and rockslides. In *Conference Proceedings INTERPRAEVENT*, volume 2, 2008.

B. Gutenberg and CF Richter. Earthquake magnitude, intensity, energy, and acceleration (Second paper). *Bulletin of the Seismological Society of America*, 46(2):105–145, 1956.

F. Guzzetti, B.D. Malamud, D.L. Turcotte, and P. Reichenbach. Power-law correlations of landslide areas in central Italy. *Earth and Planetary Science Letters*, 195(3-4):169–183, 2002.

F. Guzzetti, S. Peruccacci, M. Rossi, and C.P. Stark. Rainfall thresholds for the initiation of landslides in central and southern Europe. *Meteorology and Atmospheric Physics*, 98 (3):239–267, 2007.

S. Hainzl, T. Kraft, J. Wassermann, H. Igel, and E. Schmedes. Evidence for rainfall-triggered earthquake activity. *Geophysical Research Letters*, 33(19):L19303, 2006.

T.C. Hales and J.J. Roering. Climate-controlled variations in scree production, Southern Alps, New Zealand. *Geology*, 33(9):701–704, 2005.

T.C. Hales and J.J. Roering. Climatic controls on frost cracking and implications for the evolution of bedrock landscapes. *Journal of Geophysical Research - Earth Surface*, 112 (F2), 2007.

G.T. Hancox. The 1979 Abbotsford Landslide, Dunedin, New Zealand: a retrospective look at its nature and causes. *Landslides*, 5(2):177–188, 2008.

G.T. Hancox, N.D. Perrin, and G.D. Dellow. Recent studies of historical earthquake-induced landsliding, ground damage, and MM intensity in New Zealand. *Bulletin of the New Zealand Society for Earthquake Engineering(1999)*, 35(2):59–95, 2002.

G.T. Hancox, S. Cox, Turnbull I.M., and M.J. Crozier. Reconnaissance studies of landslides and other ground damage caused by the Mw 7.2 Fiordland earthquake of 22 August 2003. Institute of Geological and Nuclear Sciences science report 2003/30., 2003.

G.T. Hancox, D. Dellow, M. Mc Saveney, B. Scott, and P. Villamor. Reconnaissance studies of landslides caused by the M_L5.4 Lake Rotoehu earthquake and swarm of July 2004. Institute of Geological & Nuclear Sciences science report 2004/24 21p., 2004.

G.T. Hancox, M.J. McSaveney, V.R. Manville, and T.R. Davies. The October 1999 Mt Adams rock avalanche and subsequent landslide dam-break flood and effects in Poerua River, Westland, New Zealand. *New Zealand Journal of Geology and Geophysics*, 48(4): 683–705, 2005.

E.L. Harp and A.J. Crone. Landslides triggered by the October 8, 2005, Pakistan earthquake and associated landslide-dammed reservoirs. *US Geological Survey Open-file Report*, 1052, 2006.

E.L. Harp and R.W. Jibson. Landslides triggered by the 1994 Northridge, California, earthquake. *Bulletin of the Seismological Society of America*, 86(1B):S319, 1996.

E.L. Harp, R.W. Jibson, R.E. Kayen, D.K. Keefer, B.L. Sherrod, G.A. Carver, B.D. Collins, R.E.S. Moss, and N. Sitar. Landslides and liquefaction triggered by the M 7.9 Denali fault earthquake of 3 November 2002. *GSA TODAY*, 13(8):4–10, 2003.

E. Hauksson, L.M. Jones, and K. Hutton. The 1994 Northridge earthquake sequence in California: seismological and tectonic aspects. *Journal of Geophysical Research - Solid Earth*, 100(B7):12335–12356, 1995.

A. Helmstetter. Is earthquake triggering driven by small earthquakes? *Physical Review Letters*, 91(5):58501, 2003.

A. Helmstetter and S. Garambois. Seismic monitoring of Séchilienne Rockslide (French Alps): analysis of seismic signals and their correlation with rainfalls. *Journal of Geophysical Research - Earth surface*, submitted.

K. Holm, M. Bovis, and M. Jakob. The landslide response of alpine basins to post-Little Ice Age glacial thinning and retreat in southwestern British Columbia. *Geomorphology*, 57(3-4):201–216, 2004.

G. Hufschmidt and M.J. Crozier. Evolution of natural risk: analysing changing landside hazard in Wellington, Aotearoa/New Zealand. *Natural Hazards*, 45:255–276, 2008.

T. Hurst, S. Bannister, R. Robinson, and B. Scott. Characteristics of three recent earthquake sequences in the Taupo Volcanic Zone, New Zealand. *Tectonophysics*, 2008.

A.J. Izenman. Recent developments in nonparametric density estimation. *Journal of the American Statistical Association*, pages 205–224, 1991.

P.A. Johnson and X. Jia. Nonlinear dynamics, granular media and dynamic earthquake triggering. *Nature*, 437(7060):871–874, 2005.

M. Julian and E. Anthony. Aspects of landslide activity in the Mercantour Massif and the French Riviera, southeastern France. *Geomorphology*, 15(3-4):275–289, 1996.

Y.Y. Kagan and D.D. Jackson. Long-term earthquake clustering. *Geophysical Journal International*, 104(1):117–134, 1991.

D.K. Keefer. Statistical analysis of an earthquake-induced landslide distribution - the 1989 Loma Prieta, California event. *Engineering Geology*, 58(3-4):231–249, 2000.

D.K. Keefer. Investigating landslides caused by earthquakes - a historical review. *Surveys in Geophysics*, 23:573–510, 2002.

D.K. Keefer. Landslides caused by earthquakes. *Bulletin of the Geological Society of America*, 95(4):406–421, 1984.

DK Keefer and RC Wilson. Predicting earthquake-induced landslides, with emphasis on arid and semi-arid environments. *Sadler, PM, and Morton, DD. M., eds., Landslides in a semi-arid environment: Riverside. California, Inland Geological Society*, 2:118–149, 1989.

B. Khazai and N. Sitar. Evaluation of factors controlling earthquake-induced landslides caused by Chi-Chi earthquake and comparison with the Northridge and Loma Prieta events. *Engineering geology*, 71(1-2):79–95, 2004.

C.R.J. Kilburn and D.N. Petley. Forecasting giant, catastrophic slope collapse: lessons from Vajont, Northern Italy. *Geomorphology*, 54(1-2):21–32, 2003.

G.C.P. King, R.S. Stein, and J. Lin. Static stress changes and the triggering of earthquakes. *Bulletin of the Seismological Society of America*, 84(3):935–953, 1994.

O. Korup. Distribution of landslides in southwest New Zealand. *Landslides*, 2(1):43–51, 2005.

N. Lemarchand and J.R. Grasso. Interactions between earthquakes and volcano activity. *Geophysical Research Letters*, 34, 2007.

M. Leonard. One hundred years of earthquake recording in Australia. *Bulletin of the Seismological Society of America*, 98(3):1458–1470, June 2008.

H.W. Liao and C.T. Lee. Landslides triggered by the chi-chi earthquake. Asian Conference on Remote Sensing, 2000.

C.W. Lin, C.L. Shieh, B.D. Yuan, Y.C. Shieh, S.H. Liu, and S.Y. Lee. Impact of Chi-Chi earthquake on the occurence of landslides and debris flows: example from the Chenyulan River watershed, Nantou, Taiwan. *Engineering Geology*, 71:49–61, 2003.

C.W. Lin, S.H. Liu, S.Y. Lee, and C.C. Liu. Impacts of the Chi-Chi earthquake on subsequent rainfall-induced landslides in central Taiwan. *Engineering Geology*, 86(2-3):87–101, 2006.

G.W. Lin, H. Chen, Y.H. Chen, and M.J. Horng. Influence of typhoons and earthquakes on rainfall-induced landslides and suspended sediments discharge. *Engineering Geology*, 97(1-2):32–41, 2008a.

G.W. Lin, H. Chen, N. Hovius, M.J. Horng, S. Dadson, P. Meunier, and M. Lines. Effects of earthquake and cyclone sequencing on landsliding and fluvial sediment transfer in a mountain catchment. *Earth Surface Processes and Landforms*, 33(9):1354–1373, 2008b.

A.T. Linde and I.S. Sacks. Triggering of volcanic eruptions. *Nature(London)*, 395(6705): 888–890, 1998.

E. Lippiello, L. de Arcangelis, and C. Godano. Role of static stress diffusion in the spatiotemporal organization of aftershocks. *Physical Review Letters*, 103(3):38501, 2009.

K.F. Ma, C.H. Chan, and R.S. Stein. Response of seismicity to Coulomb stress triggers and shadows of the 1999 Mw= 7.6 Chi-Chi, Taiwan, earthquake. *Journal of Geophysical Research - Solid Earth*, 110(5), 2005.

D.F. Macfarlane. Observations and predictions of the behaviour of large, slow-moving landslides in schist, Clyde Dam reservoir, New Zealand. *Engineering Geology*, 2009.

B.D. Malamud, D.L. Turcotte, F. Guzzetti, and P. Reichenbach. Landslide inventories and their statistical properties. *Earth Surface Processes and Landforms*, 29(6):687–711, 2004.

M. Manga and E. Brodsky. Seismic Triggering of Eruptions in the Far Field: Volcanoes and Geysers. *Annual Reviews of Earth and Planetary Sciences*, 34:263–91, 2006.

W. Marzocchi and L. Zaccarelli. A quantitative model for the time-size distribution of eruptions. *Journal of Geophysical Research - Solid Earth*, 111, 2006.

N. Matsuoka and J. Murton. Frost weathering: recent advances and future directions. *Permafrost and Periglacial Processes*, 19(2), 2008.

N. Matsuoka and H. Sakai. Rockfall activity from an alpine cliff during thawing periods. *Geomorphology*, 28(3-4):309–328, 1999.

A. McGarr, D. Simpson, and L. Seeber. Case histories of induced and triggered seismicity. *International Geophysics Series*, 81(A):647–664, 2002.

P. McGinty and R. Robinson. The 2003 Mw 7.2 Fiordland subduction earthquake, New Zealand: aftershock distribution, main shock fault plane and static stress changes on the overlying Alpine Fault. *Geophysical Journal International*, 169(2):579–592, 2007.

M.J. McSaveney. Recent rock-falls and rock avalanches in Mount Cook National Park, New Zealand. *Catastrophic Landslides: Effects, Occurrence and Mechanisms*, pages 35–70, 2002.

M.J. McSaveney and G. Downes. Application of landslide seismology to some New Zealand rock avalanches. In *Landslides: Proceedings of the First European Conference on Landslides, Prague, Czech Republic, June 24-26, 2002*, page 649. Taylor & Francis Group, 2002.

P. Meunier, N. Hovius, and A.J. Haines. Regional patterns of earthquake-triggered landslides and their relation to ground motion. *Geophysical Research Letters*, 34(20):1–L20408, 2007.

P. Meunier, N. Hovius, and J.A. Haines. Topographic site effects and the location of earthquake induced landslides. *Earth and Planetary Science Letters*, 275(3-4):221–232, 2008.

M. Michael-Leiba, K. Andrews, and R. Blong. The impact of landslides in Australia. *Australian Journal of Emergency Management*, 12(1):23–26, 1997.

S.A. Miller, C. Collettini, L. Chiaraluce, M. Cocco, M. Barchi, and B.J.P. Kaus. Aftershocks driven by a high-pressure CO 2 source at depth. *Nature*, 427(6976):724–727, 2004.

W.J. Miller. The landslide at Point Firmin, California. *The Scientific Monthly*, 32(5): 464–469, 1931.

A.S. Miner, P. Flentje, C. Mazengrab, J.M. Selkirk-Bell, and P. Dalhaus. Some geomorphological techniques used in constraining the likelihood of landsliding–selected Australian examples. *Faculty of Engineering-Papers*, page 451, 2008.

P. Molnar, R.S. Anderson, and S.P. Anderson. Tectonics, fracturing of rock, and erosion. *Journal of Geophysical Research*, 112(F3), 2007.

J.L. Monteith. Evaporation and surface temperature. *Quarterly Journal of the Royal Meteorological Society*, 107(451):1–27, 1981.

B. Muço. Statistical investigation on possible seasonality of seismic activity and rainfall-induced earthquakes in Balkan area. *Physics of the Earth and Planetary Interiors*, 114 (3):119–127, 1999.

NIWA. http://www.niwa.co.nz/education-and-training/schools/resources/climate/overview, September 2009.

H. Ogasawara, K. Fujimori, N. Koizumi, N. Hirano, S. Fujiwara, S. Otsuka, S. Nakao, K. Nishigami, K. Taniguchi, Y. Iio, et al. Microseismicity induced by heavy rainfall around flooded vertical ore veins. *Pure and Applied Geophysics*, 159(1):91–109, 2002.

Y. Ogata. Statistical models for earthquake occurrences and residual analysis for point processes. *Journal of the American Statistical Association*, 83(401):9–27, 1988.

Y. Ogata and K. Katsura. Analysis of temporal and spatial heterogeneity of magnitude frequency distribution inferred from earthquake catalogues. *Geophysical Journal International*, 113(3):727–738, 1993.

T. Parsons. Global Omori law decay of triggered earthquakes: Large aftershocks outside the classical aftershock zone. *Journal of Geophysical Research - Solid Earth*, 107(B9): 2199, 2002.

A. Pasuto and S. Silvano. Rainfall as a trigger of shallow mass movements. A case study in the Dolomites, Italy. *Environmental Geology*, 35(2):184–189, 1998.

O. Peters and K. Christensen. Rain: Relaxations in the sky. *Physical Review E*, 66(3): 36120, 2002.

O. Peters, C. Hertlein, and K. Christensen. A complexity view of rainfall. *Physical review letters*, 88(1):18701, 2001.

D.N. Petley, S.A. Dunning, N.J. Rosser, and A.B. Kausar. Incipient landslides in the Jhelum Valley, Pakistan following the 8th October 2005 earthquake. *Disaster Mitigation of Debris Flows, Slope Failures and Landslides, Frontiers of Science Series*, 47:47–56, 2005.

M. Pirulli. The Thurwieser rock avalanche (Italian Alps): Description and dynamic analysis. *Engineering Geology*, in press.

A. Pitarka, L.A. Dalguer, S.M. Day, P.G. Somerville, and K. Dan. Numerical Study of Ground-Motion Differences between Buried-Rupturing and Surface-Rupturing Earthquakes. *Bulletin of the Seismological Society of America*, 99(3):1521, 2009.

W.H. Press, B. Flannery, S.A. Teukolsky, and W.T. Vetterling. *Numerical recipes in C: the art of scientific computing.* Cambridge University Press New York, 2nd edition, 1992.

R.L. Ray and J.M. Jacobs. Relationships among remotely sensed soil moisture, precipitation and landslide events. *Natural Hazards*, 43(2):211–222, 2007.

L.M. Reid and M.J. Page. Magnitude and frequency of landsliding in a large New Zealand catchment. *Geomorphology*, 49(1-2):71–88, 2002.

M. Reyners, P. McGinty, S. Cox, I. Turnbull, T. O'Neill, K. Gledhill, G. Hancox, J. Beavan, D. Matheson, G. McVerry, et al. The Mw 7.2 Fiordland earthquake of August 21, 2003: Background and preliminary results. *Bulletin of the New Zealand Society for Earthquake Engineering(1999)*, 36(4):233–248, 2003.

N. Rosser, M. Lim, D. Petley, S. Dunning, and R. Allison. Patterns of precursory rockfall prior to slope failure. *Journal of Geophysical Research - Earth Surface*, 112(F4):F04014, 2007.

N. Rousseau. *Study of seismic signals associated with rockfalls at 2 sites on the Reunion island (Mahavel Cascade and Souffriere cavity)*. PhD thesis, PhD Thesis, IPG, Paris, 1999, 1999.

F. Sandersen, S. Bakkehoi, E. Hestnes, and K. Lied. The influence of meteorologial factors on the initiation of debris flow, rockfall, rockslides and rockmass stability. In *Proc. of the 7th Int. Symp. on Landslides, Trondheim*, volume 1, pages 97–114., Balkema, Rotterdam, 1996.

K. Sassa, H. Fukuoka, F. Wang, and G. Wang. Landslides induced by a combined effect of earthquake and rainfall. *Progress in Landslide Science (Editors: K. Sassa, H. Fukuoka, F. Wang, G. Wang), Springer*, pages 193–207, 2007.

H.P. Sato, H. Hasegawa, S. Fujiwara, M. Tobita, M. Koarai, H. Une, and J. Iwahashi. Interpretation of landslide distribution triggered by the 2005 Northern Pakistan earthquake using SPOT 5 imagery. *Landslides*, 4(2):113–122, 2007.

P. Segall, E.K. Desmarais, D. Shelly, A. Miklius, and P. Cervelli. Earthquakes triggered by silent slip events on Kilauea volcano, Hawaii. *Nature*, 442(7098):71–74, 2006.

S.A. Sepúlveda, W. Murphy, R.W. Jibson, and D.N. Petley. Seismically induced rock slope failures resulting from topographic amplification of strong ground motions: The case of Pacoima Canyon, California. *Engineering geology*, 80(3-4):336–348, 2005.

R.C. Sidle and H. Ochiai. *Landslides: processes, prediction, and land use*. American Geophysical Union, 2006.

G.M. Smith, T.R. Davies, M.J. McSaveney, and D.H. Bell. The Acheron rock avalanche, Canterbury, New Zealand: morphology and dynamics. *Landslides*, 3(1):62–72, 2006.

C.G. Smyth and S.A. Royle. Urban landslide hazards: incidence and causative factors in Niterói, Rio de Janeiro State, Brazil. *Applied Geography*, 20(2):95–118, 2000.

A. Špičák and J. Horálek. Possible role of fluids in the process of earthquake swarm generation in the West Bohemia/Vogtland seismoactive region. *Tectonophysics*, 336(1-4):151–161, 2001.

C.P. Stark and N. Hovius. The characterization of landslide size distributions. *Geophysical Research Letters*, 28(6):1091–1094, 2001.

T.D. Stark, W.D. Arellano, R.P. Hillman, R.M. Hughes, N. Joyal, and D. Hillebrandt. Effect of toe excavation on a deep bedrock landslide. *Journal of Performance of Constructed Facilities*, 19(3):244–255, 2005.

R.S. Stein. The role of stress transfer in earthquake occurrence. *Nature*, 402(6762):605–609, 1999.

L. Tatard, J.R. Grasso, A. Helmstetter, and G.D. Dellow. Interactions between landslides, seismicity and climate in New Zealand. *Journal of Geophysical Research - Earth Surface*, Submitted.

M.T.J. Terlien. The determination of statistical and deterministic hydrological landslide-triggering thresholds. *Environmental geology*, 35(2):124–130, 1998.

S. Touati, M. Naylor, and I.G. Main. Origin and Nonuniversality of the Earthquake Interevent Time Distribution. *Physical Review Letters*, 102(16):168501, 2009.

D.M. Tralli, R.G. Blom, V. Zlotnicki, A. Donnellan, and D.L. Evans. Satellite remote sensing of earthquake, volcano, flood, landslide and coastal inundation hazards. *ISPRS Journal of Photogrammetry and Remote Sensing*, 59(4):185–198, 2005.

P. Traversa and J.R. Grasso. Brittle Creep Damage as the Seismic Signature of Dyke Propagations within Basaltic Volcanoes. *Bulletin of the Seismological Society of America*, 99(3):2035, 2009.

Y.B. Tsai and M.W. Huang. Strong ground motion characteristics of the Chi-Chi, Taiwan earthquake of September 21, 1999. *Earthquake Engineering and Engineering Seismology*, 2(1):1–21, 2000.

T. Utsu. A statistical study on the occurrence of aftershocks. *Geophys. Mag*, 30(4):521–605, 1961.

W.G. Vahrson. Macrozonation methodology for landslide hazard determination. *Bulletin-Association of Engineering Geologists*, page 49, 1994.

D.J. Wald, T.H. Heaton, and KW Hudnut. The slip history of the 1994 Northridge, California, earthquake determined from strong-motion, teleseismic, GPS, and leveling data. *Bulletin of the Seismological Society of America*, 86(1B):S49, 1996.

M. Walter and M. Joswig. Seismic monitoring of fracture processes from a creeping landslide in the Vorarlberg Alps. In EGU General Assembly, editor, *Geophysical Research Abstracts*, volume 10, 2008.

D.L. Wells and K.J. Coppersmith. New empirical relationships among magnitude, rupture length, rupture width, rupture area, and surface displacement. *Bulletin of the Seismological Society of America*, 84(4):974–1002, 1994.

K.X. Whipple. The influence of climate on the tectonic evolution of mountain belts. *Nature Geoscience*, 2(2):97–104, 2009.

I.E. Whitehouse and G.A. Griffiths. Frequency and hazard of large rock avalanches in the central Southern Alps, New Zealand. *Geology*, 11(6):331–334, 1983.

G.F. Wieczorek. Catastrophic rockfalls and rockslides in the Sierra Nevada, USA. *Catastrophic Landslides: Effects, Occurrence, and Mechanisms*, page 165, 2002.

G.F. Wieczorek, S.R. Nishenko, and D.J. Varnes. Analysis of rock falls in the Yosemite Valley, California1. In *Rock mechanics: proceedings of the 35th US Symposium, University of Nevada/Reno/5-7 June 1995*, page 85. Taylor & Francis, 1995.

C.A. Wright. The AD 930 long-runout Round Top debris avalanche, Westland, New Zealand. *New Zealand Journal of Geology and Geophysics*, 41:493–498, 1998.

C. Xu, J. Wang, Z. Li, and J. Drummond. Applying the Coulomb failure function with an optimally oriented plane to the 2008 Mw 7.9 Wenchuan earthquake triggering. *Tectonophysics*, in press.

Y. Zeng and C.H. Chen. Fault rupture process of the 20 September 1999 Chi-Chi, Taiwan, earthquake. *Bulletin of the Seismological Society of America*, 91(5):1088, 2001.

VL Zimmer, GM Stock, and N. Sitar. Seismic Monitoring of Rock Falls in Yosemite National Park. In *American Geophysical Union, Fall Meeting 2008, abstract H51F-0897*, 2008.

Statistical analysis of triggered landslides: implications for earthquake and weather controls

We analyse the 1996-2004 New Zealand landslide time series in time and rate and find a strong correlation in landslide occurrences. This time correlation is not found to be driven by the earthquake-landslide nor the landslide-landslide interactions but by climate-landslide interactions. We compare the occurrence of landslides in time, space and rate of New Zealand, Yosemite (California, USA), Grenoble (French Alps), Val d'Arly (French Alps), Australia and Wollongong (New South Wales, Australia) as indicated by the corresponding catalogues. The New Zealand, Yosemite, Australia and Wollongong landslide daily rates between 1 and 1000 events per day are well fitted by a power law, suggesting that the same mechanism(s) are driving both the large landslide daily crises and the single events. The joint analysis of the six catalogues reveals parameters that allow sorting of the relative landslide occurrences in each of the six areas. Finally, we compare earthquake aftershock spatial distributions with the spatial distributions of landslides triggered by the Chi-Chi Mw7.6 earthquake (Taiwan), by the Mw7.6 Kashmir earthquake (Pakistan), by the Mw7.2 Fiordland earthquake (New Zealand), by the Mw6.6 Northridge earthquake (California) and by the Mw5.6 Rotoehu earthquake (New Zealand). We show the seismic aftershocks and landslides to display roughly similar patterns with distances for given seismic events. We find no linear scaling of the number of landslides or aftershocks with any of the ground motion variables. We suggest that landslides and aftershocks are driven by the same mechanisms and shed light on the Peak Ground Displacement and static stress changes on landslide triggering.

Keywords: landslides, earthquake-triggered landslides, time series, earthquake, rainfall, temperature.

Analyse statistique des glissements de terrain déclenchés : implications sur les contrôles sismiques et climatiques

Nous analysons les séries temporelles des glissements de terrain de Nouvelle-Zélande (NZ) en temps et en taux et mettons en évidence une corrélation dans les occurrences de glissements. Cette corrélation n'est pas due aux interactions glissement-séisme ou glissement-glissement mais aux interactions glissement-climat. Nous comparons la dynamique des glissements en temps, espace et taux pour la NZ, le Yosemite (Californie, Etats-Unis), Grenoble (Isère), Val d'Arly (Haute-Savoie), l'Australie et le Wollongong (New South Wales, Australie). Les taux journaliers de glissements de la NZ, du Yosemite, de l'Australie et du Wollongong acceptent une loi puissance pour des taux variant de 1 à 1000 glissements/jour. Cela suggère que les mêmes méchanismes sont à l'oeuvre pour le déclenchement de plusieurs centaines de glissements comme de un seul glissement. L'analyse jointe de ces six catalogues nous a permis de dériver des paramètres permettant de classer la dynamique de chaque endroit en terme de glissements. Enfin, nous comparons les distributions en espace des répliques sismiques et des glissements de terrain déclenchés par les séismes de Chi-Chi (Mw7.6 - Taiwan), du Kashmir (Mw7.6 - Pakistan), de Fiordland (Mw7.2 - NZ), de Northridge (Mw6.6 - Californie) et de Rotoehu (MW5.6 - NZ). Les répliques sismiques et les glissements présentent des distributions spatiales similaires. Nous ne trouvons pas de réponse linéaire entre les glissements et/ou les répliques et les observations de mouvements du sol. Nous suggérons que les glissements et les répliques sont contrôlés par les mêmes méchanismes et donc qu'il existe un rôle de la contrainte statique sur le déclenchement des glissements de terrain.

Mots clés : Glissements de terrain, glissements de terrain déclenchés par les séismes, séries temporelles, séisme, pluie, température.